Contract DAHC-04-71-C-0026
Report IITRI-J6248-II

BLAST PRESSURES FROM SEQUENTIAL EXPLOSIONS

Department of Defense Explosives Safety Board
Forrestal Building, GB-270
Washington, D.C. 20314

Prepared by

James J. Swatosh, Jr.

IIT Research Institute
10 West 35th Street
Chicago, Illinois 60616

Final Report January 1972

FOREWORD

This final report on "Blast Pressures from Sequential Explosions" covers the period from April 1971 through September 1971. The work was conducted by IIT Research Institute for the Department of Defense Explosives Safety Board under Contract DAHC-04-71-C-0026. Personnel who have made material contributions to the report are R. P. Joyce, D. C. Anderson, and J. J. Swatosh.

Prepared by

James J. Swatosh, Jr.
Research Engineer
Shock Dynamics and
Safety Analysis

Approved by:

D. C. Anderson, Manager
Shock Dynamics and Safety Analysis

UNCLASSIFIED

Security Classification

DOCUMENT CONTROL DATA - R & D

(Security classification of title, body of abstract and indexing annotation must be entered when the overall report is classified)

1 ORIGINATING ACTIVITY *(Corporate author)*

IIT Research Institute
10 W. 35th Street
Chicago, Illinois 60616

2a. REPORT SECURITY CLASSIFICATION

2b. GROUP

3 REPORT TITLE

BLAST PRESSURES FROM SEQUENTIAL EXPLOSIONS

4 DESCRIPTIVE NOTES *(Type of report and inclusive dates)*

Final Report (April 1971 through September 1971)

5 AUTHOR(S) *(First name, middle initial, last name)*

James J. Swatosh

6 REPORT DATE	7a. TOTAL NO. OF PAGES	7b. NO. OF REFS
January 1972	126	2

8a. CONTRACT OR GRANT NO	9a. ORIGINATOR'S REPORT NUMBER(S)
DAHC-04-71-C-0026	J6248-II
b. PROJECT NO	
c.	9b. OTHER REPORT NO(S) *(Any other numbers that may be assigned this report)*
d.	

10 DISTRIBUTION STATEMENT

Distribution of this document is unlimited.

11 SUPPLEMENTARY NOTES	12. SPONSORING MILITARY ACTIVITY
	Dept.of Defense Explosives Safety Bd. Forrestal Building, GB-270 Washington, D.C. 20314

13 ABSTRACT

An experimental program was conducted, for the Department of Defense Explosives Safety Board, to determine blast pressures, total impulse, and catchup times of shock waves generated by sequentially detonating two explosive charges. The parameters varied in this experimental series included charge spacing, time delay between detonations, and orientation of the charges with respect to two right-angle blast lines. It was found that the peak overpressure at a given point in the blast field around the charges is greatest when the two shock waves just coalesce at that point. It was also found that the peak pressure from two sequentially detonated charges can be greater than a total weight equivalent one-charge detonation in some directions or orientations.

DD FORM 1 NOV 68 1473

UNCLASSIFIED

Security Classification

14 KEY WORDS	LINK A		LINK B		LINK C	
	ROLE	WT	ROLE	WT	ROLE	WT

ABSTRACT

An experimental program was conducted, for the Department of Defense Explosives Safety Board, to determine blast pressures, total impulse, and catchup times of shock waves generated by sequentially detonating two explosive charges. The parameters varied in this experimental series include charge spacing, time delay between detonations, and orientation of the charges with respect to two right-angle blast lines. It was found that the peak overpressure at a given point in the blast field around the charges is greatest when the two shock waves just coalesce at that point. It was also found that the peak pressure from two sequentially detonated charges can be greater than a total weight equivalent one-charge detonation in some directions or orientations.

BLANK

CONTENTS

LIST OF FIGURES

LIST OF FIGURES (continued)

LIST OF FIGURES (continued)

LIST OF FIGURES (continued)

LIST OF FIGURES (concluded)

BLAST PRESSURES FROM SEQUENTIAL EXPLOSIONS

1. INTRODUCTION

This final report documents an experimental program which was designed to determine blast pressures, peak impulse, and catchup times of shock waves generated by sequentially detonating two explosive charges. The parameters varied in this experimental series included charge spacing, time delay between detonations, and orientation of the charges with respect to two right-angle blast measurement lines.

1.1 Previous Investigations

Previous work[1] in this area indicated that there is a strong directional effect on the coalescence of successive blast pulses from sequentially detonated charges. Criteria for deciding conditions under which closely spaced sequential explosions must be considered simultaneous in calculating safe distances from explosive stores were determined. Theoretical analysis and model experiments were conducted. In that work, 20 experiments were carried out with small plastic explosive charges totaling 2 lbs in weight in each experiment. The weights of the two successively fired charges in each experiment were in the ratio of 1/2, 1, or 2, with emphasis on the equal-charge case. A few tests were also run with three explosive charges in each test.

Blast pressure measurements were made at six stations on each of two blast lines. One blast line, termed the axial line, was directed along the extended line of centers of the charges, while the other, termed the lateral line, extended from the center of the charge array in a direction perpendicular to the axial line.

In the theoretical effort, calculations were made of the blast fields from sequential explosions with the assumption of spherical symmetry. That is, the sequential explosions were considered to be spatially coincident,

---

[1] Zaker, T. A., "Blast Pressures from Sequential Explosions," IITRI Final Report J6166, Contract DAHC-04-69-C-0020 for ASESB (October 1969)

and details of placement in the charge array were neglected. Blast pressures and pulse separation times were determined theoretically as functions of time delay between explosions, ratio of weights of successively fired charges, and distance from the explosion site.

The completed series of experiments was designed to determine the main effects of time delay, charge weight ratio, and distance. Other factors, such as charge separation distance and firing sequence with respect to charge position were not investigated. The experiments were performed with a single fixed value of separation distance of about 0.8 ft.

In the previous work, it was found that:

- The results obtained agree quite well with properly scaled data from similar studies with widely different explosive weights, thus blast coalescence phenomena can be investigated quite adequately with scale model experiments.

- There is a strong directional effect on the coalescence of successive blast pulses from sequentially detonated charges due to the sequence in which the charges are fired.

- There is enhancement of coalescence along an observation line axial to the line of charge centers relative to a lateral observation line.

- The effects of initial charge separation and explosion time delay, and the interactions of these effects, are strong functions of the angle that the observation line makes with the axis of the charges. Based on blast measurements in axial and lateral directions only, there was a wide possible variation of the locus of coalescence for two equal charges at a given time delay, and hence a wide variation of safe distance, as a function orientation.

1.2 Present Investigation

As a result of the conclusions and inadequate coverage of all the control parameters of the previous work on sequential explosions this current program was undertaken.

In this program a total of 60 experiments were planned, each using two equal 1 lb charges (1:1 charge weight ratio). These 60 experiments represent a full factorial experimental plan for the following set of control variable values.

Time delay, milliseconds: 2.2, 2.9, 3.6, 4.3, 5.0
Orientation, degrees: (9,90), (18,72), (36,54)
Spacing, inches: 10, 20, 40, 80

The results of these experiments allow one to map contours of the blast field (i.e., pressure isobars, and peak impulse and shock wave coalescence contours) around 180 deg of the charges.

This report is divided into three major sections. Chapter 2, describes details of the field experiments. Chapter 3, presents an overall view of the results obtained and Chapter 4 presents some conclusions and recommendations based upon these results. All of the experimental data obtained in this program are illustrated in Appendix A in such a manner as to be useful to those seeking answers to specific problems. Appendix B gives details of the test instrumentation used in the experimental program.

2. EXPERIMENTS

The series of 60 experiments was designed to investigate effects of detonation time delay, charge separation, and orientation between two sequentially detonated charges. Pressure-time and impulse-time histories were recorded at 12 specific locations for each test so that peak pressures, peak impulse, and shock wave separation time and coalescence could be determined for the range of parameter variations tested.

2.1 Test Arrangement

A schematic diagram of the physical arrangement of the test setup is shown as Figure 1. The area consists of two 75-ft-long by 10-ft-wide concrete slabs located at right angles to one another. Pressure transducers were installed flush with the top surface of the concrete slabs in mechanically isolated steel plates. The steel plates cover a channel in which gage leads are laid. Further isolation of the gages occurs because the pressure transducers are installed in mylar mounting plugs. Pressure gages were located on both concrete slabs at the same relative distances with respect to the center.

The center area of the test setup, at the common ends of the concrete slab, is sand. The explosive charges were placed in this area. Before each test this area was leveled even with the two concrete slabs. Zero distance was measured at the intersection of the centerlines of the two concrete slabs. The charges were equally spaced from this point.

Each charge was taped to a 6 by 6 by 0.5 in. steel plate. The charges were always separated by a 1-in.-thick steel dividing wall. The wall was 6 in. high by 15 in. long. The dividing wall was located at the center of the charge area and was oriented normal to a centerline through the charges. The dividing wall had four legs that were driven into the sand to minimize its movement. The dividing wall was used to minimize the possibility of sympathetic detonation of the second charge. Figure 2 is an overall view of the test area. Figure 3 is preshot and postshot views of the detonation area.

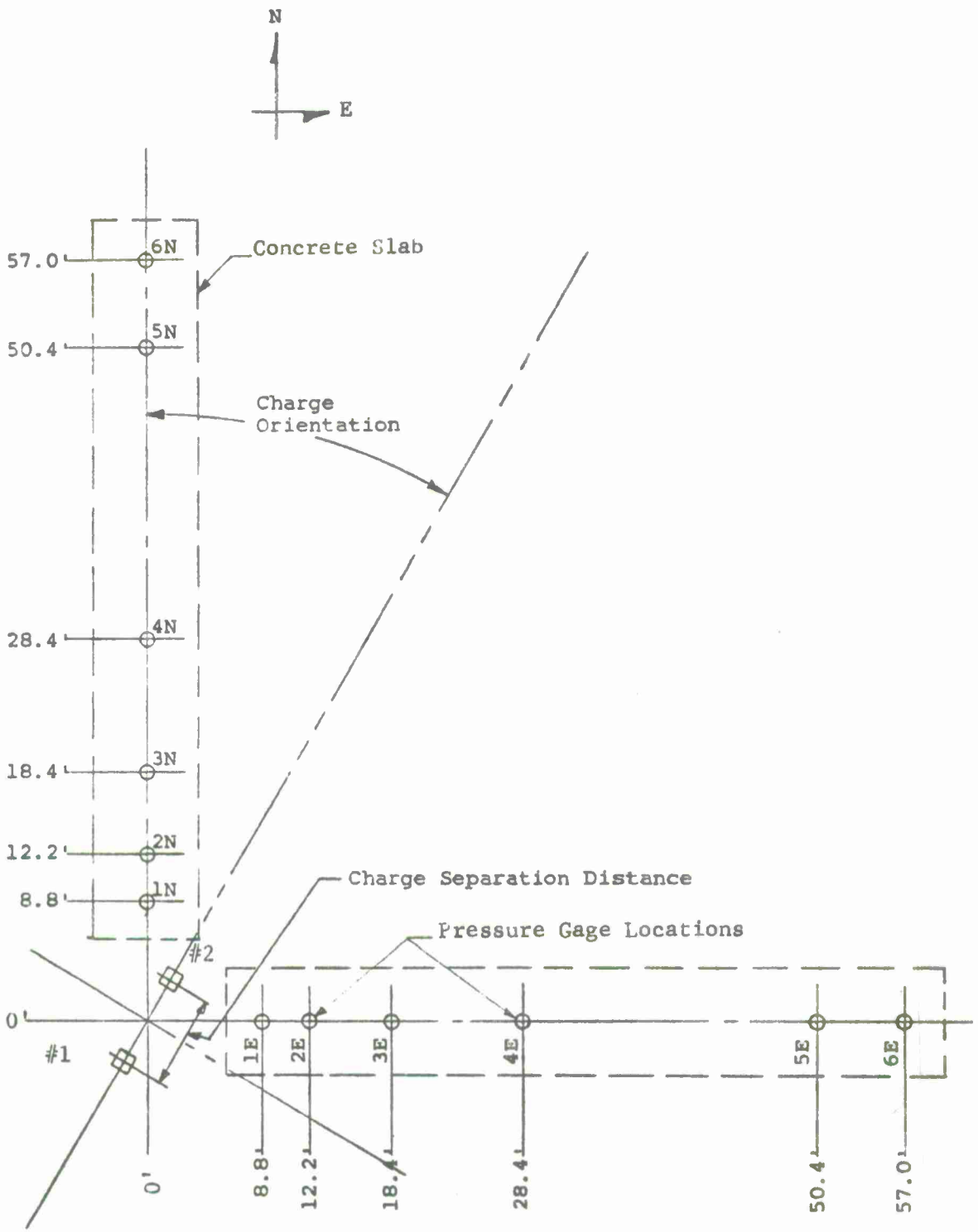

Figure 1 Sequential Explosion Test Setup

Figure 2 Overall View of Test Area

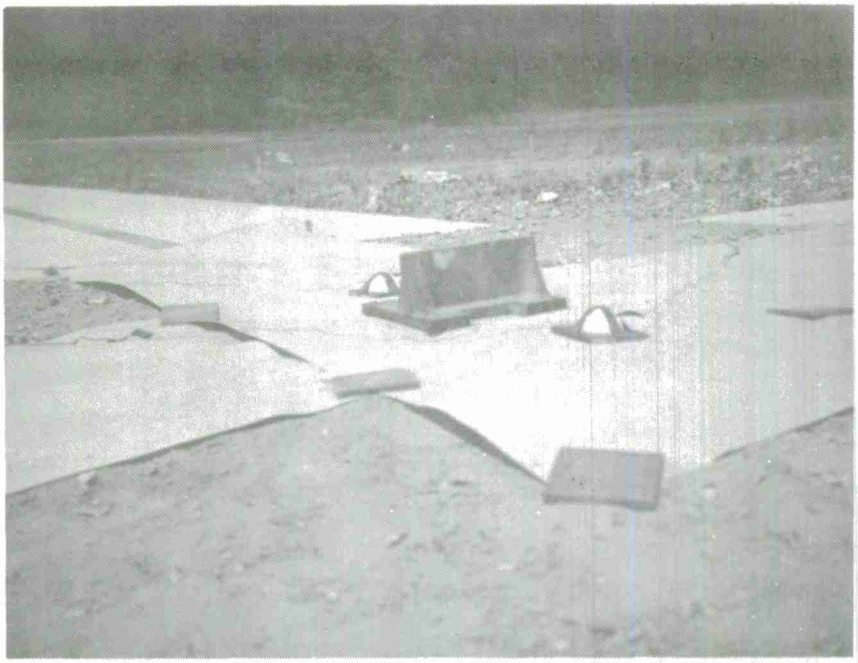

a. Preshot Photo

b. Postshot Photo

Figure 3 Detonation Area

2.2 Explosive Charges

Two hemispherical charges of C-4 plastic explosive (91 percent RDX and 9 percent plasticizer) were used for all tests. These charges were formed by pressing a preweighed quantity of explosive into a specially fabricated mold. Pressing is done by remote control. The 1 lb charges are approximately 4 in. in diameter and are initiated with fast-functioning 106B National Northern Detonators using 0.25 by 0.25 in. cylindrical tetryl pellets as boosters.

The time delay between the first and second detonation was obtained by using electronic waveform and pulse generators (Tektronix Type 162 and 161 respectively), to trigger a thyratron-controlled 4 mfd 330 volt firing circuit to energize the second detonator at the preselected time delay.

The explosive C-4 is about 25 percent more energetic per unit weight than TNT, since its heat of detonation is 1.37 kcal/g compared with 1.10 kcal/g for TNT. All the scaled quantities in this report are based on the TNT equivalent of a 2-lb C-4 charge (i.e., 2-lb C-4 is equivalent to 2.50 lb TNT). The scaling quantity $(2.50)^{1/3}$ becomes 1.357.

2.3 Experimental Procedures and Test Schedule

In order to preserve uniformity between these tests, and have them compatible with those previously conducted, a strict preshot experimental procedure was followed.

First the detonation area was cleared of debris and leveled. The concrete slabs were also swept and the face of each gage was examined for possible debris damage from the previous test. Brown wrapping paper, 4 ft wide, was spread over the detonation area. It was taped to the ends of the concrete slabs and weighted at the ends away from the slabs. This paper provided a means whereby one could accurately mark the center of the detonation area and charge locations.

Prior to the test sequence a surveyor's transit was used to locate stakes in the field to mark the charge orientation angles. When twine was stretched between the appropriate stakes it extended through the center of the detonation area, thereby enabling one to mark the orientation angle, separation distance, and hence charge locations on the brown paper.

After the charge locations and center of detonation were identified, the divider plate and two 1-lb C-4 charges were respectively set in place. The ionization probes and detonator leads were then connected to their respective instrumentation. Just prior to the actual detonation, a calibration pulse (known voltage) was recorded on the magnetic tape.

The test schedule for this program is included as Table 1. It consists of 60 shots to determine the effects of time delay between detonations, charge orientation, and separation distance. Time delays were varied between 2.2 msec to 5.0 msec in 0.7 msec increments. Charge orientations were varied between 0 and 90 deg in 18 deg increments. The charge separation distances tested were 10, 20, 40 and 80 in.

All of the tests, with the exception of S1 and S2 were conducted with two 1-lb hemispherical charges located as indicated by the test schedule and Figure 1. The charge furthest away from the concrete slabs (charge number 1, Figure 1) was always detonated first. After the appropriate time delay, the second charge (charge number 2, Figure 1) was detonated.

Test S1 and S2 were special shots taken to obtain pre- and postscheduled test calibration data. They consisted of detonating a 2 lb spherical C-4 charge in the center of the detonation area. Since gage placement was identical on both gage lines equal pressure measurements at respective stations is a good indication of recording accuracy. Test S1 was shot at the start of the scheduled test series and S2 was shot at the end of the test series. A good comparison between these two tests is an indication of the accuracy and consistency of the measuring system.

Table 1

TEST SCHEDULE

Test Number	Time Delay (msec)	Charge Orientation (deg)	Charge Separation Distance (in.)
1	2.2	0,90	10
2	2.2	0,90	20
3	2.2	0,90	40
4	2.2	0,90	80
5-8	2.9	same as above series	
9-12	3.6	same as above series	
13-16	4.3	same as above series	
17-20	5.0	same as above series	
21	2.2	18,72	10
22	2.2	18,72	20
23	2.2	18,72	40
24	2.2	18,72	80
25-28	2.9	same as above series	
29-32	3.6	same as above series	
33-36	4.3	same as above series	
37-40	5.0	same as above series	
41	2.2	36,54	10
42	2.2	36.54	20
43	2.2	36,54	40
44	2.2	36,54	80
45-48	2.9	same as above series	
49-52	3.6	same as above series	
53-56	4.3	same as above series	
57-60	5.0	same as above series	
S1	0	—	0
S2	0	—	0

Shots 1 through 60 conducted with 1:1 charge weight ratio, i.e., two 1-lb charges.

Shots S1 and S2 conducted with one 2-lb charge located at center of detonation area.

3. EXPERIMENTAL RESULTS

Typical results are presented in the figures that are presented in this chapter. An infinite number of pressure isobars and coalescence contours could be plotted for the range of parameters tested, however, only a few are presented for discussion purposes.

3.1 Reference Tests

Two reference tests, S1 and S2, were performed for use as a standard when making pressure and impulse comparisons with the sequentially detonated charges. The reference tests consisted of detonating one 2-lb charge at ground zero. Pressure and total impulse were measured on both blast lines. Results of these tests are shown on Figure 4.

Test S1 was shot at the beginning of the program and S2 was shot at the end. Results indicate good agreement between pretest and posttest measurement capabilities, and also agree with other published free field data. Impulse and distance in Figure 4 are scaled by the TNT equivalent of the charge weight.

3.2 Shock Wave Coalescence

The detonation delay time required to obtain shock wave coalescence at a given location can be determined from Figures 5 through 8. Note that when the two shock waves coalesce they remain coalesced. These curves give the radial distance at which coalescence begins for a particular detonation delay time. These curves were formulated by extrapolating the shock separation time versus distance plots in Appendix A to zero shock separation time. The dashed lines indicate regions in which experimental data were not obtained, however it was thought that reasonable extrapolations could be made with the assistance of the pressure versus delay time plots in Appendix A. Coalescence plots as a straight line on the latter curves, but further experiments would be required to confirm the validity of the extrapolations. Coalescence contours for four charge separation distances are illustrated in Figures 9 through 12. The contours represent the radial distances around the charges at which the shock waves will have just coalesced for a given detonation delay time. The parameter variation between the four plots is the charge separation distance. Note that the shock waves have coalesced in relatively short radial distances in the 0 deg orientation when the charges are far apart. The 0 deg orientation is directed along a line extended through the centers of both charges.

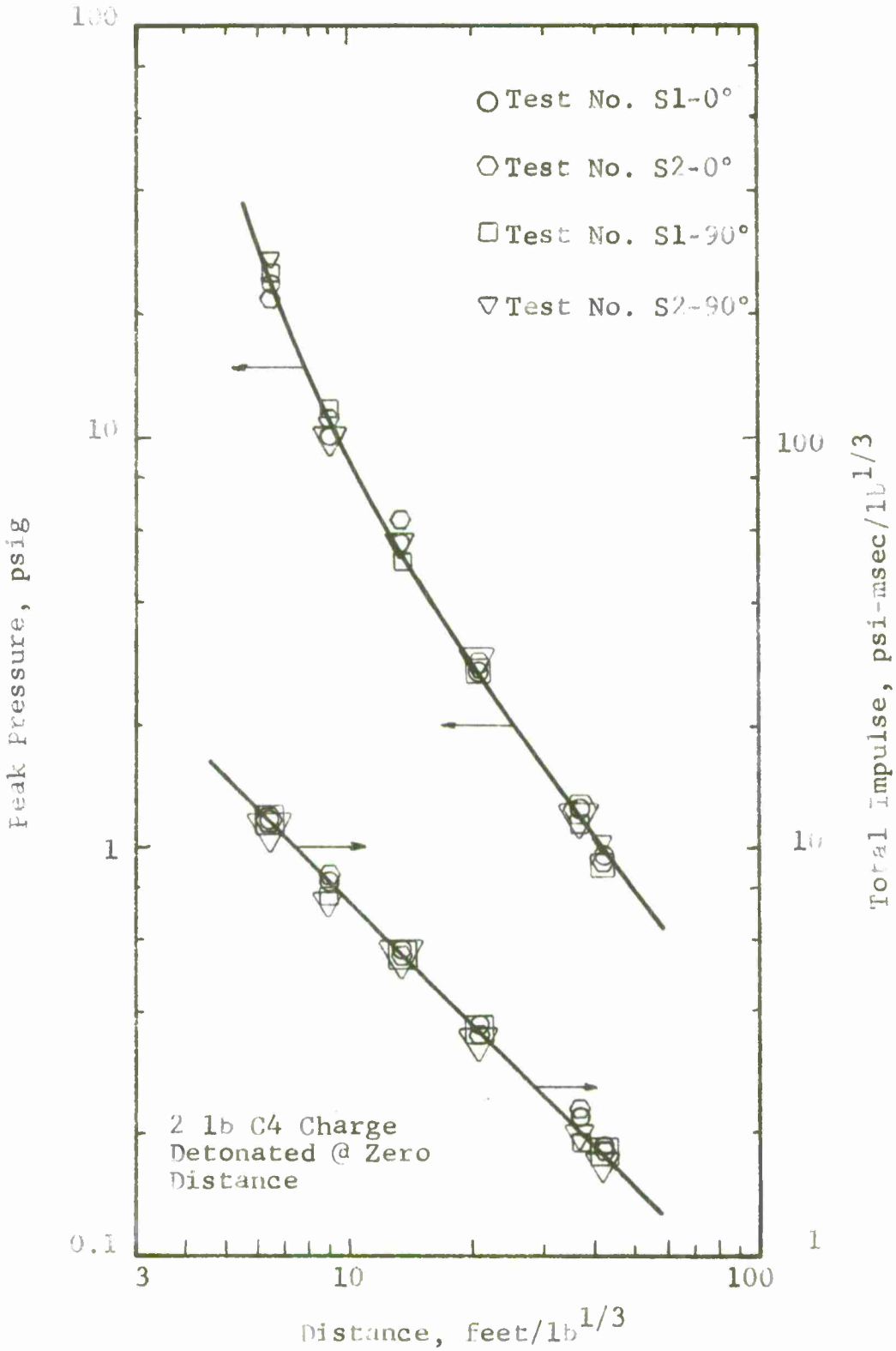

Figure 4 Pressure and Impulse for C-4 Explosive

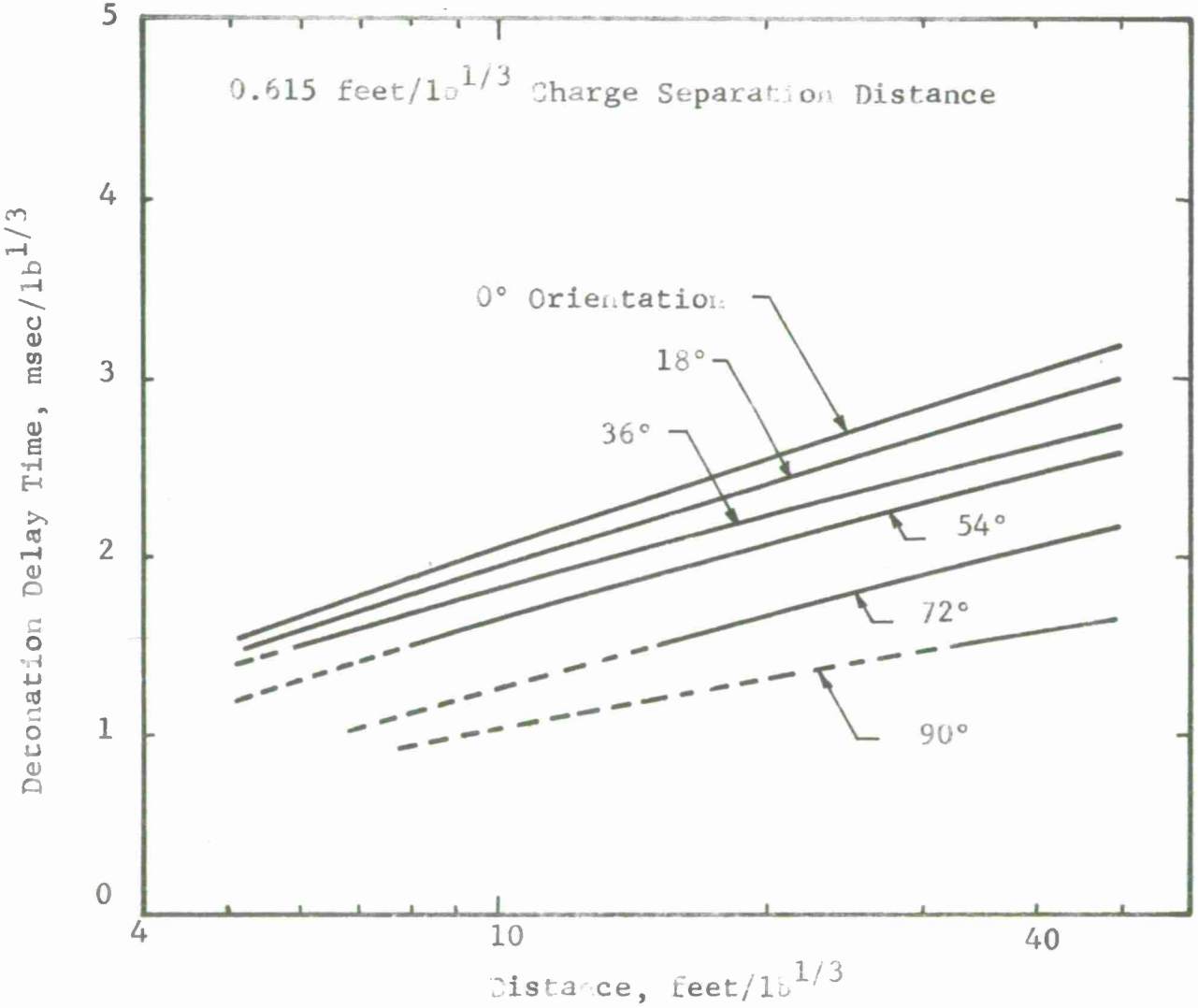

Figure 5 Delay Time for Coalescence (0.615 feet/lb$^{1/3}$)

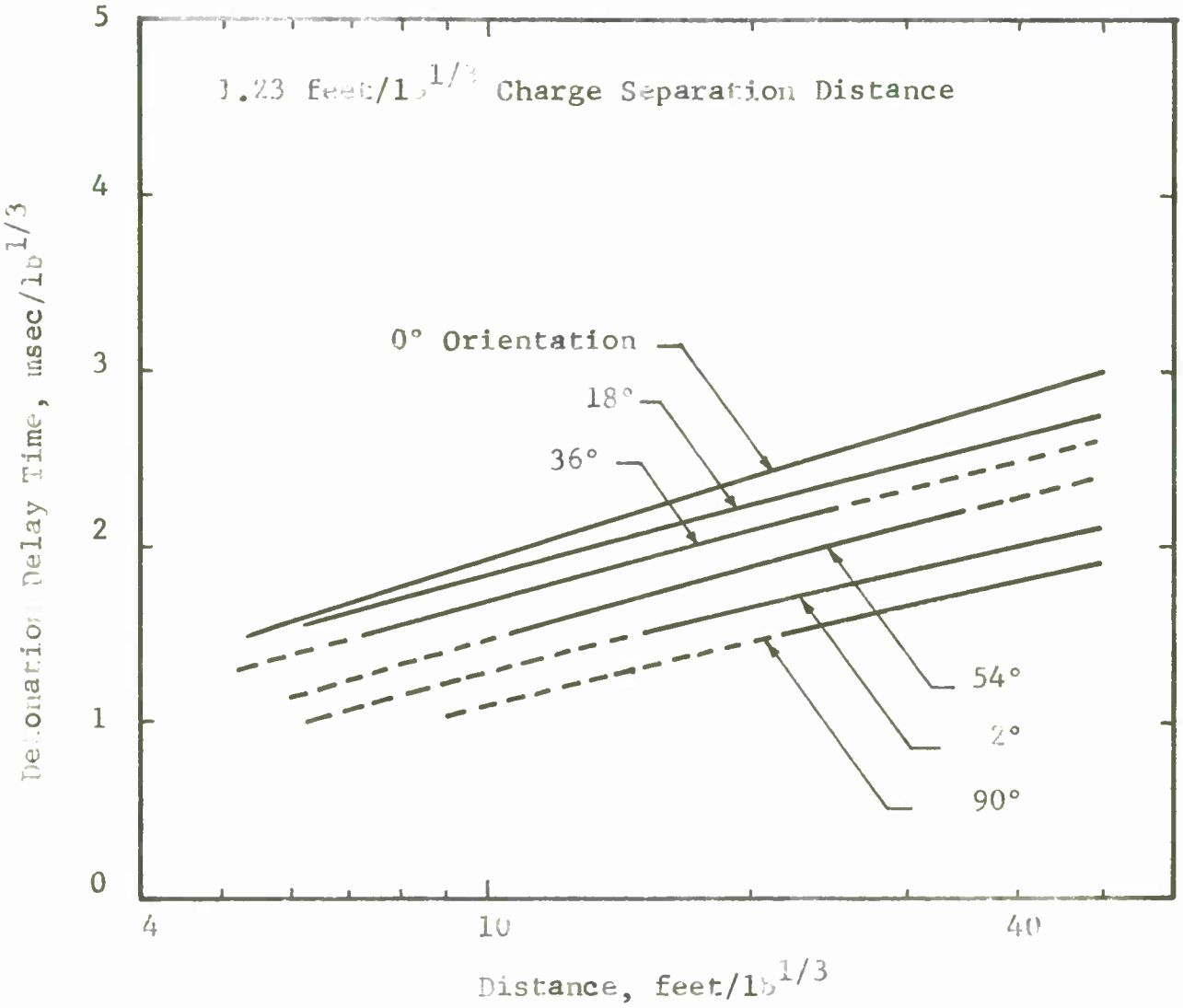

Figure 6 Delay Time for Coalescence (1.23 feet/lb$^{1/3}$)

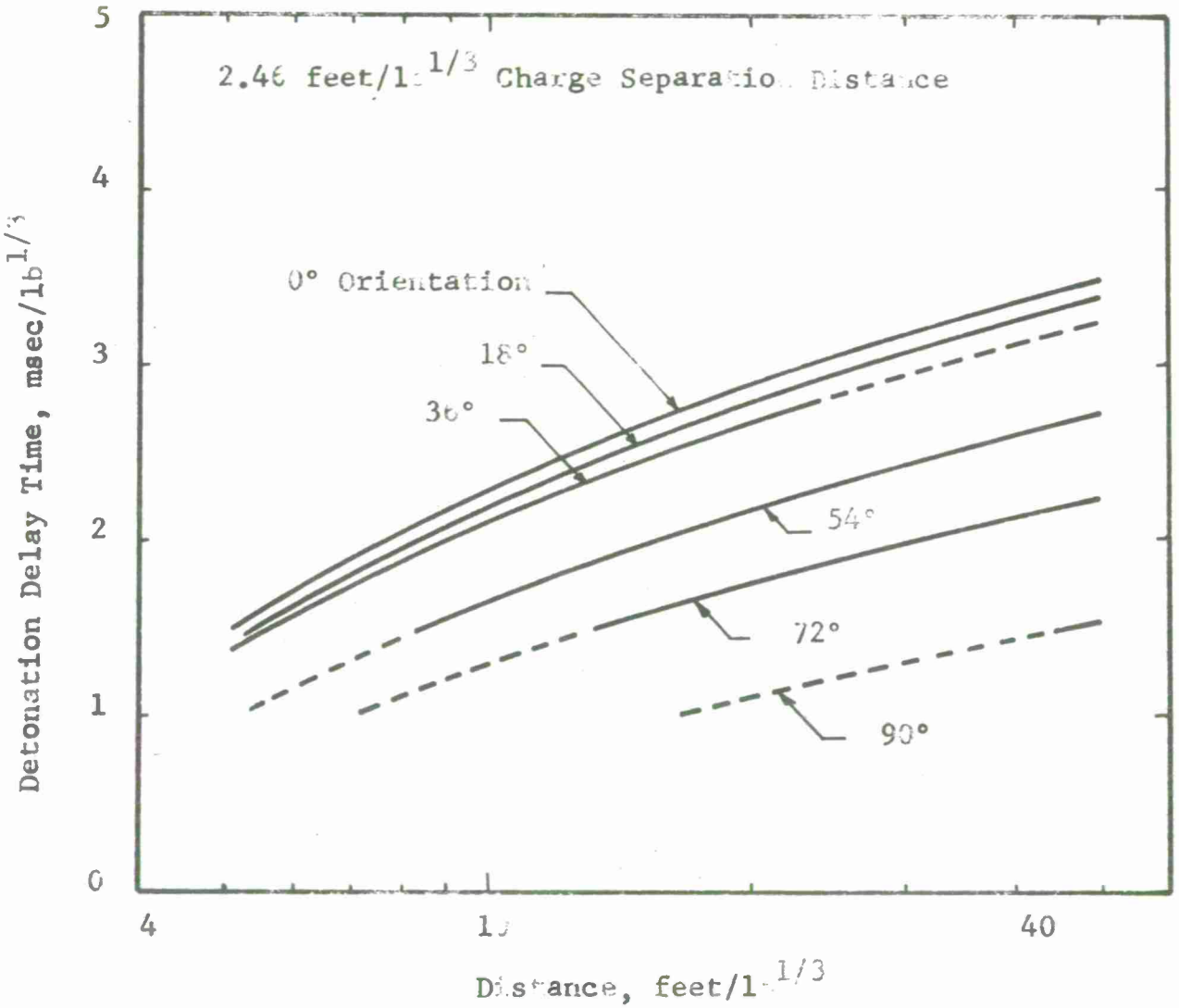

Figure 7 Delay Time for Coalescence (2.46 feet/lb$^{1/3}$)

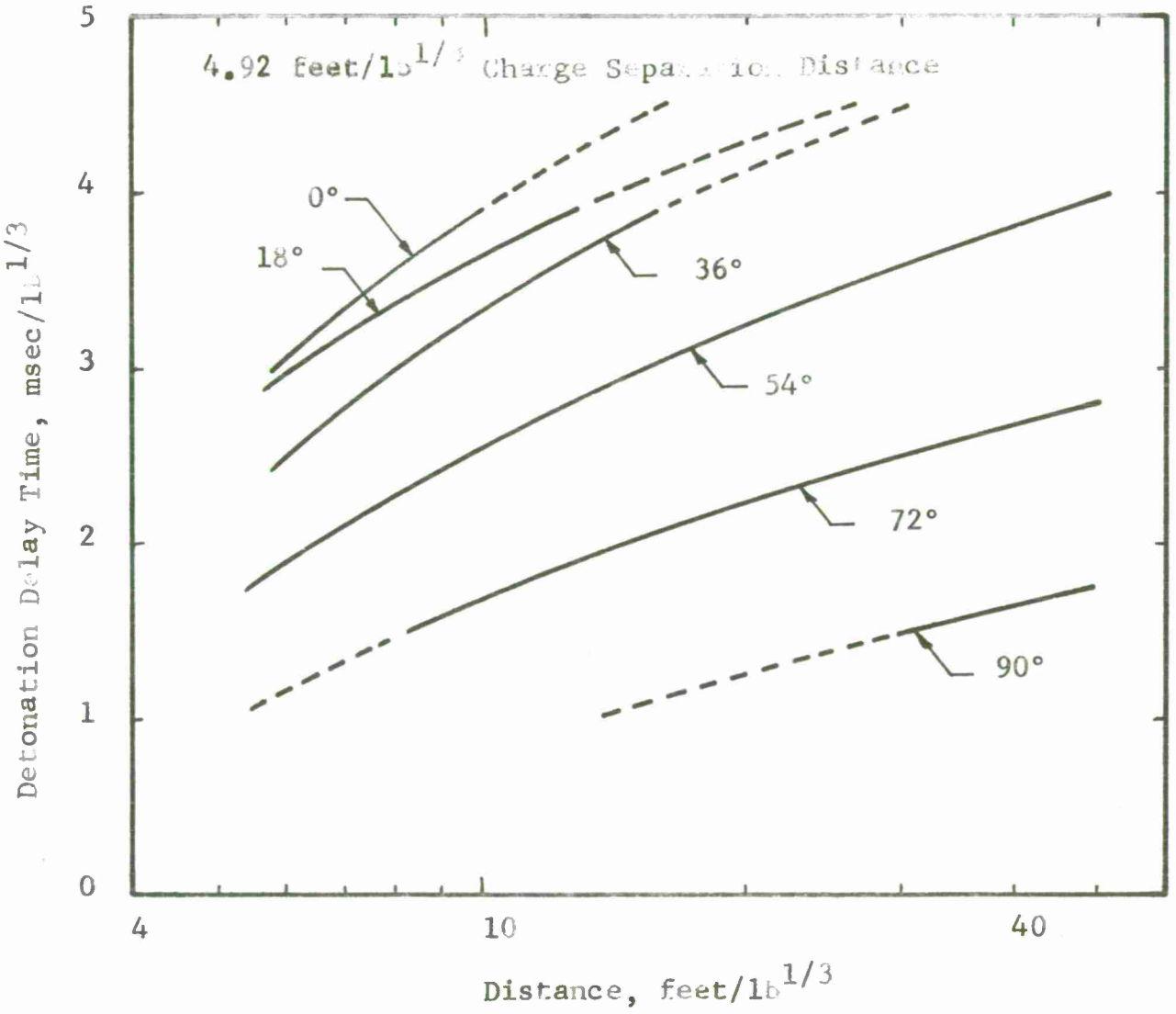

Figure 8 Delay Time for Coalescence (4.92 feet/$lb^{1/3}$)

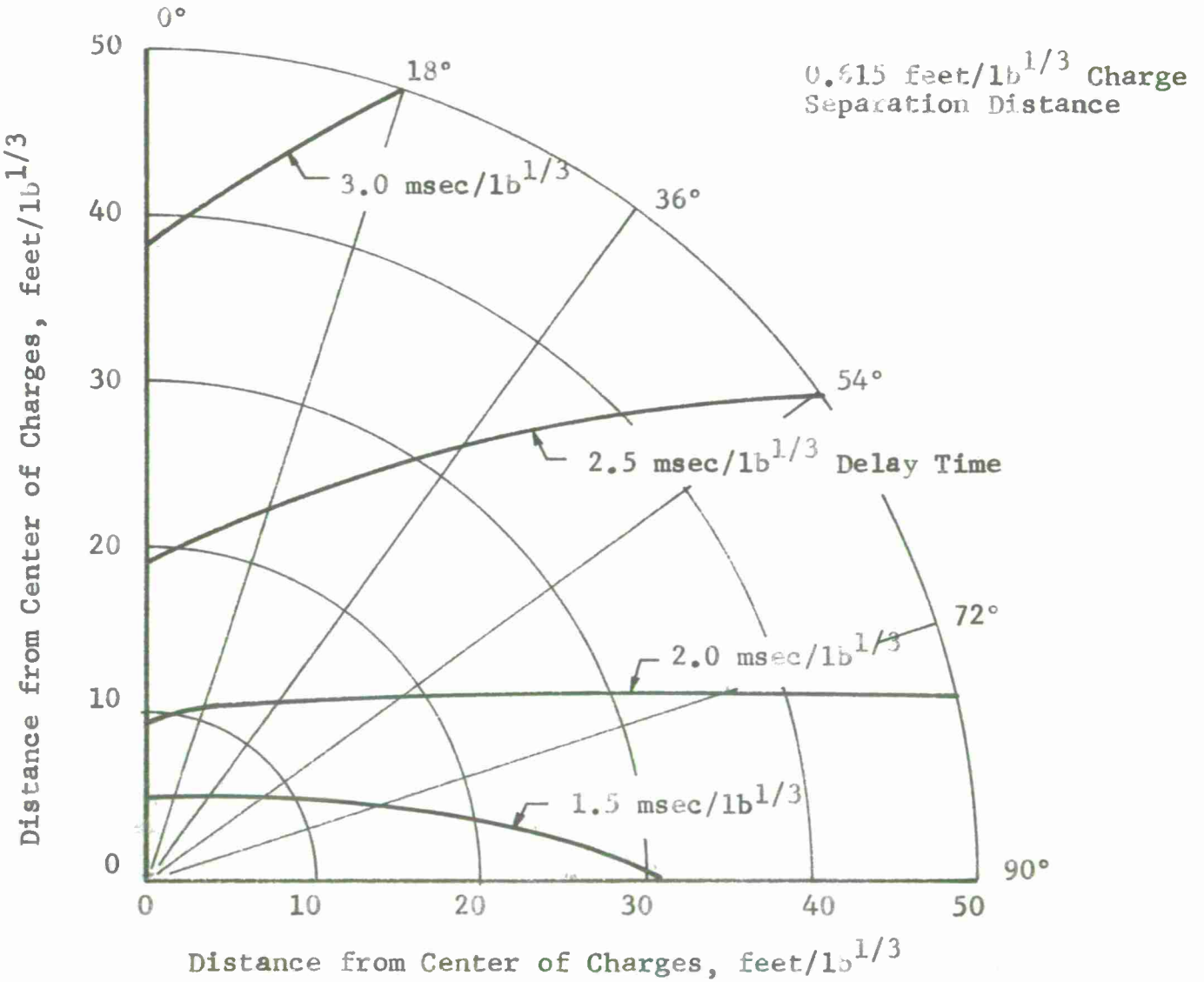

Figure 9 Coalescence-Distance Contours (0.615 feet/lb$^{1/3}$)

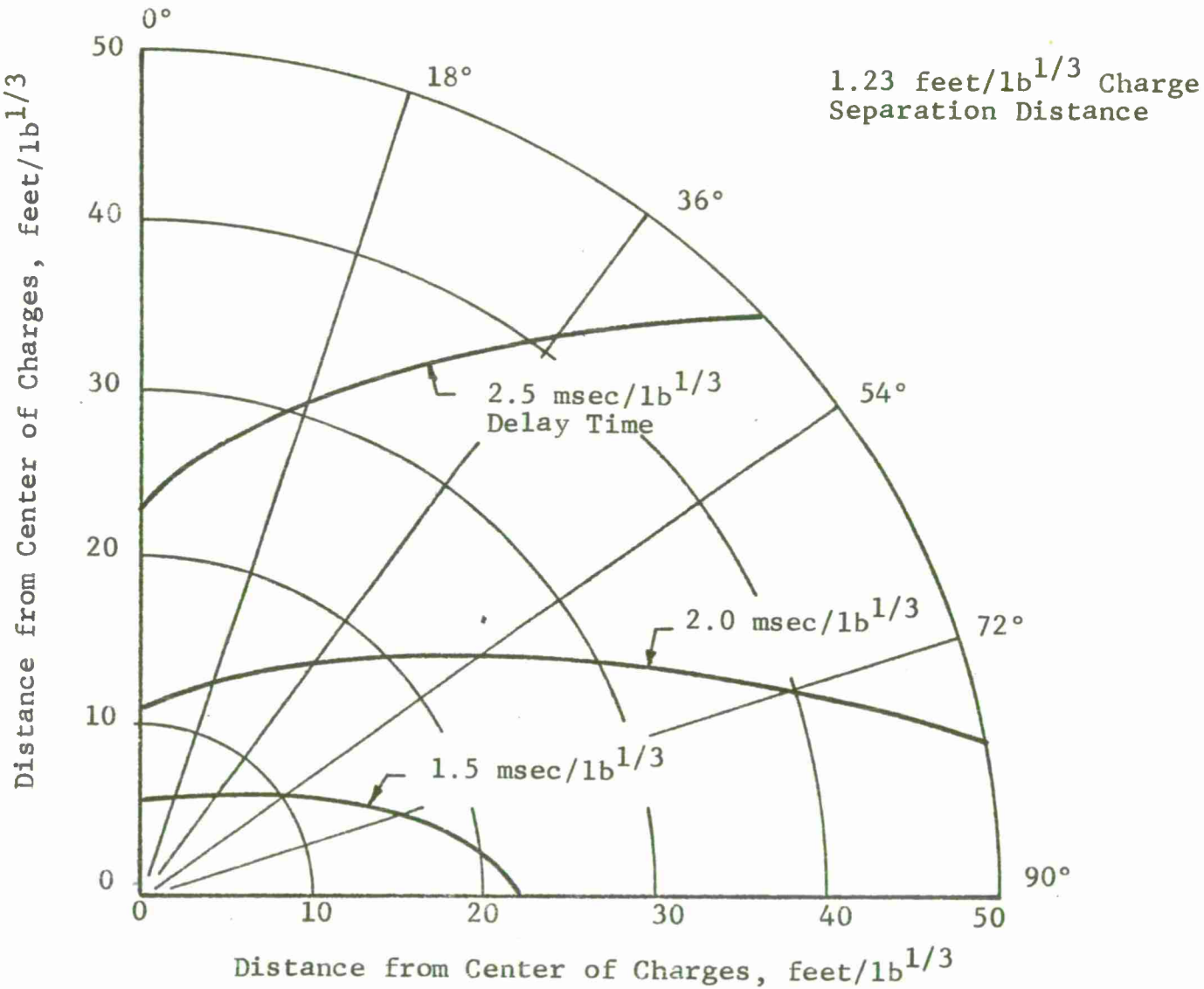

Figure 10 Coalescence-Distance Contours (1.23 feet/lb$^{1/3}$)

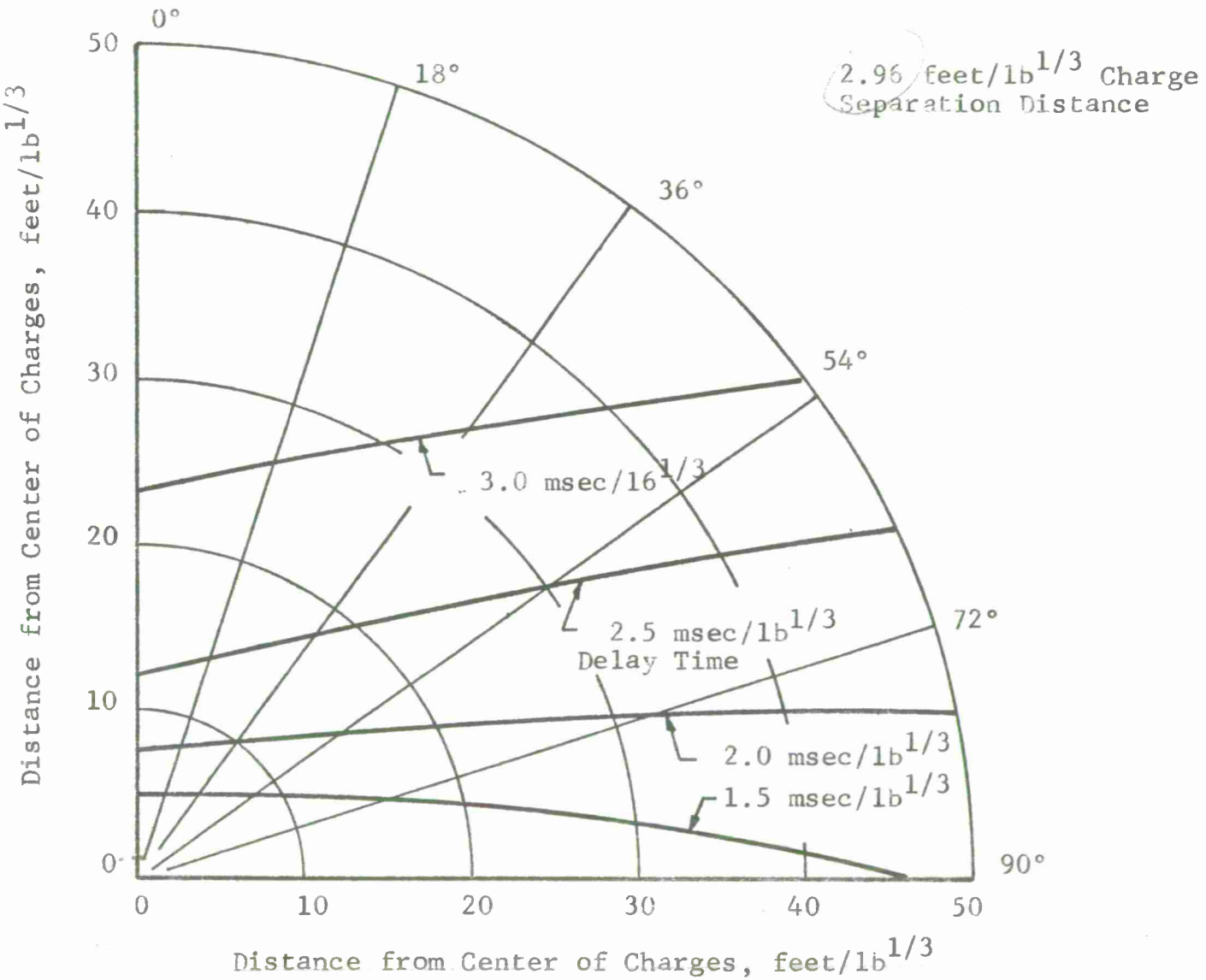

Figure 11 Coalescence-Distance Contours (2.46 feet/lb$^{1/3}$)

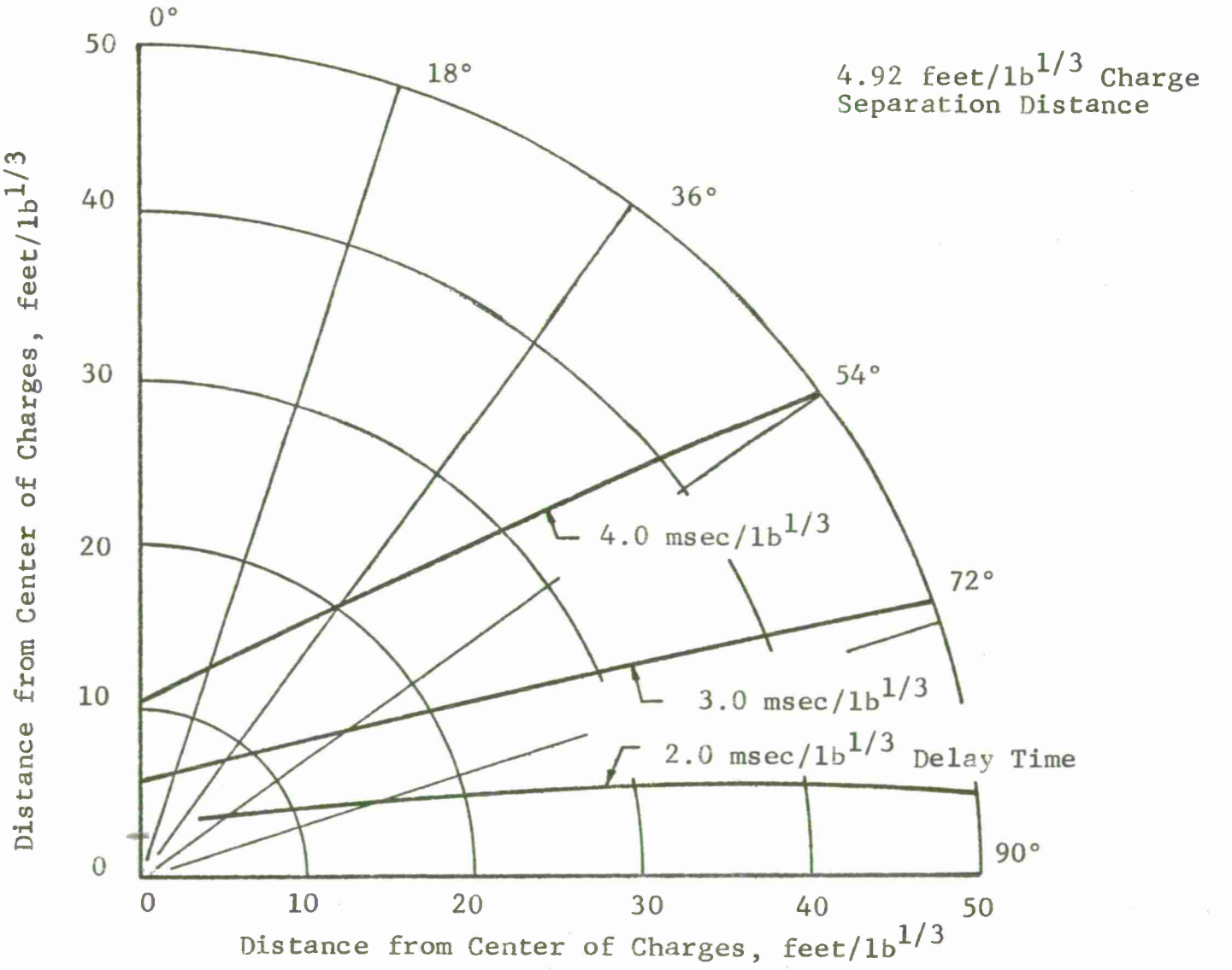

Figure 12 Coalescence-Distance Contours (4.92 feet/lb$^{1/3}$)

In the 0 deg orientation, coalescence occurs at shorter radial distances for large charge separation distances because the second charge is physically closer to the first shock wave when it is detonated, and hence has a shorter distance to travel for coalescence. Obviously if the detonation delay time is very long no coalescence would occur. In the 90 deg orientation, coalescence only occurs for short detonation delay times.

The effect of the barrier between the two charges is illustrated in Figure 13. Plotted thereon are curves of detonation delay time required to obtain coalescence at two radial distances, namely 10 and 42 feet/$lb^{1/3}$. The four curves for each radial distance represent the four charge separation distances. Note that for each radial distance the 0.615 feet/$lb^{1/3}$ charge separation distance curve lies above the 1.23 feet/$lb^{1/3}$ curve for small orientation angles. One would expect the reverse of this to occur. In these experiments the barrier wall or charge separation plate is slowing down the first shock wave such that the second shock is able to catch up sooner or at a shorter radial distance, for a given detonation delay time. As the charges are moved further apart, and consequently further from the barrier, the barrier becomes less significant. It should be noted that the linear dimensions of the barrier scale with the cube root of the charge weight, as do all other distances. Thus one would expect to observe this influence of the barrier for the same scaled charge separations in an experiment with larger explosive charges, provided the barrier dimensions are similarly scaled.

3.3 Pressure Isobars

Representative peak pressure isobar plots are illustrated in Figures 14 through 21. The solid lines are peak pressure isobars from charges detonated at the delay times and separation distances shown. Two different delay times and four charge separation distances have been graphically illustrated. The long dashed lines are peak pressure isobars from a single charge. Scaling is based upon the total quantity of explosive detonated in each case. Also shown on these figures are the regions where the shock waves have coalesced -- the short dashed line in each figure is the boundary between the region in which the shocks have coalesced and the region in which they have not.

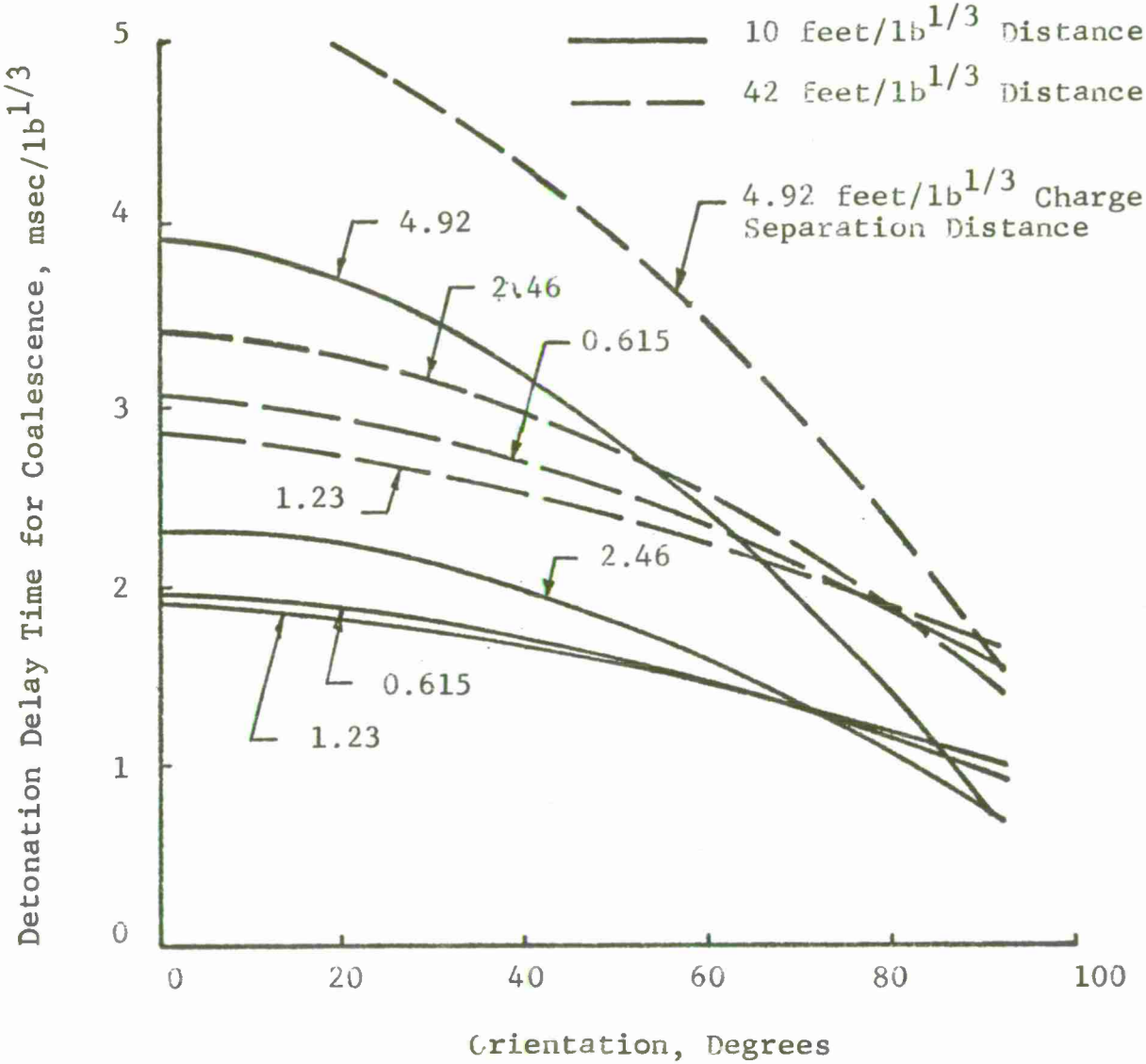

Figure 13 Effect of Barrier on Shock Coalescence

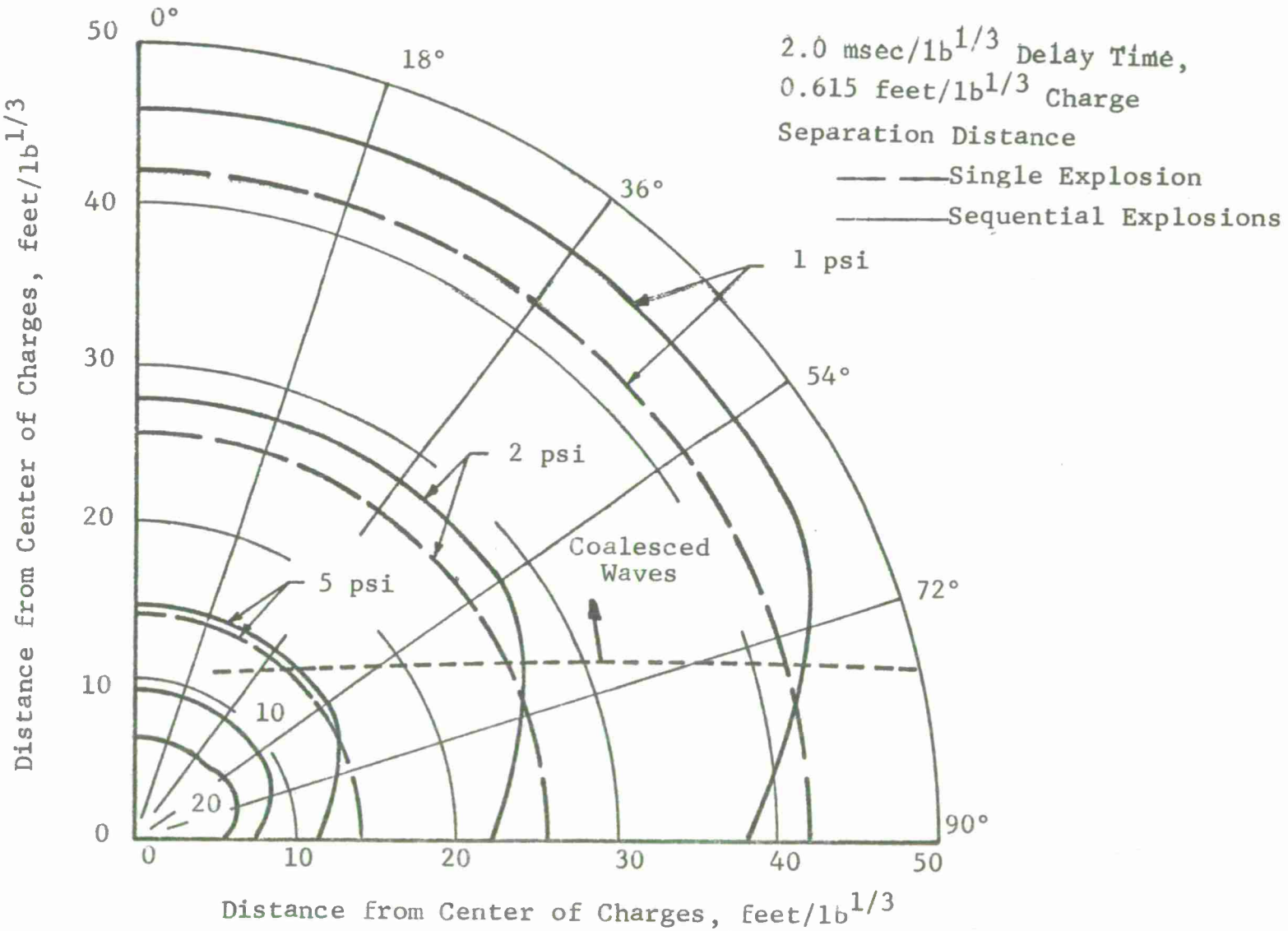

Figure 14 Peak Pressure Isobars (2.0 msec/lb$^{1/3}$, 0.615 feet/lb$^{1/3}$)

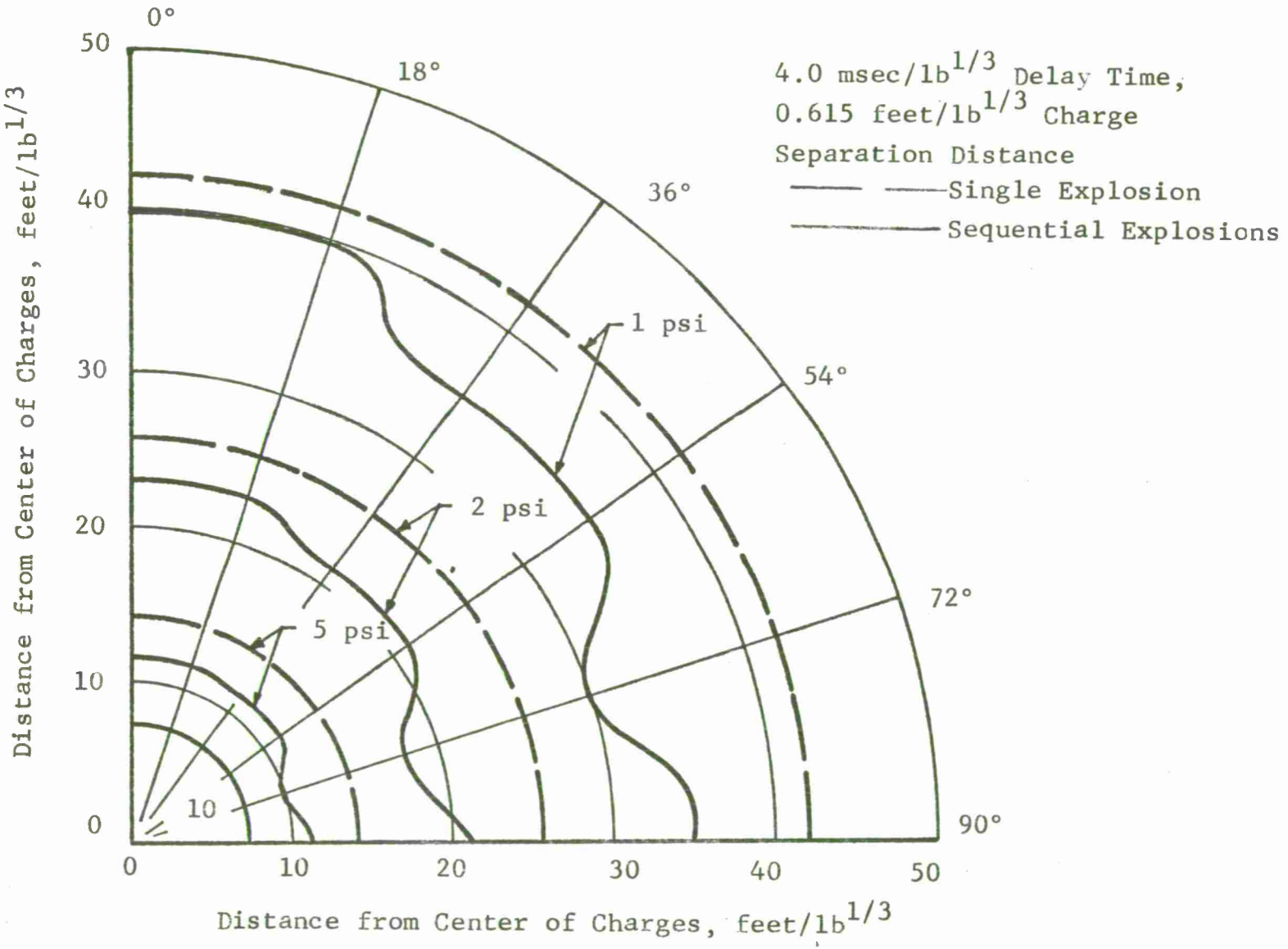

Figure 15 Peak Pressure Isobars (4.0 msec/$lb^{1/3}$, 0.615 feet/$lb^{1/3}$)

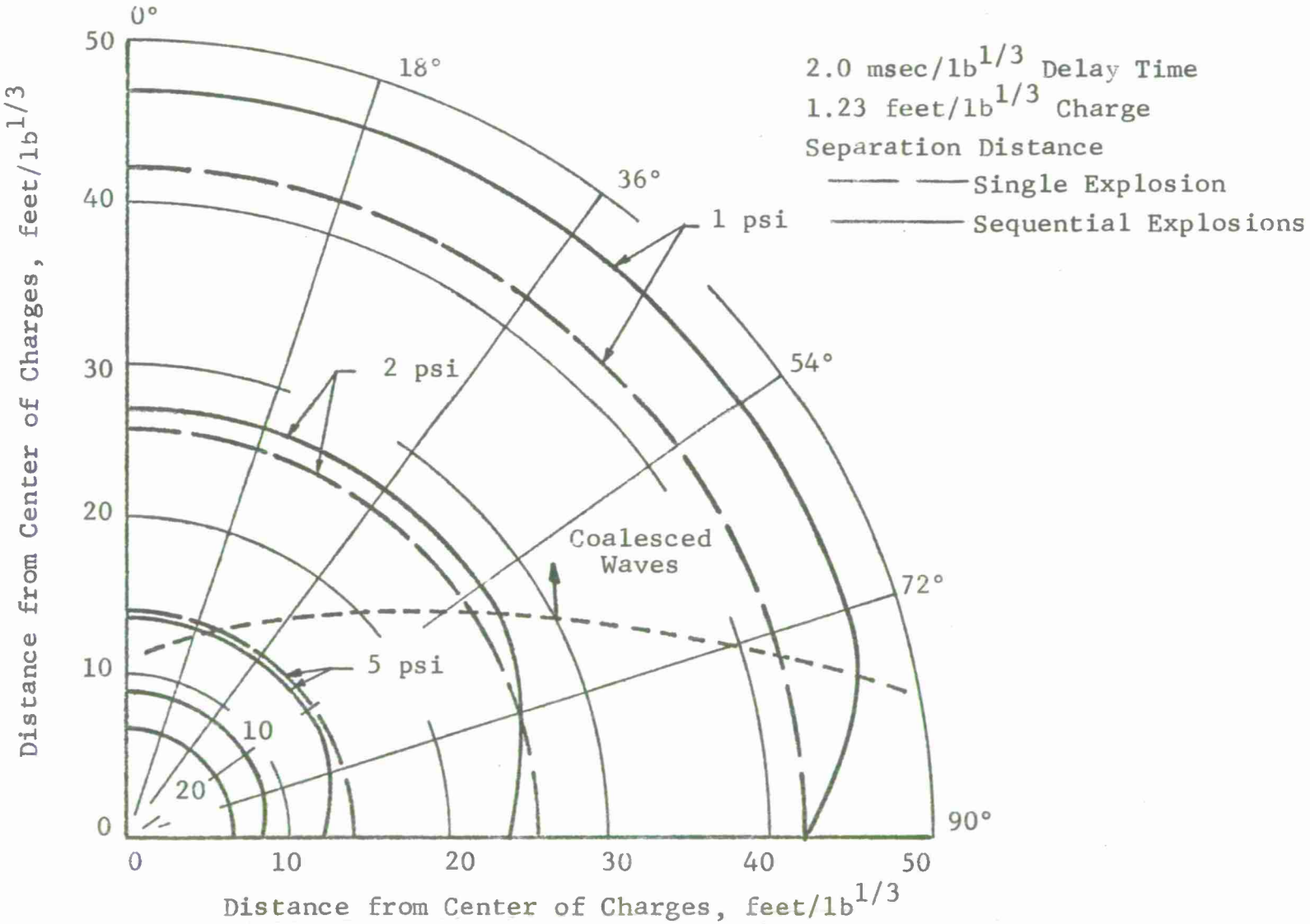

Figure 16 Peak Pressure Isobars (2.0 msec/lb$^{1/3}$, 1.23 feet/lb$^{1/3}$)

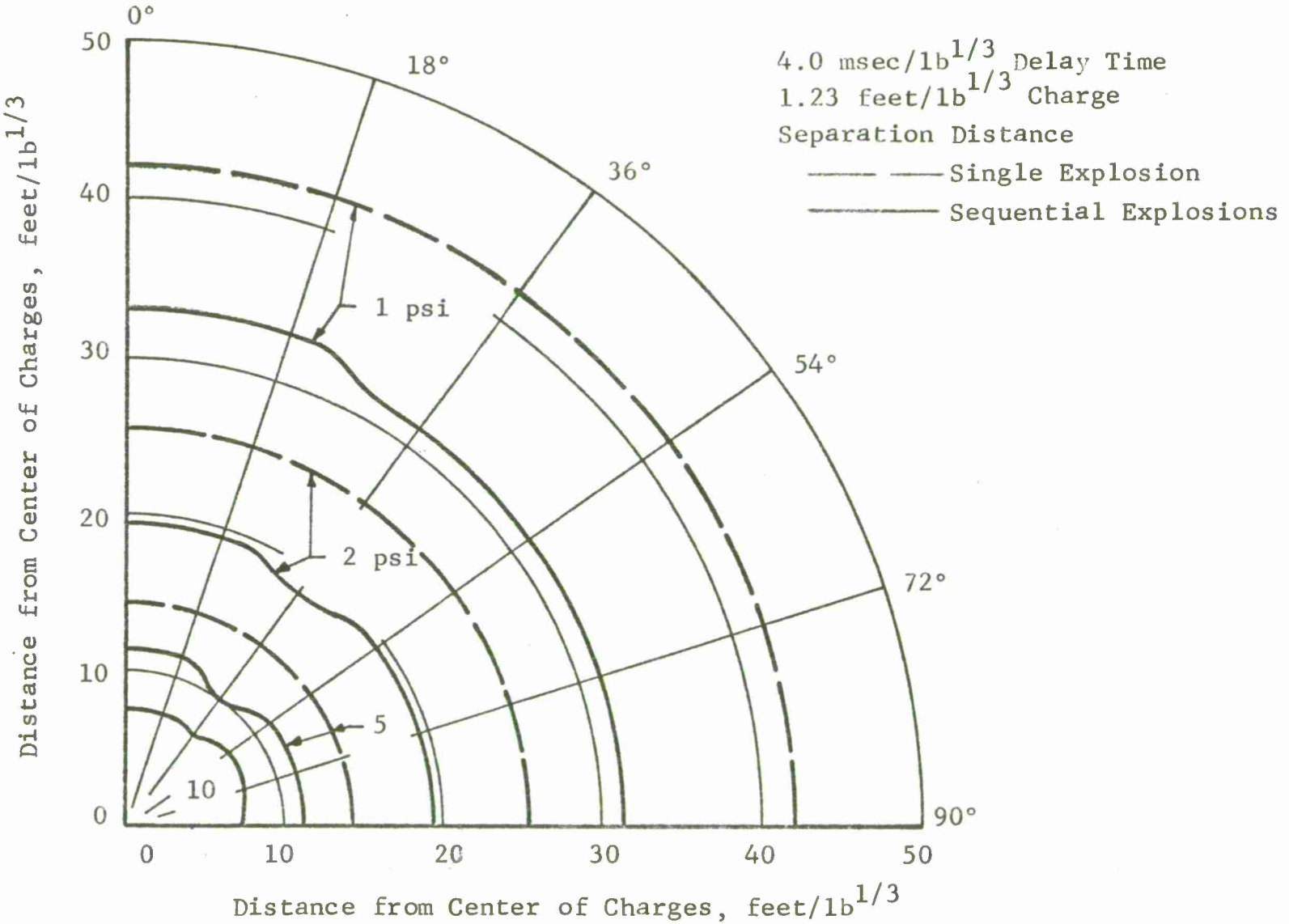

Figure 17 Peak Pressure Isobars (4.0 msec/lb$^{1/3}$, 1.23 feet/lb$^{1/3}$)

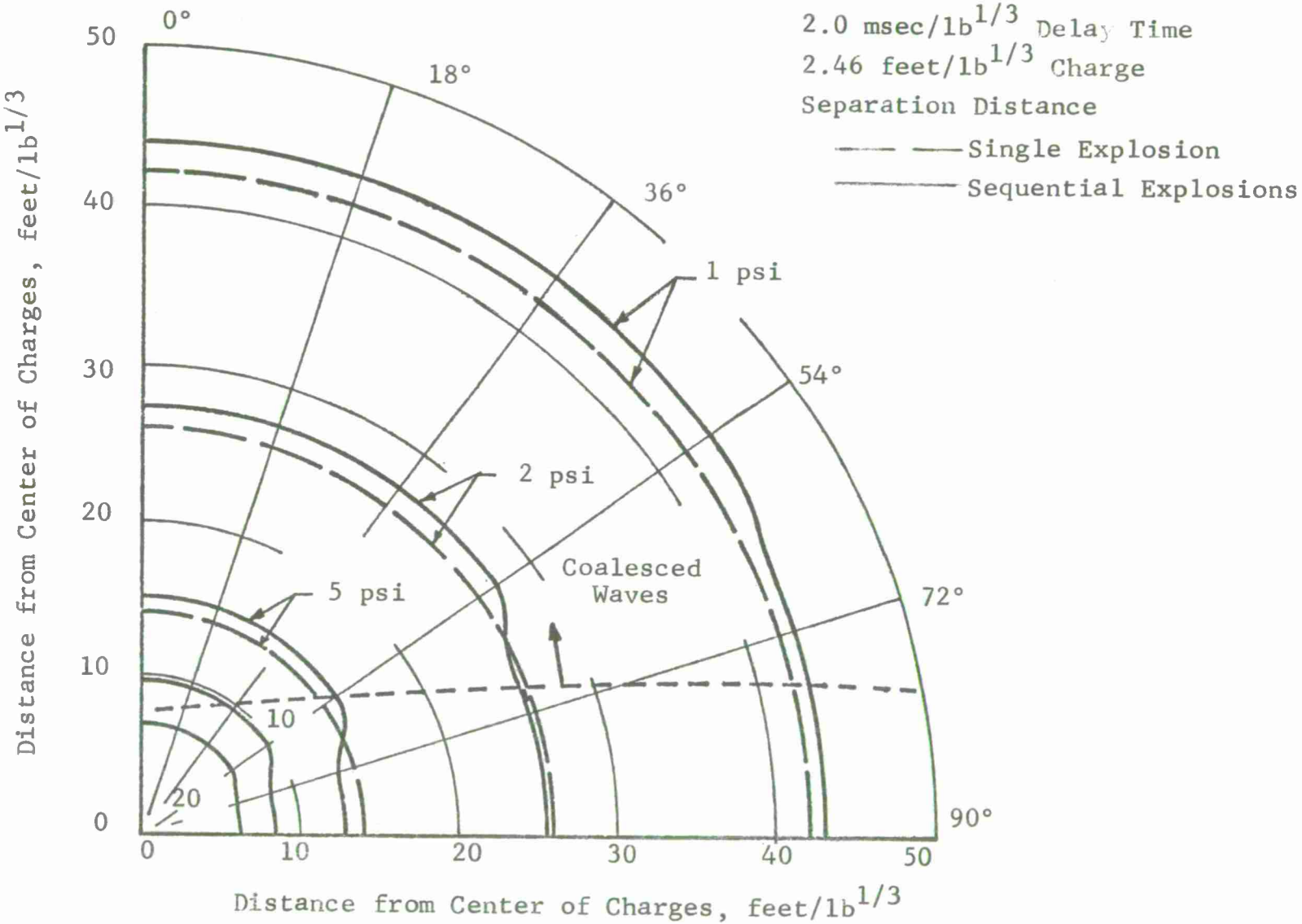

Figure 18 Peak Pressure Isobars (2.0 msec/lb$^{1/3}$, 2.46 feet/lb$^{1/3}$)

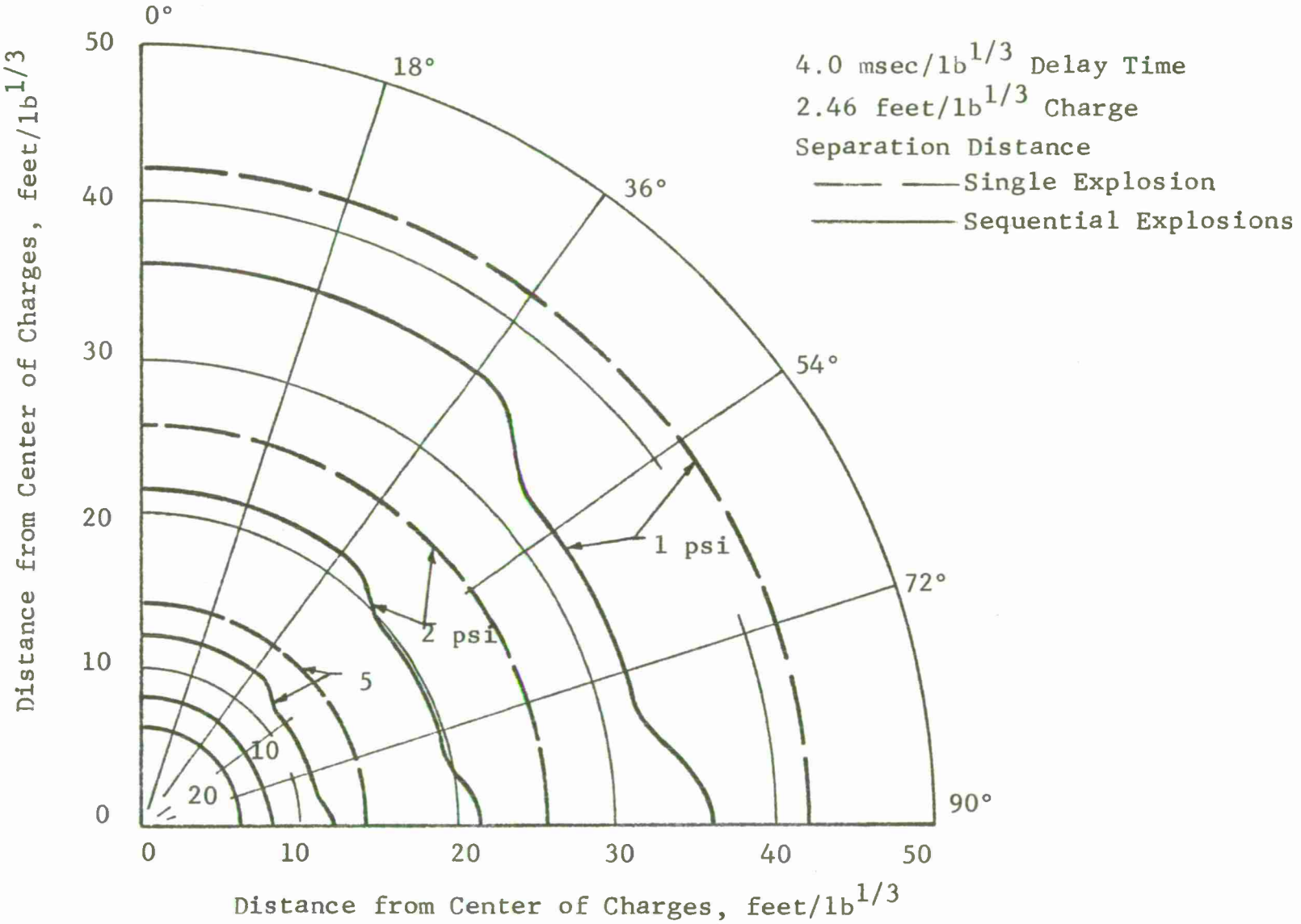

Figure 19 Peak Pressure Isobars (4.0 msec/lb$^{1/3}$, 2.46 feet/lb$^{1/3}$)

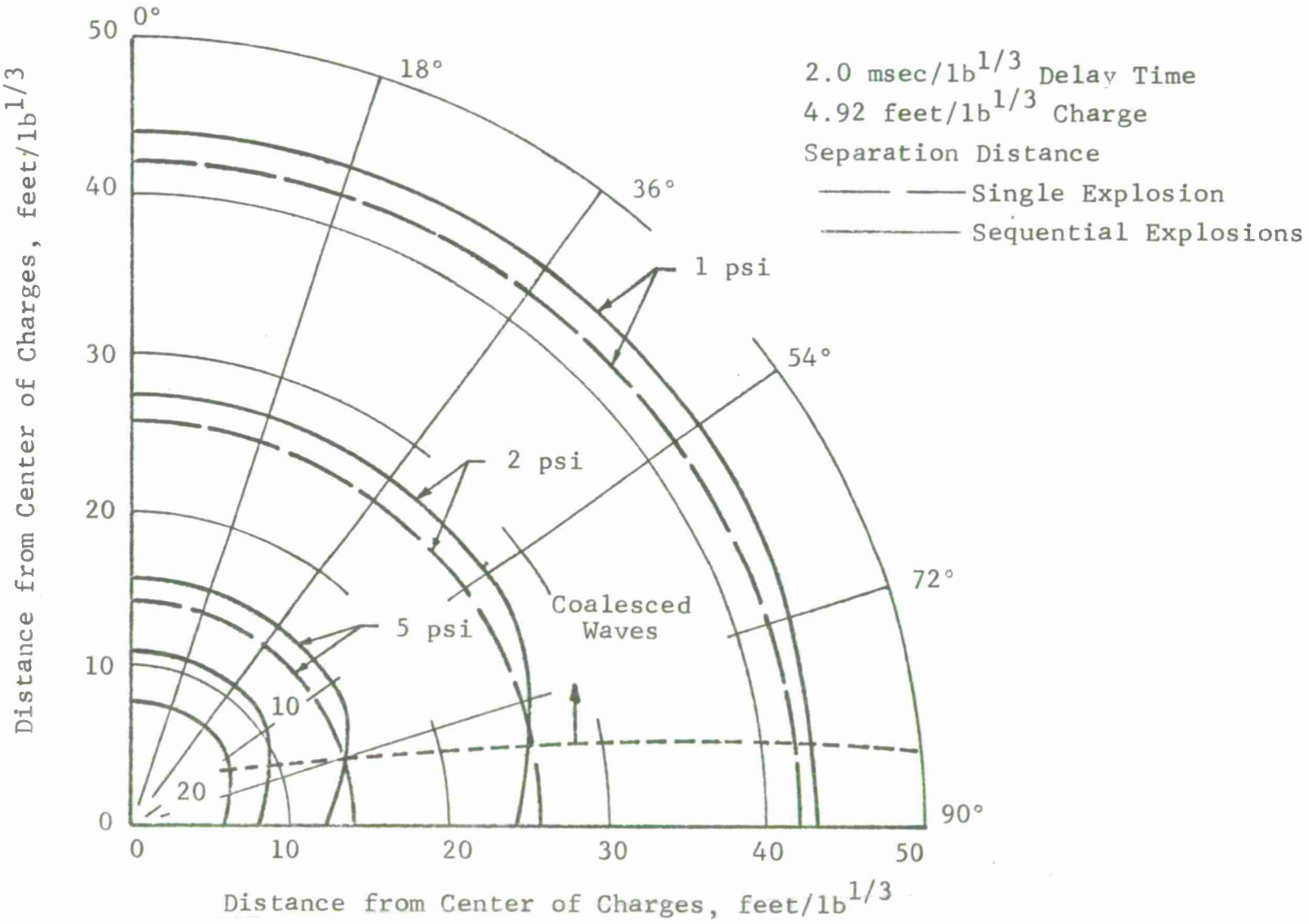

Figure 20 Peak Pressure Isobars (2.0 msec/lb$^{1/3}$, 4.92 feet/lb$^{1/3}$)

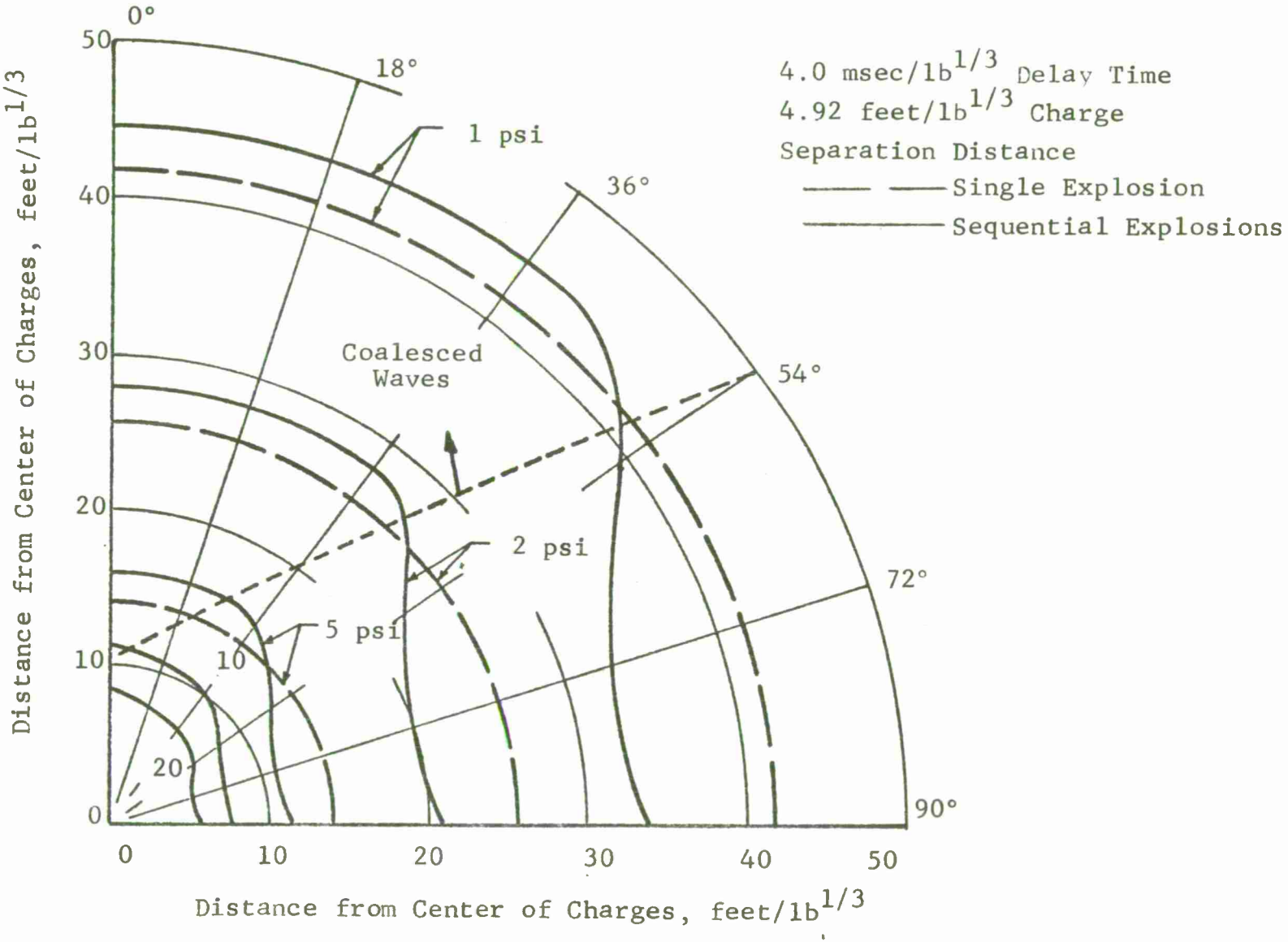

Figure 21 Peak Pressure Isobars (4.0 msec/lb$^{1/3}$, 4.92 feet/lb$^{1/3}$)

A cursory examination of these eight figures reveals many interesting phenomena. Peak pressure is strongly dependent upon orientation, detonation delay time, and charge separation distance. When the delay time is large the shock waves do not coalesce (Figures 15, 17, and 19) and the peak pressures are less than those observed from a single charge detonation at comparable radial distances. In those regions where coalescence has occured and the peak pressure at a given radial distance is higher from two charges sequentially detonated that it is from an equivalent single charge weight detonation.

3.4 Total Impulse

Total impulse appears to be insensitive to detonation delay time, charge separation distance, and orientation within the range of parameters tested. The impulse data obtained during these experiments have been plotted and are presented in Appendix A.

At a given radial distance from the detonation area the total impulse measured is the same for two sequential detonations and for an equivalent single point source detonation. It is recommended that constant radius contours be used when estimating damage criteria based on total impulse. However, it should be kept in mind that the pressure-time histories themselves are not independent of direction.

3.5 Illustrative Example

Assume two ships with high explosive cargos are to be docked at a pier. It is required that estimates be made of the potential damage to buildings in the surroudning area in case of an accidential explosion. Three cases are considered:

Case I - Cargo detonates on only one ship

Case II - Cargos on both ships detonate and damage estimates are based upon a point source explosion midway between the two ships

Case III - Cargo on one ship detonates and causes the second ship's cargo to detonate later as a result of fragment damage

Problem Parameters:

Cargo is 3.5×10^6 lbs TNT per ship

Ship separation distance is 950 ft

Delay time between detonations is 760 msec (i.e., based upon an average fragment velocity of 1250 fps, applicable only to Case III).

Regions where peak pressure is $\geq$ 6 psi, damage[2] is 100 percent

Regions where peak pressure is $\approx$ 3.5 psi, damage is 50 percent

Regions where peak pressure is $\approx$ 1 psi, damage is 20 percent

Problem Solution Case I:

Compute scale factor $(3.5 \times 10^6)^{1/3} = 1.52 \times 10^2 - \text{lb}^{1/3}$

Use scale factor and determine radial distances at which the pressures (percent damage) occur from Figure 4

6 psi - 12.5 feet/$\text{lb}^{1/3}$ - 1900 feet

3.5 psi - 17.5 feet/$\text{lb}^{1/3}$ - 2660 feet

1 psi - 42 feet/$\text{lb}^{1/3}$ - 6380 feet

Problem Solution Case II:

Compute scale factor $(2 \times 3.5 \times 10^6)^{1/3} = 1.91 \times 10^2 - \text{lb}^{1/3}$

Using this scale factor the radial distances become

6 psi - 2390 feet

3.5 psi - 3340 feet

1 psi - 8030 feet

---

[2] Damage in percent of building cost. C. Wilton, "Building Damage Surveys from Explosion Tests," Minutes, Twelfth ASESB Seminar, 267-286 (August 1970).

Problem Solution Case III:

The scale factor is the same as Case II; 1.91×10^2-lb$^{1/3}$

The scaled charge separation distance becomes

$$950/1.91 \times 10^2 \quad 4.92 \text{ feet/lb}^{1/3}$$

and the scaled time delay becomes

$$760/1.91 \times 10^2 \quad 4.0 \text{ msec/lb}^{1/3}$$

Plot peak pressure-distance curves (Figure 22) using applicable pressure-delay time curves from Appendix A. Peak pressure isobars, or in this case, percent damage contours can now be readily determined.

The results of these three cases are illustrated in Figure 23. The first case is highly improbable because the second ship is located in a very severe region, very high pressures, high velocity fragments, and thermal exposure. However if proper protection was afforded the second ship it would not detonate and the resulting blast damage from the first ship to the surrounding area, would be considerably lessened as shown. When damage estimates are made using point source criteria (Case II), they would be conservative in some regions and not in others. Along the shoreline, 90 deg orientation for this docking configuration, the actual damage contours are closer-in than the point source predictions. In the inland or 0 deg orientation the actual damage contours extend further out from the source. One can conclude from these examples that placement of the charges should be a consideration in explosive storage. For example, less damage to land facilities would be realized if the ships were docked parallel to the shoreline during an accidental detonation.

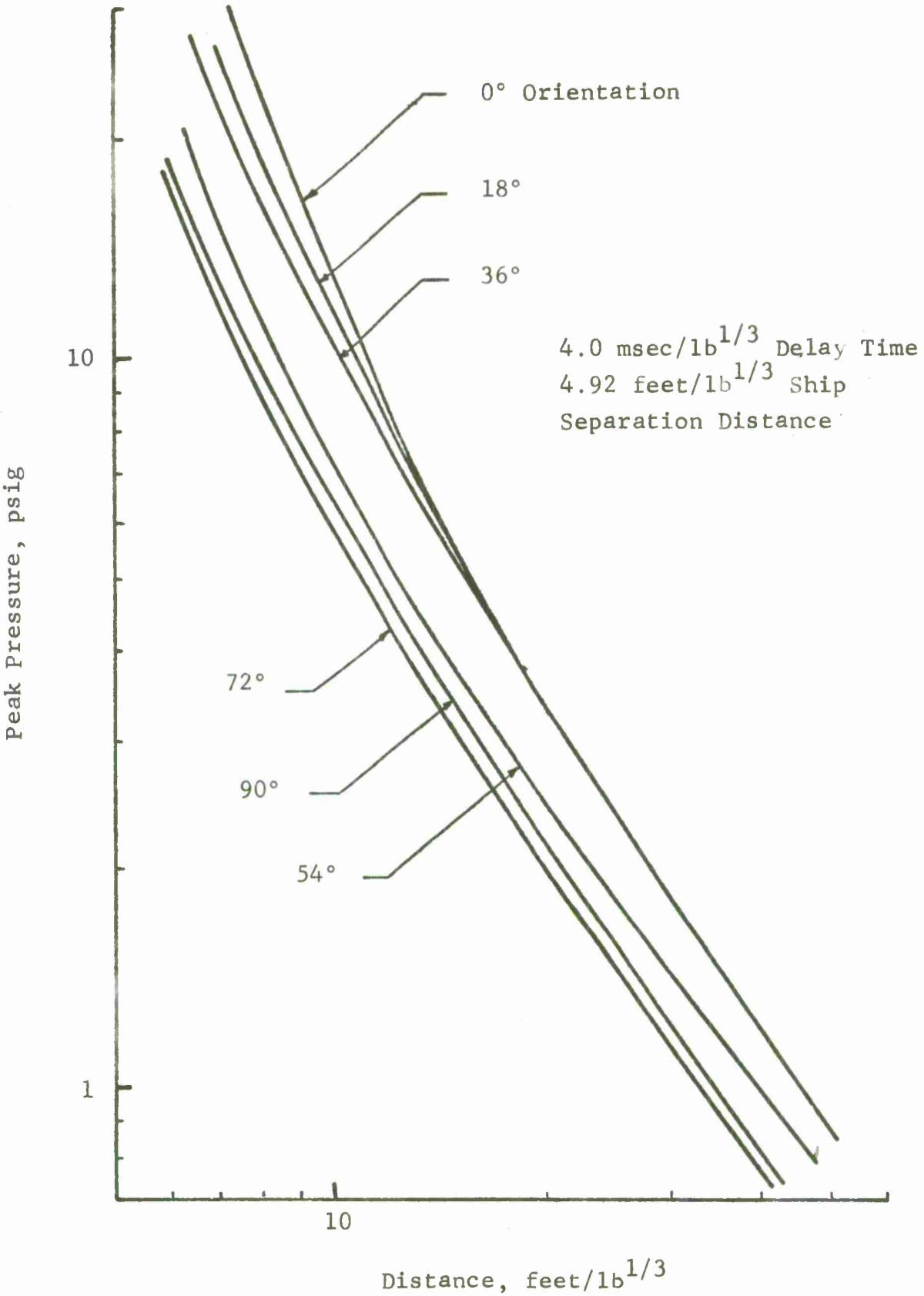

Figure 22 Pressure-Distance Example Problem

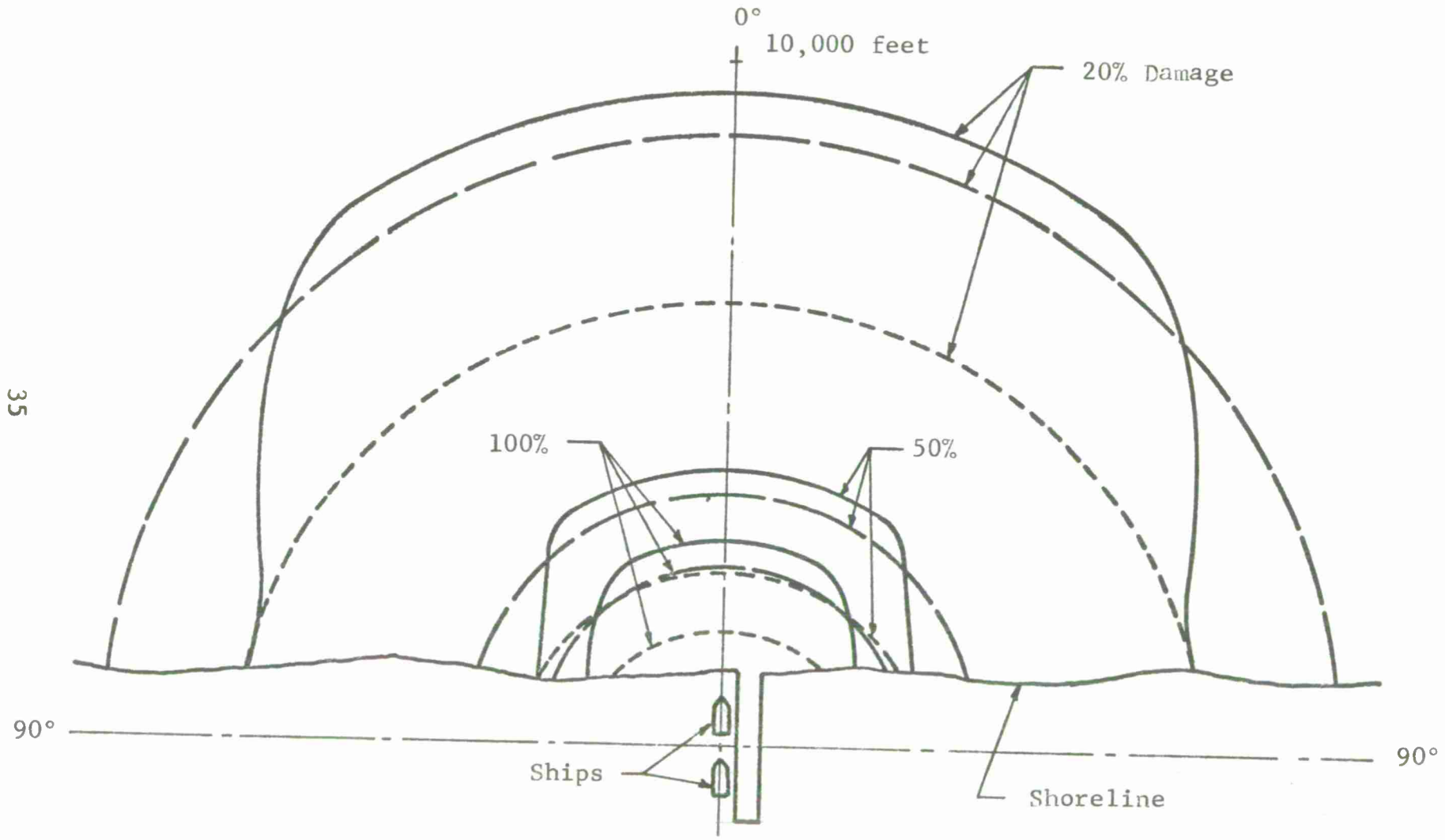

Figure 23 Illustrative Example

4. CONCLUSION AND RECOMMENDATIONS

The following principal conclusions can be drawn from the experimental program.

- When a shock wave is formed by coalescence of the waves from two sequential explosions, the peak overpressure is somewhat greater than that from a single explosion of the total quantity.

- The peak overpressure at a particular station is greatest when the shock waves coalesce at that station.

- It is not conservative to assume point source total explosive weight equivalency in estimating pressure-distance hazards when two detonations and shock wave coalescence are possible.

- Total impulse is not a function of orientation, delay time, or separation distance (i.e., within the range of parameters tested herein) and is the same as that from a single explosion of the total quantity.

The following specific recommendations are made as a result of the cursory analysis given the data herein.

- All of the data herein should be computerized so that specific problems or explosive storage configurations can be quickly analyzed.

- The data herein should be carefully analyzed using computer methods to determine best explosive storage configurations.

- Current point source total explosive weight equivalency can be used to estimate safe storage distances for the 1 to 2 psi range if an amplification factor of 1.25 is applied to the total explosive weight. An amplification factor of 1.50 is indicated for the higher overpressure levels.

- Further experiments should be performed to extend the range of test parameters. Specifically, the small charge separation distances should be tested at shorter delay times and the large separation distances at longer delay times. Also tests should be conducted to determine the effects of the barrier wall separating the two charges, especially for small charge separation distances.

APPENDIX A

TEST DATA

This appendix contains test data obtained during this experimental program. Figure A1 illustrates the nomenclature used to differentiate data points in the figures which follow. Table A1 is a listing of the tests performed. All data have been scaled to TNT equivalence using the total charge weight (i.e., 2 lbs C-4).

A.1 Pressure Data

Pressure data are plotted on Figures A2 thru A25. Pressure is plotted as shock pressure, P1 and P2, versus detonation delay time for each measuring station or distance. Straight lines have been drawn through the averaged nonshaded, P2, data points only. The shaded data points are shock pressure P1. Each figure is for a different orientation and charge separation distance, note upper left hand corner and title of each figure.

A.2 Shock Separation Time

Shock separation time data are plotted on Figures A26 through A49. Shock separation time versus distance is plotted as a function of detonation delay time. Data nomenclature of Figure A1 are not applicable in these figures, each curve represents one test. Each figure is for a different orientation and charge separation distance.

A.3 Impulse Data

Total impulse data are plotted on Figures A50 thru A73. Total impulse versus detonation delay time is plotted as a function of distance. Each figure is for a different orientation and charge separation distance.

Typical Pressure-Time Wave

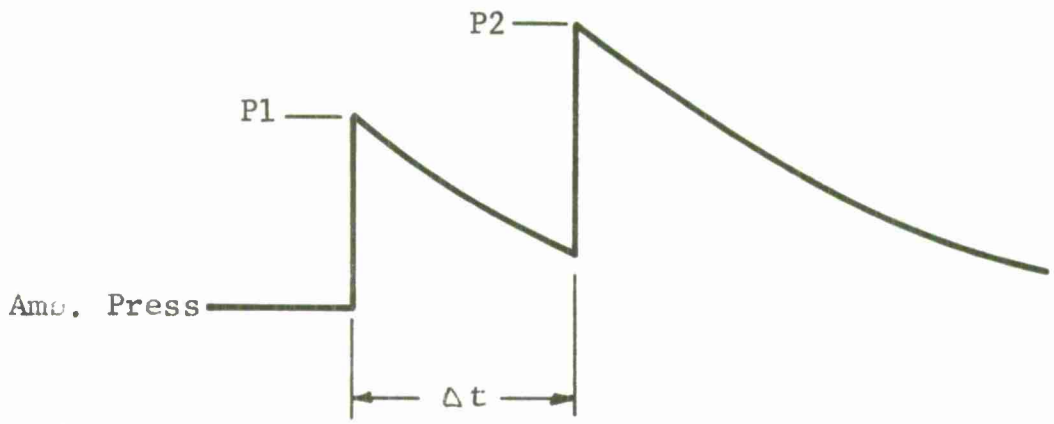

P1 - Pressure of first shock wave, psig.

P2 - Pressure of second shock wave, psig.

Δt - Shock separation time, msec/$lb^{1/3}$.

○ Data measured at 8.8 feet distance, 6.5 feet/$lb^{1/3}$.

○ Data measured at 12.2 feet distance, 9.0 feet/$lb^{1/3}$.

□ Data measured at 18.4 feet distance, 13.6 feet/$lb^{1/3}$.

△ Data measured at 28.4 feet distance, 20.9 feet/$lb^{1/3}$.

◇ Data measured at 50.4 feet distance, 37.1 feet/$lb^{1/3}$.

▽ Data measured at 57.0 feet distance, 42.0 feet/$lb^{1/3}$.

Note: P1 data points are shaded.
P2 data points are nonshaded.

Figure A1 Data nomenclature

TABLE A1 TEST SCHEDULE

Test No.	Delay Time msec/lb$^{1/3}$	Orientation deg	Separation Distance feet/lb$^{1/3}$
1	1.48	0.90	0.615
1A	1.51	0.90	0.615
2	1.64	0.90	1.23
3	1.61	0.90	2.46
4	1.61	0.90	4.92
5	2.17	0.90	0.615
6	2.16	0.90	1.23
7	2.17	0.90	2.46
8	2.19	0.90	4.92
9	2.68	0.90	0.615
10	-	0.90	1.23
10A	2.70	0.90	1.23
11	2.67	0.90	2.46
12	2.65	0.90	4.92
13	3.22	0.90	0.615
14	3.18	0.90	1.23
15	3.26	0.90	2.46
16	3.26	0.90	4.92
16A	3.25	0.90	4.92
17	3.85	0.90	0.615
18	3.88	0.90	1.23
19	3.85	0.90	2.46
20	3.81	0.90	4.92
21	1.69	18.72	0.615
22	1.66	18.72	1.23
23	1.62	18.72	2.46
24	1.72	18.72	4.92
25	2.16	18.72	0.615
26	2.16	18.72	1.23
27	2.27	18.72	2.46
28	2.16	18.72	4.92
29	2.63	18.72	0.615
30	2.65	18.72	1.23
31	2.73	18.72	2.46
32	2.73	18.72	4.92
33	3.21	18.72	0.615
34	3.52	18.72	1.23
34A	3.23	18.72	1.23
35	3.23	18.72	2.46

TABLE A1 TEST SCHEDULE
(concluded)

Test No.	Delay Time msec/lb$^{1/3}$	Orientation deg	Separation Distance feet/lb$^{1/3}$
36	3.21	18.72	4.92
37	3.76	18.72	0.615
38	3.75	18.72	1.23
39	3.78	18.72	2.46
40	3.75	18.72	4.92
41	-	36.54	0.615
41A	1.70	36.54	0.615
42	1.69	36.54	1.23
43	1.63	36.54	2.46
44	1.70	36.54	4.92
45	2.20	36.54	0.615
46	2.20	36.54	1.23
47	2.20	36.54	2.46
48	2.16	36.54	4.92
49	2.68	36.54	0.615
50	2.69	36.54	1.23
51	2.70	36.54	2.46
52	2.72	36.54	4.92
53	3.21	36.54	0.615
54	3.25	36.54	1.23
55	3.22	36.54	2.46
56	3.46	36.54	4.92
57	3.79	36.54	0.615
58	3.77	36.54	1.23
59	3.85	36.54	2.46
60	3.75	36.54	4.92

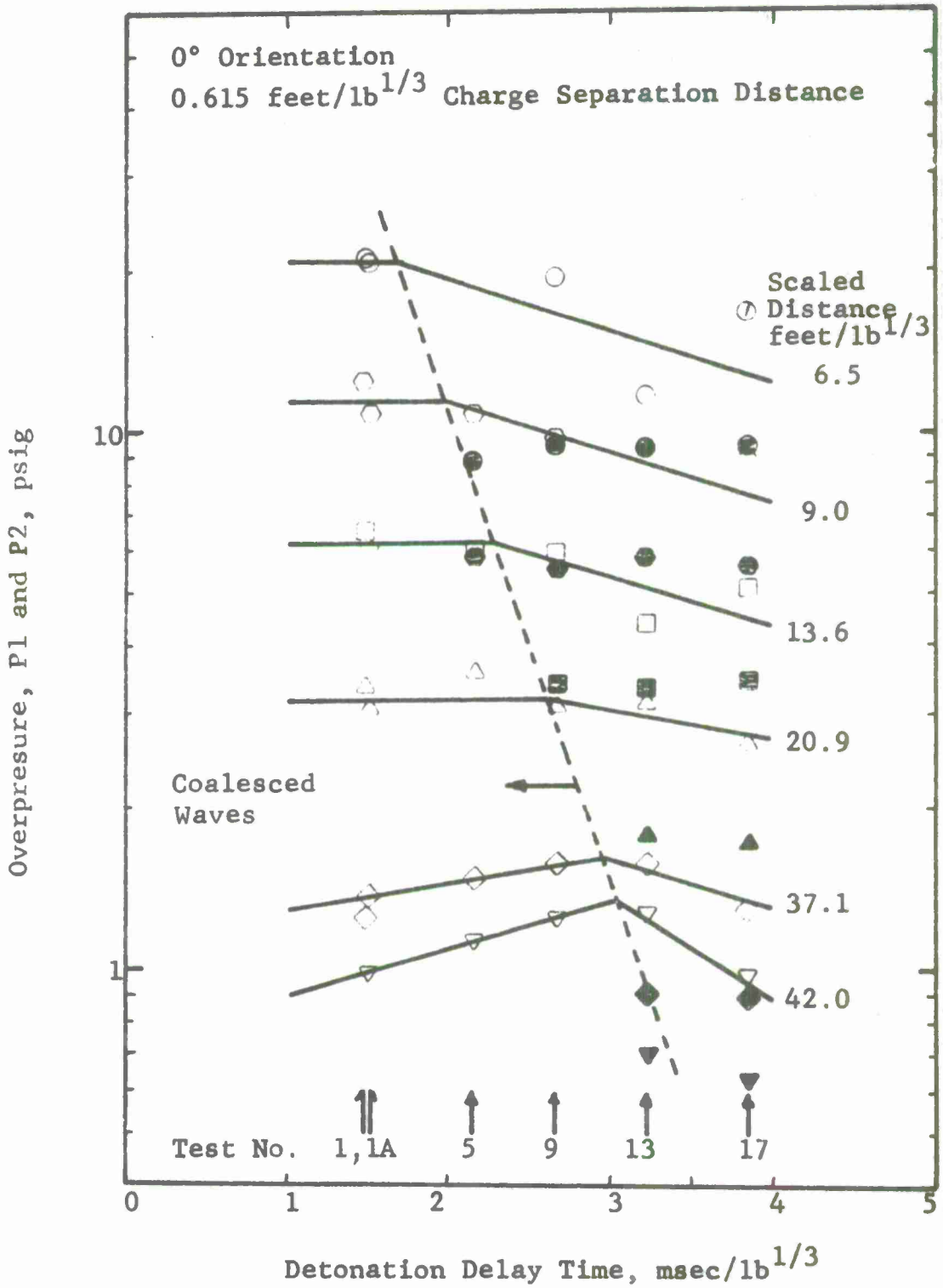

Figure A2 Pressure (0°, 0.615 feet/lb$^{1/3}$)

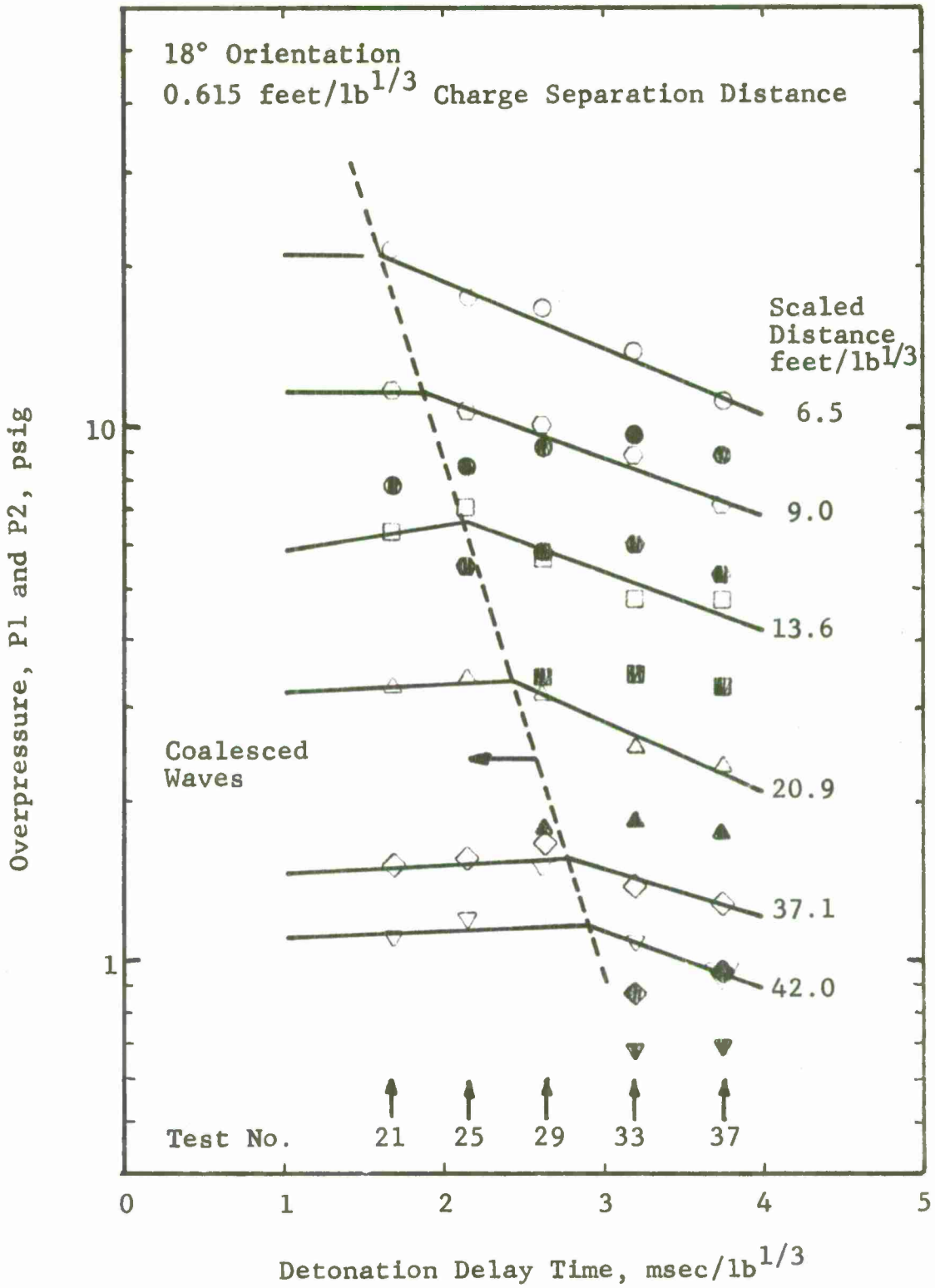

Figure A3 Pressure (18°, 0.615 feet/lb$^{1/3}$)

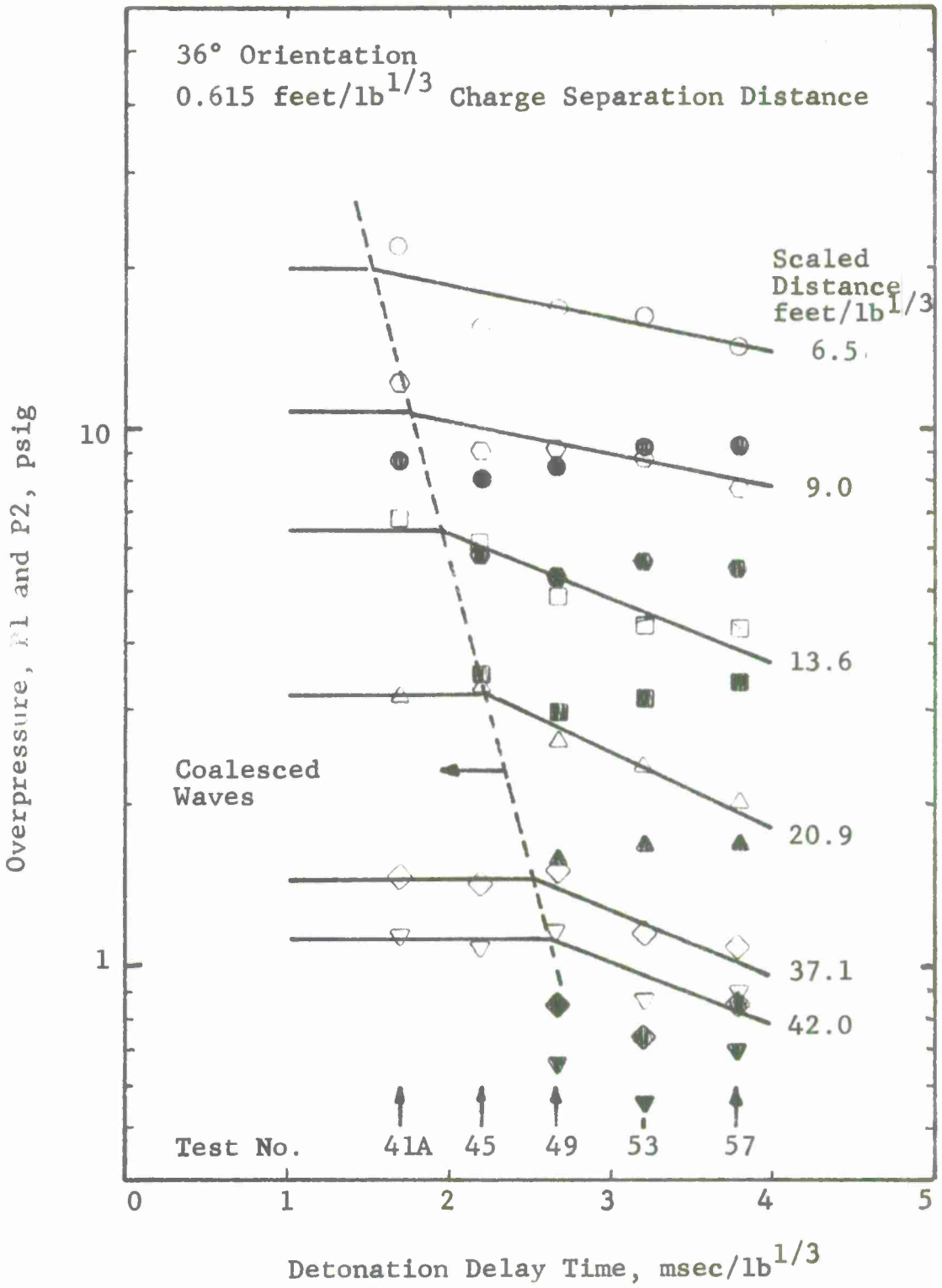

Figure A4 Pressure (36°, 0.615 feet/lb$^{1/3}$)

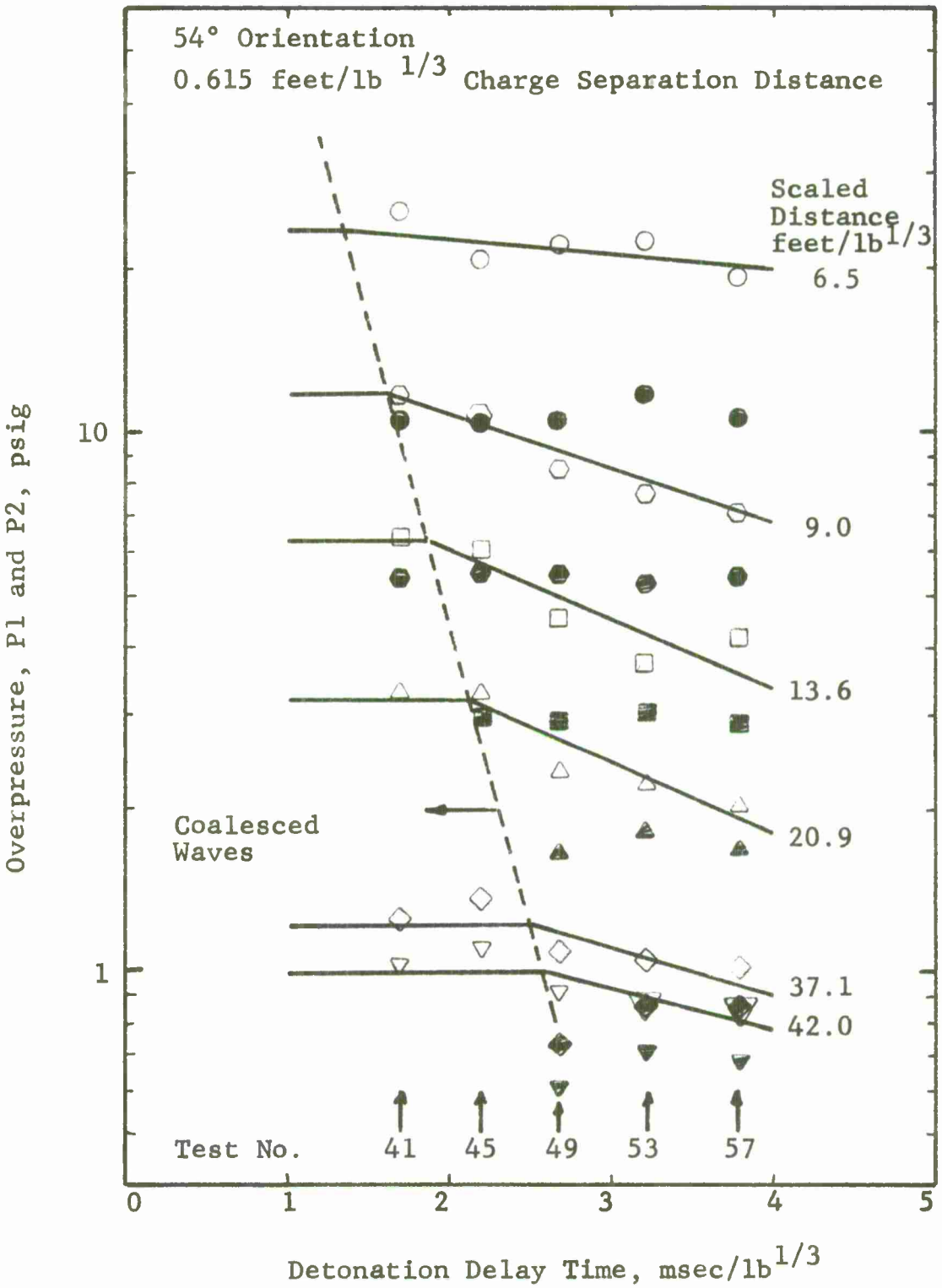

Figure A5 Pressure (54°, 0.615 feet/lb$^{1/3}$)

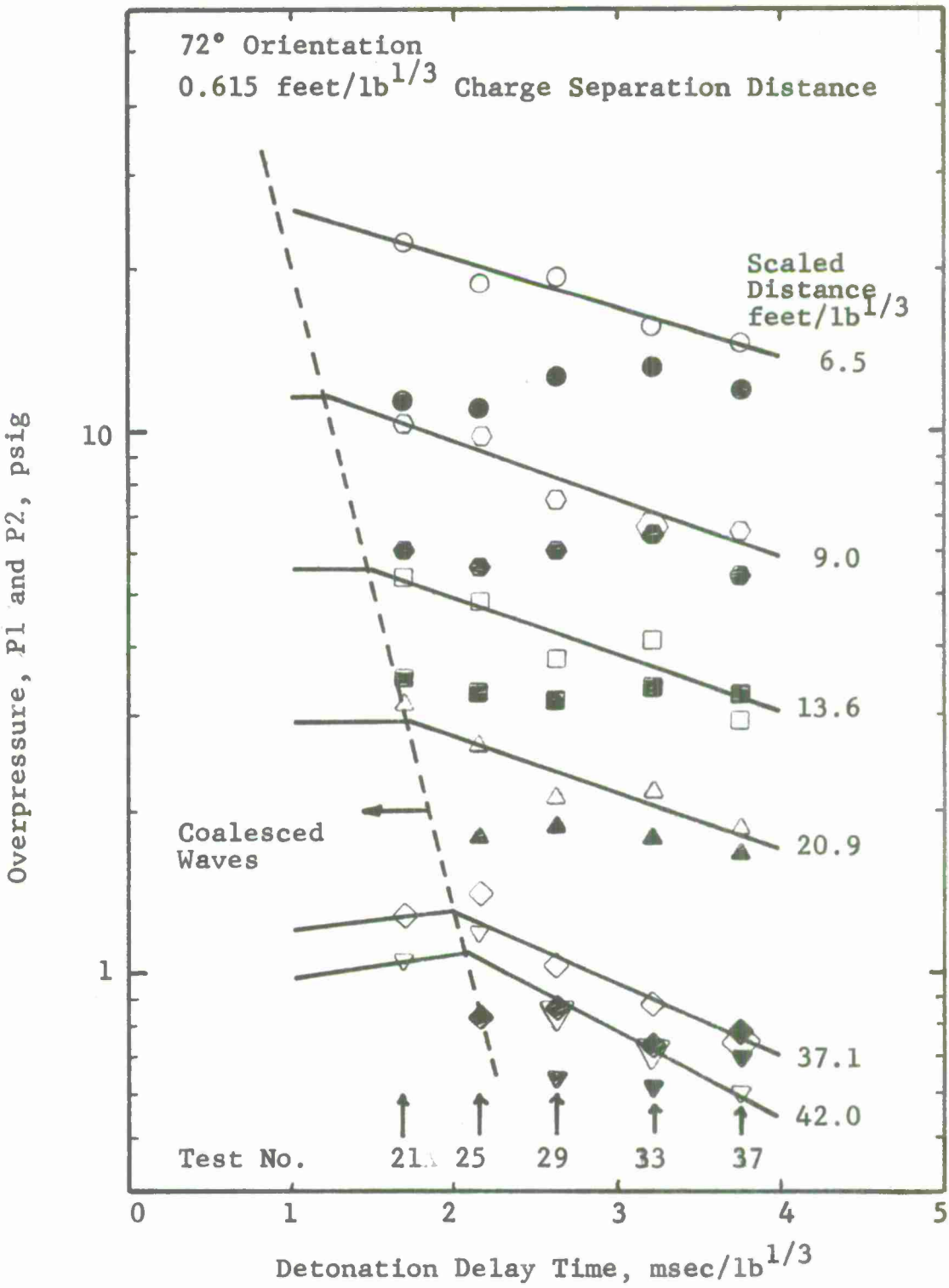

Figure A6 Pressure (72°, 0.615 feet/lb$^{1/3}$)

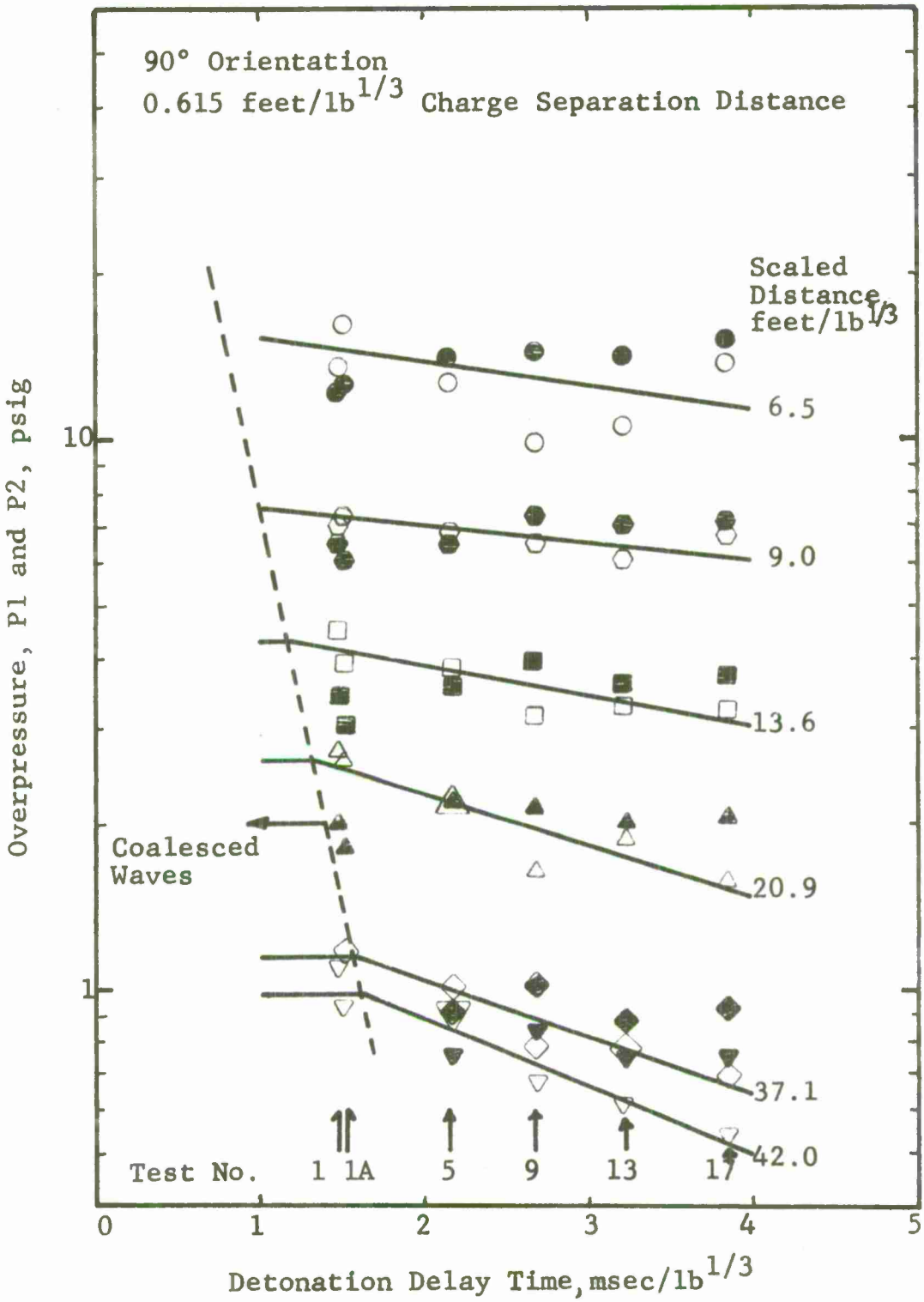

Figure A7 Pressure (90°, 0.615 feet/lb$^{1/3}$)

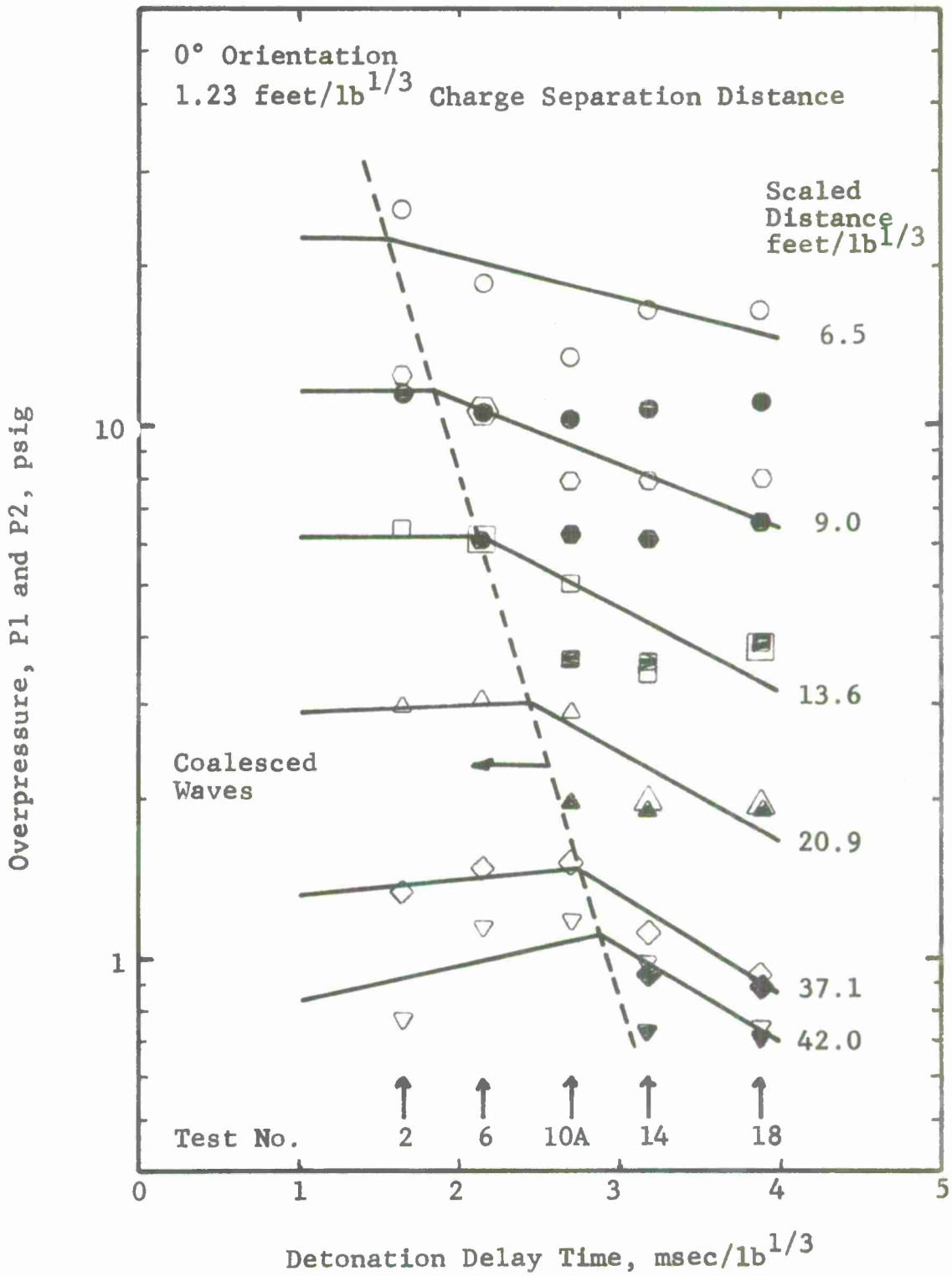

Figure A8 Pressure (0°, 1.23 feet/lb$^{1/3}$)

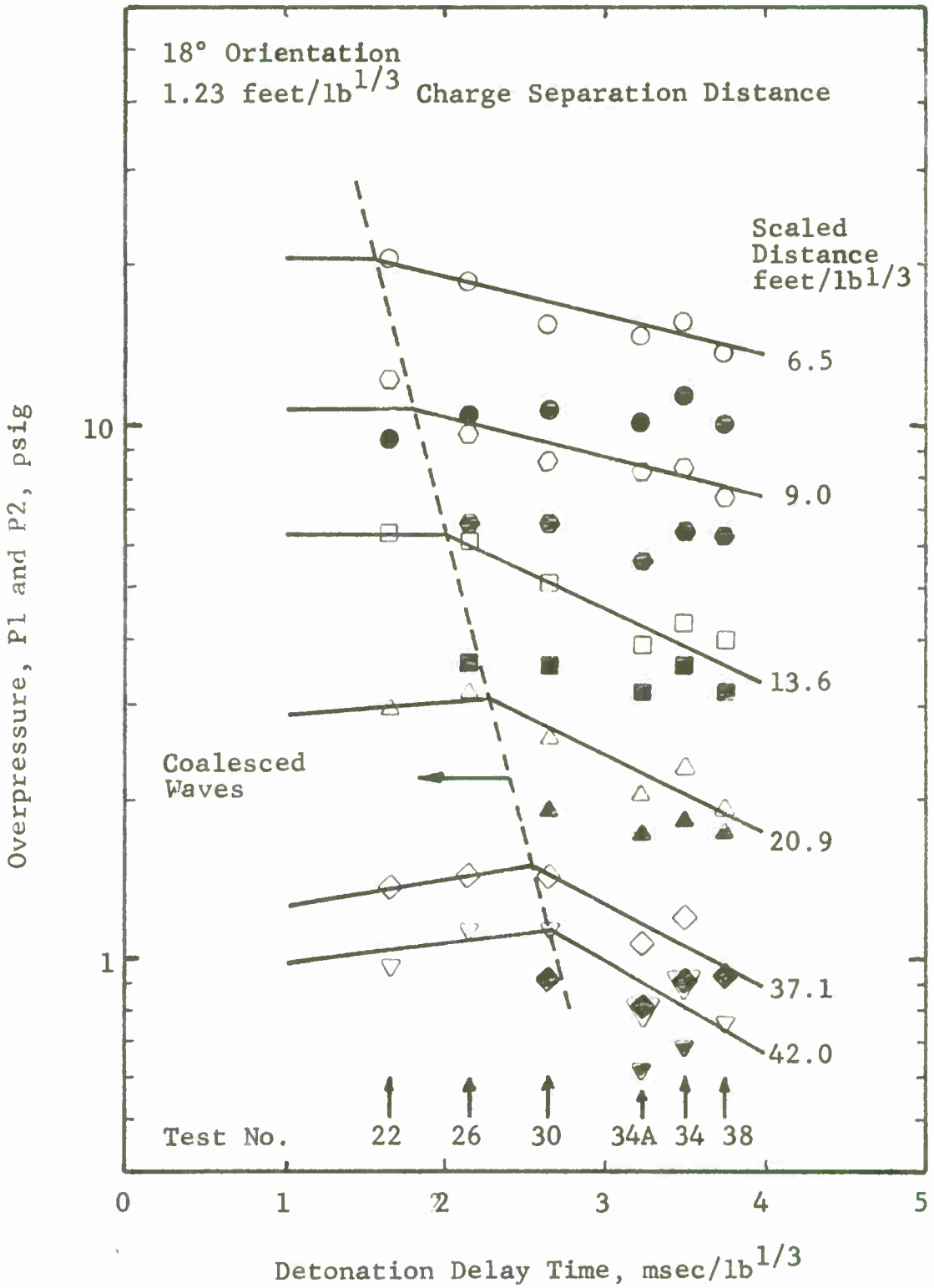

Figure A9 Pressure (18°, 1.23 feet/lb$^{1/3}$)

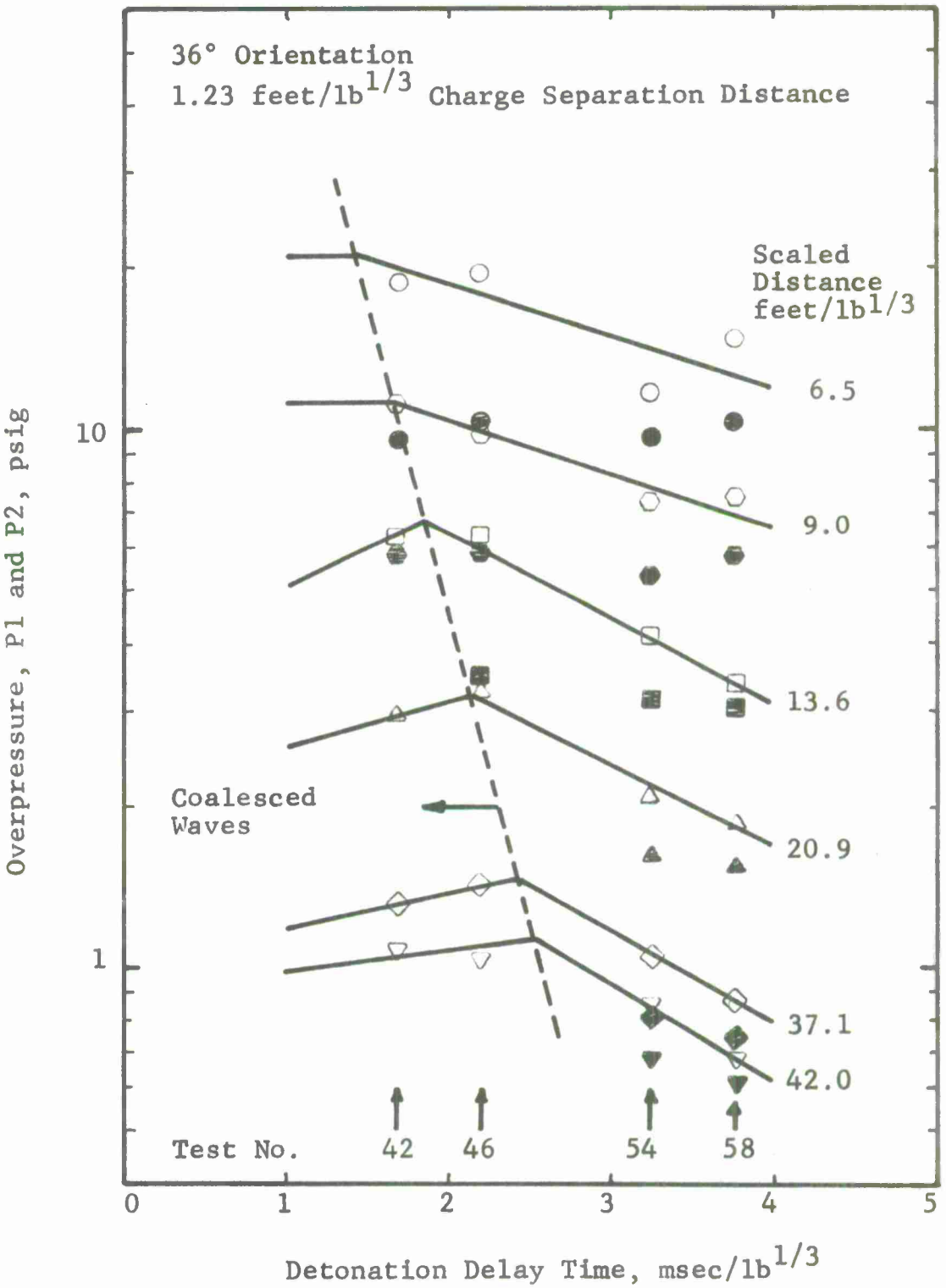

Figure A10 Pressure (36°, 1.23 feet/lb$^{1/3}$)

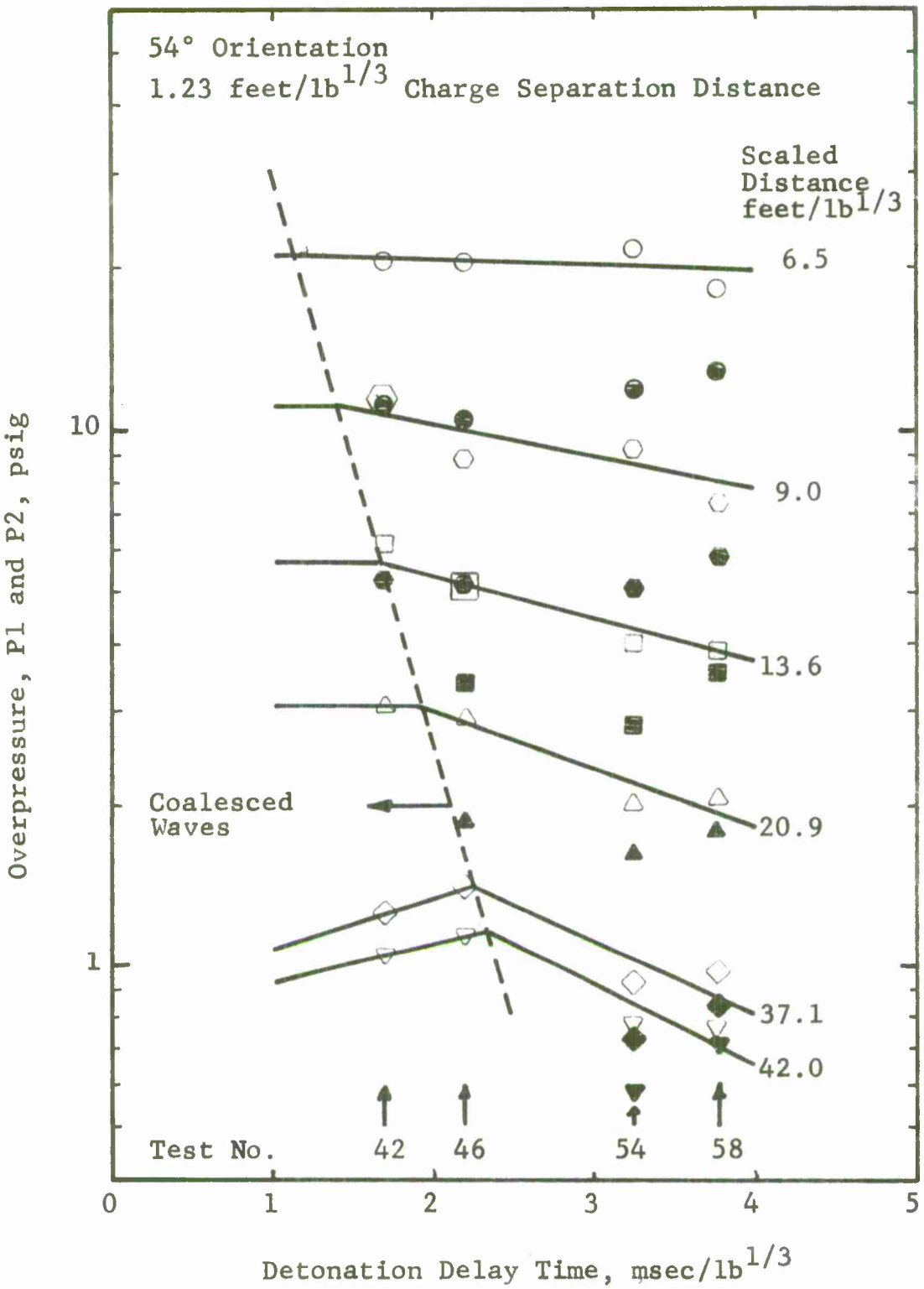

Figure A11 Pressure (54°, 1.23 feet/lb$^{1/3}$)

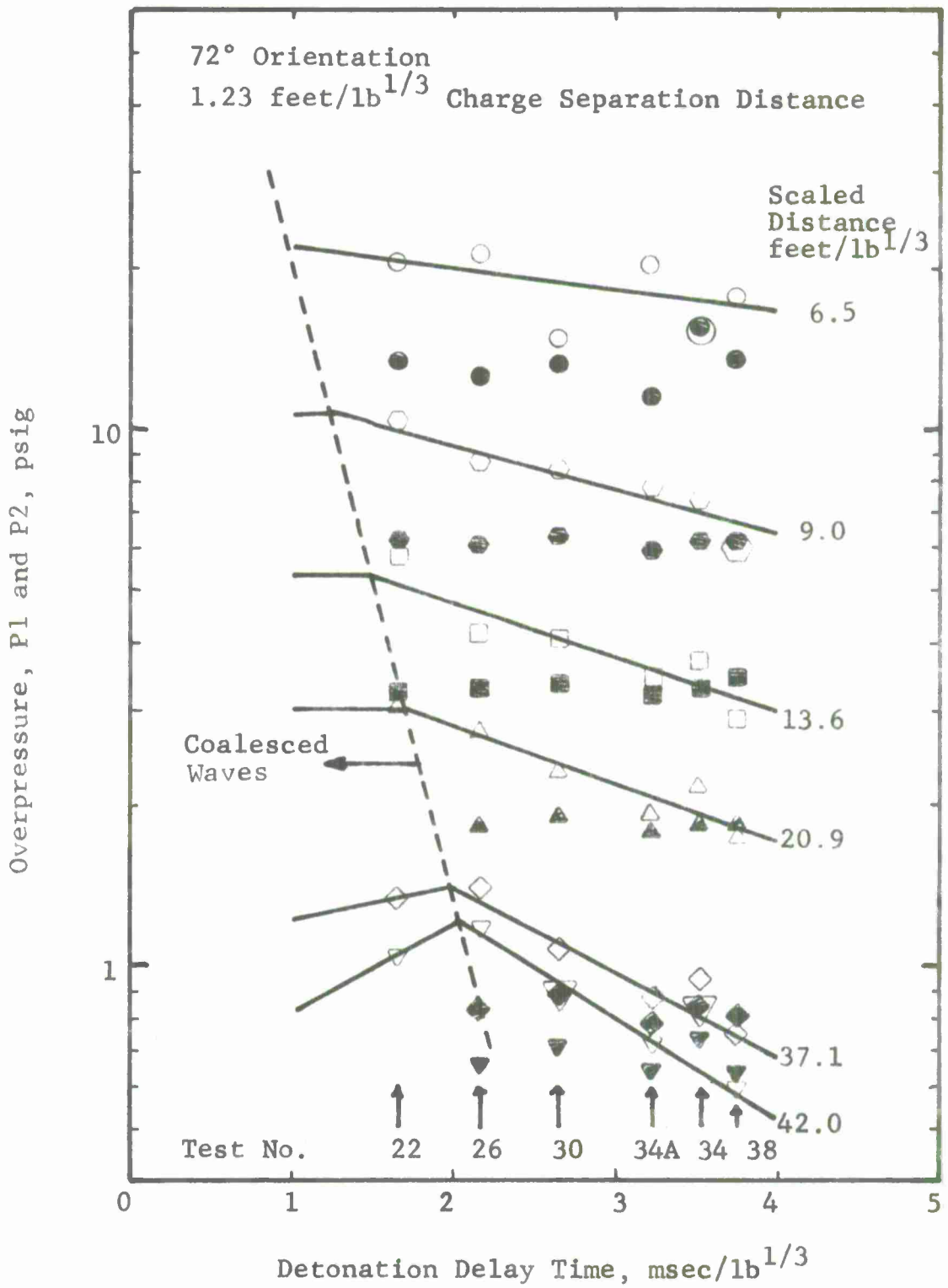

Figure A12 Pressure (72°, 1.23 feet/lb$^{1/3}$)

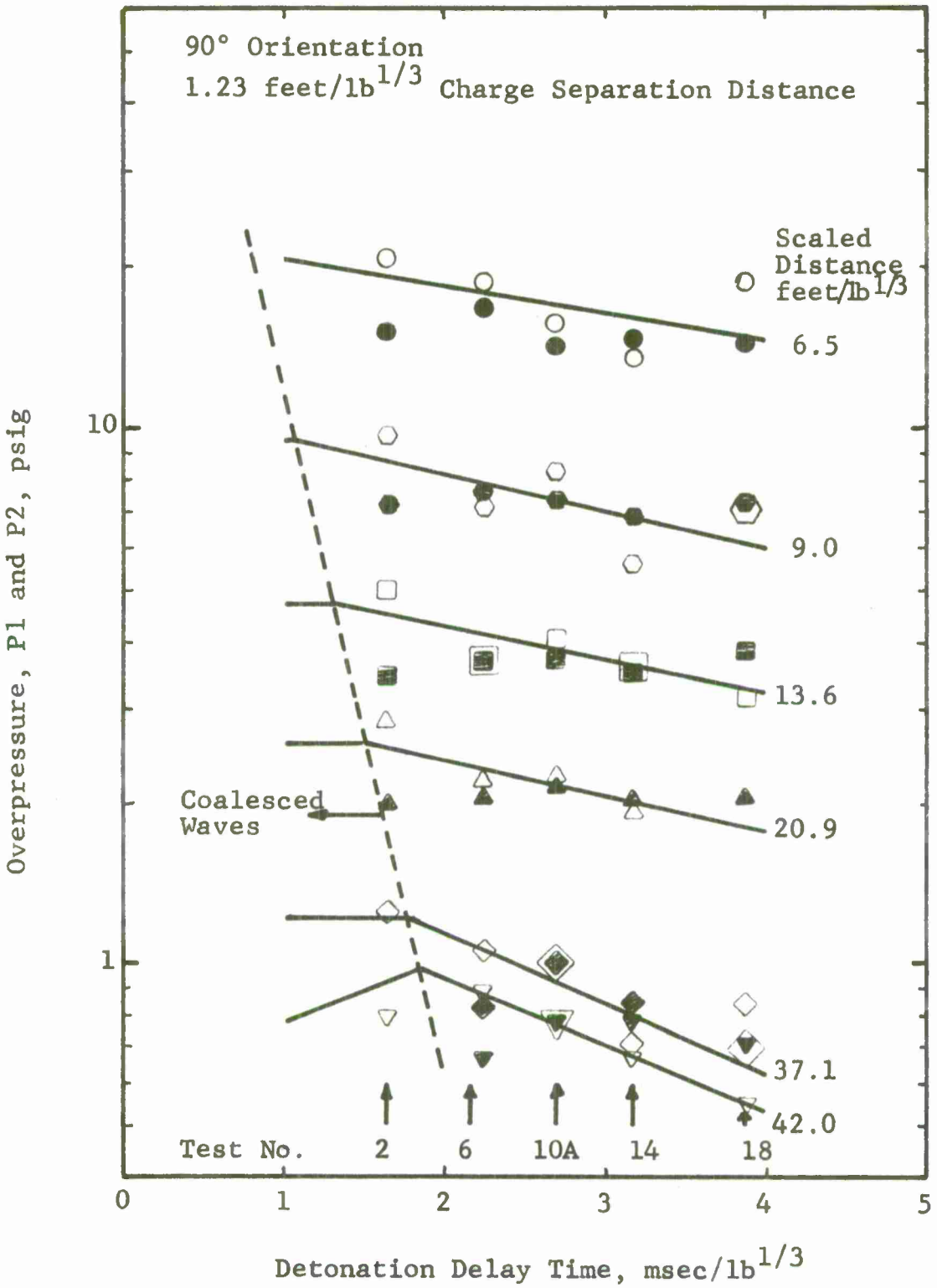

Figure A13 Pressure (90°, 1.23 feet/lb$^{1/3}$)

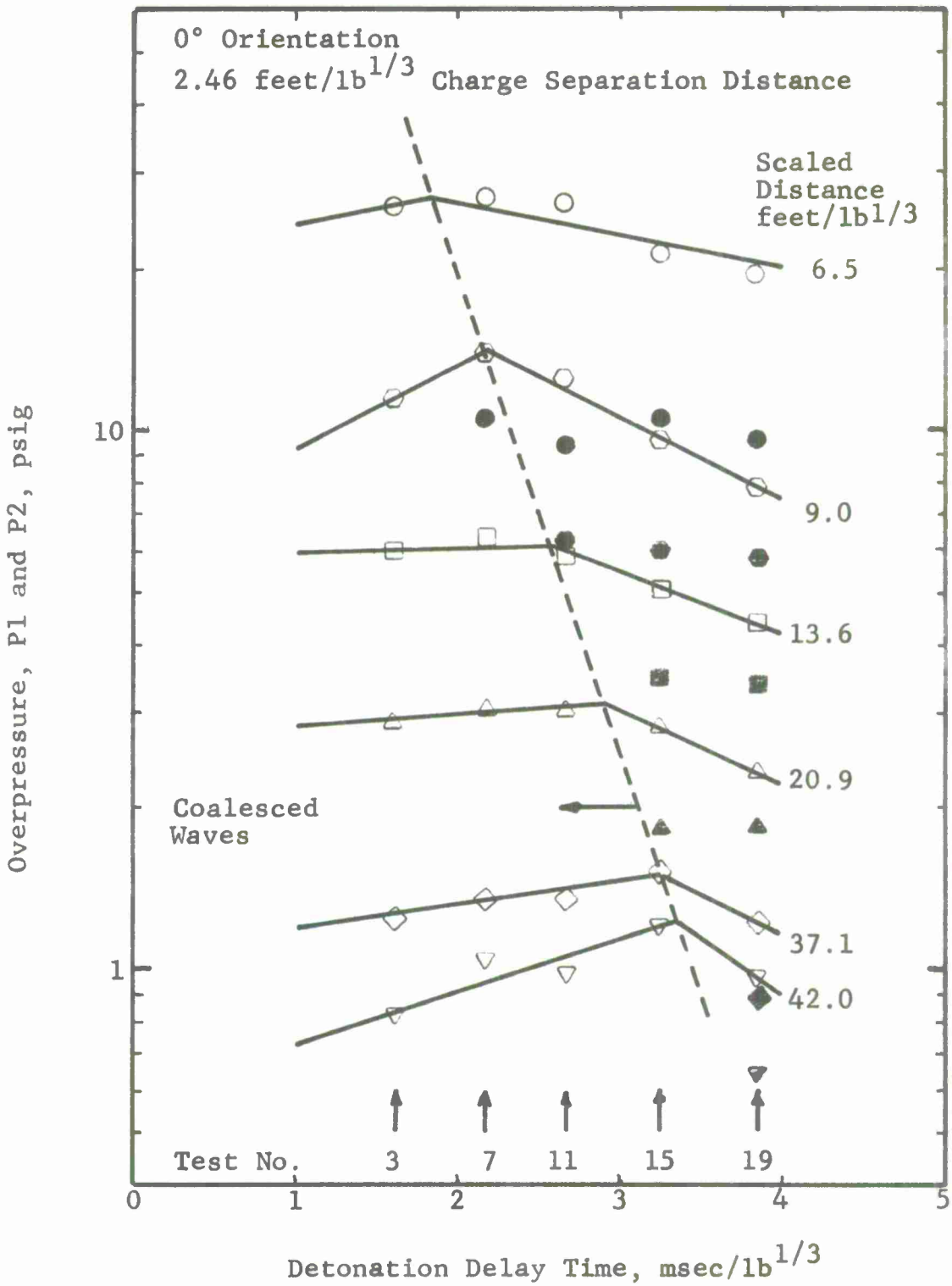

Figure A14 Pressure (0°, 2.46 feet/lb$^{1/3}$)

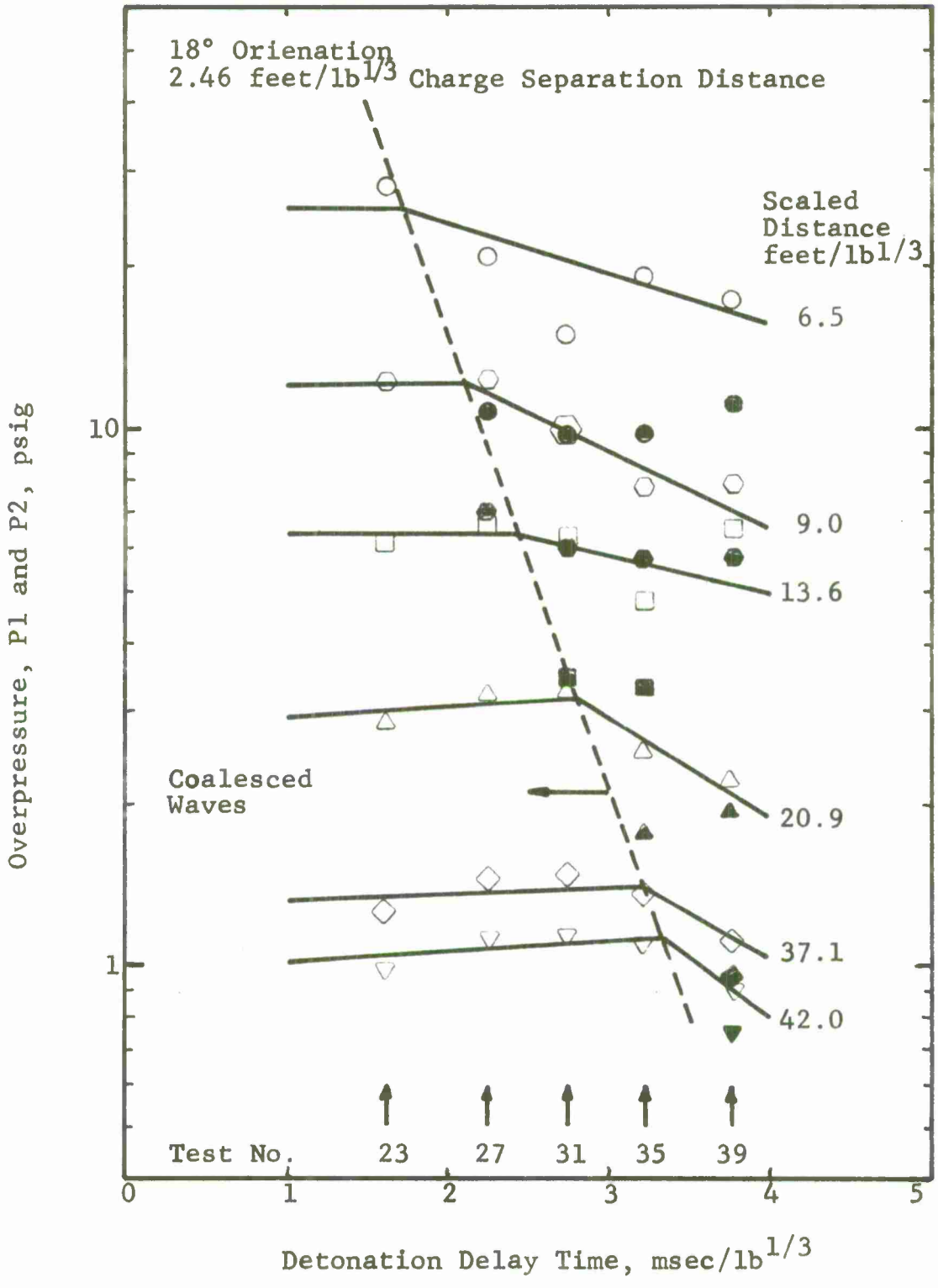

Figure A15 Pressure (18°, 2.46 feet/lb$^{1/3}$)

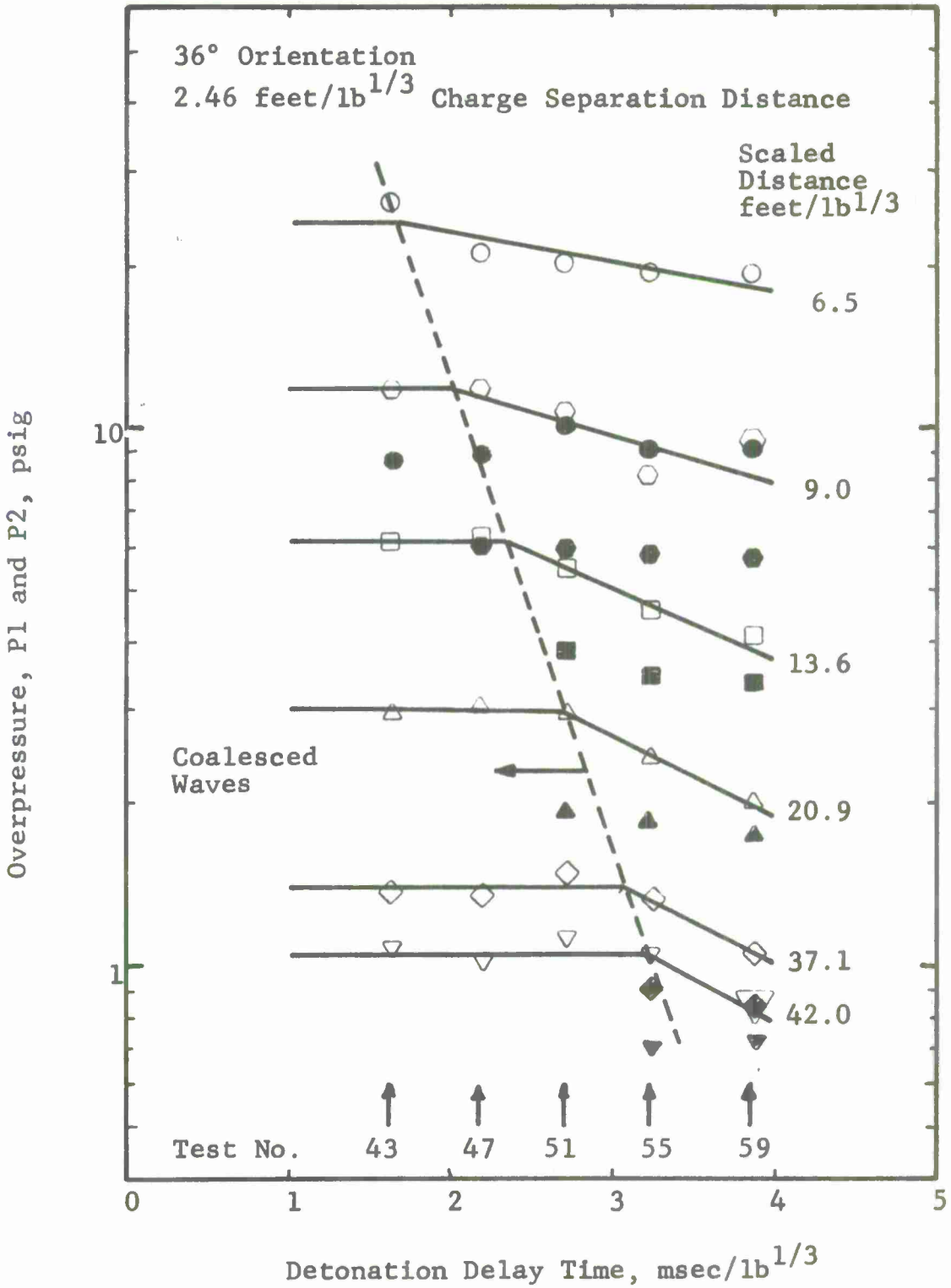

Figure A16 Pressure (36°, 2.46 feet/lb$^{1/3}$)

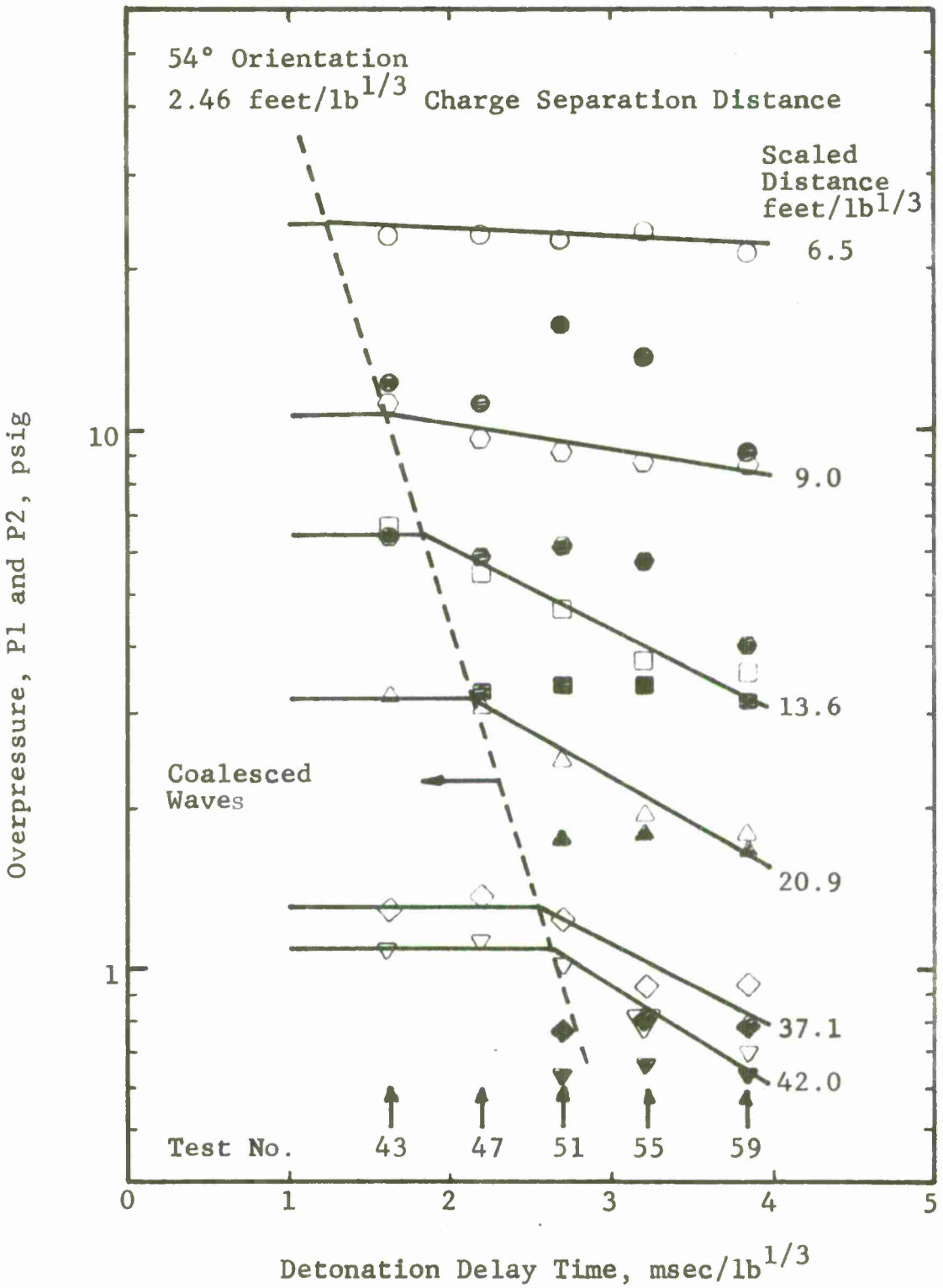

Figure A17 Pressure (54°, 2.46 feet/lb$^{1/3}$)

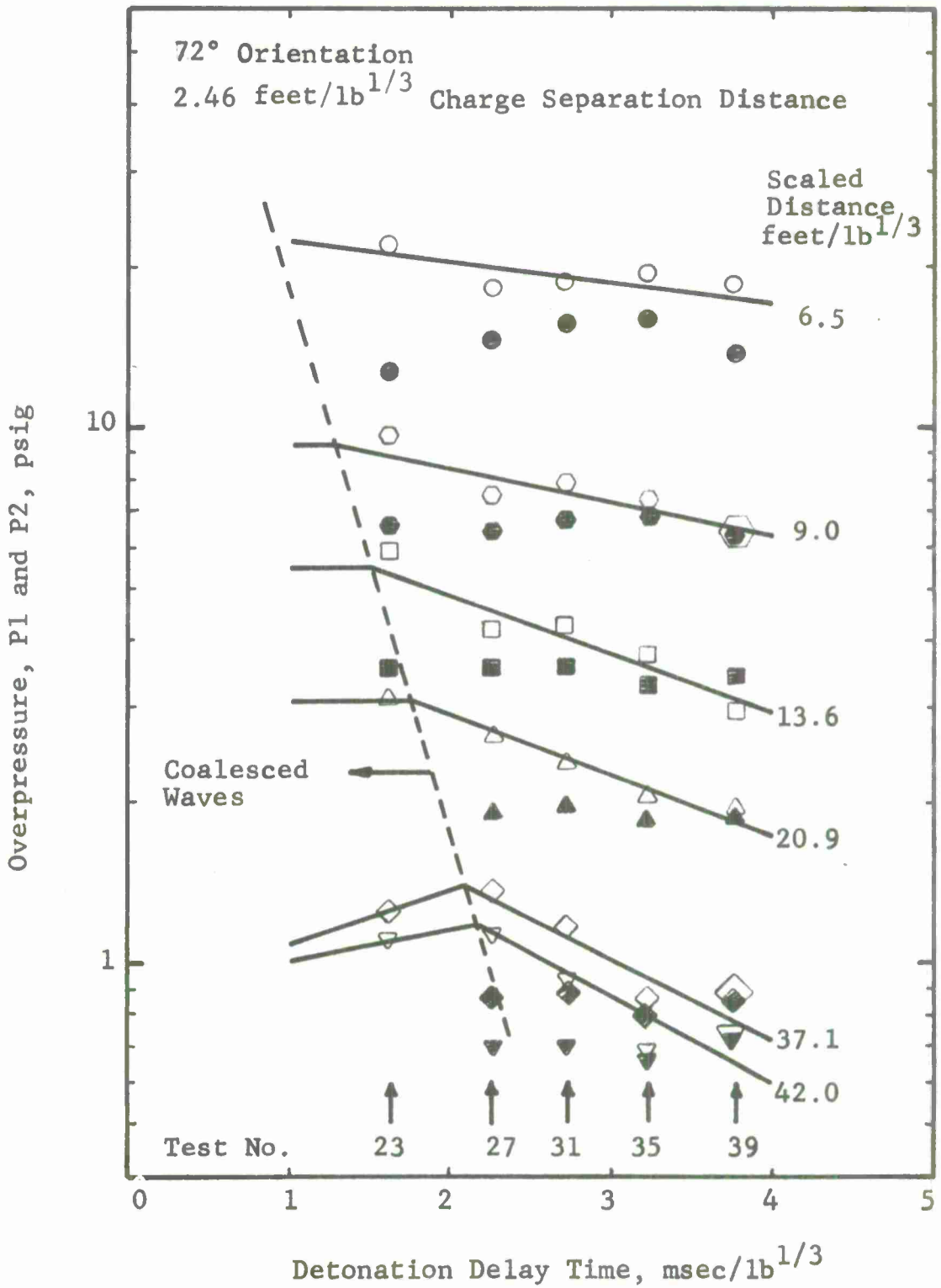

Figure A18 Pressure (72°, 2.46 feet/lb$^{1/3}$)

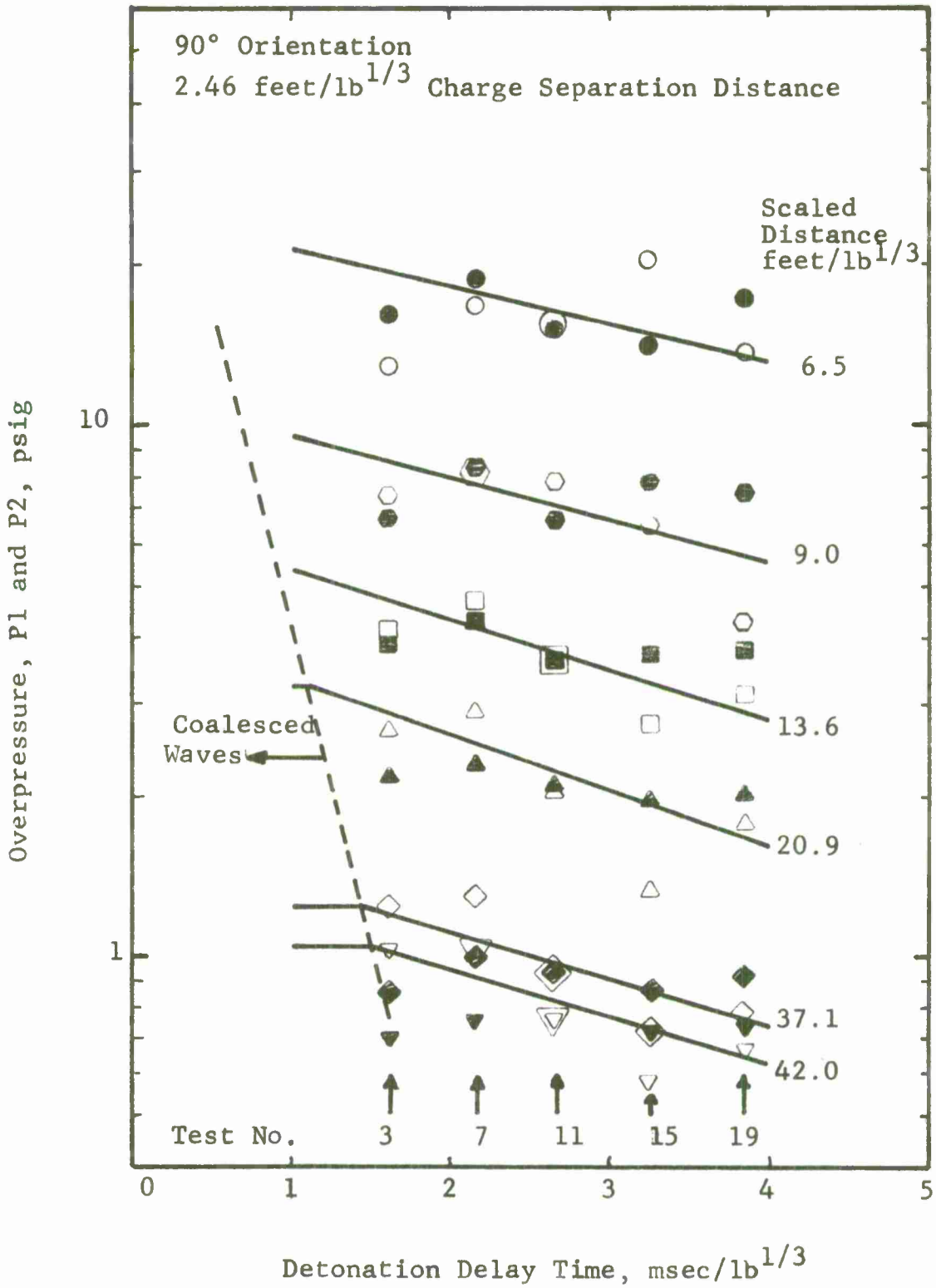

Figure A19 Pressure (90°, 2.46 feet/lb$^{1/3}$)

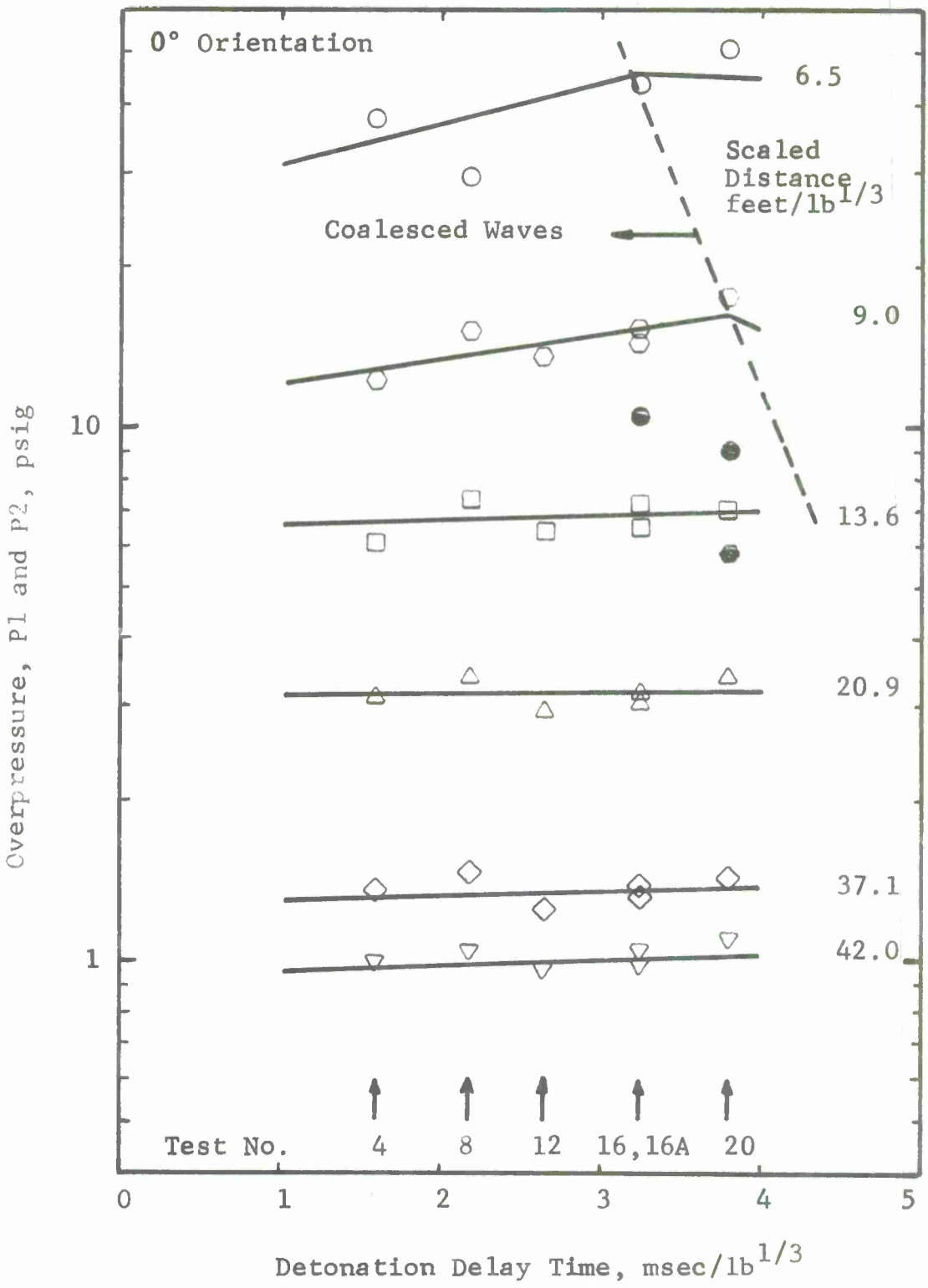

Figure A20 Pressure (0°, 4.92 feet/lb$^{1/3}$)

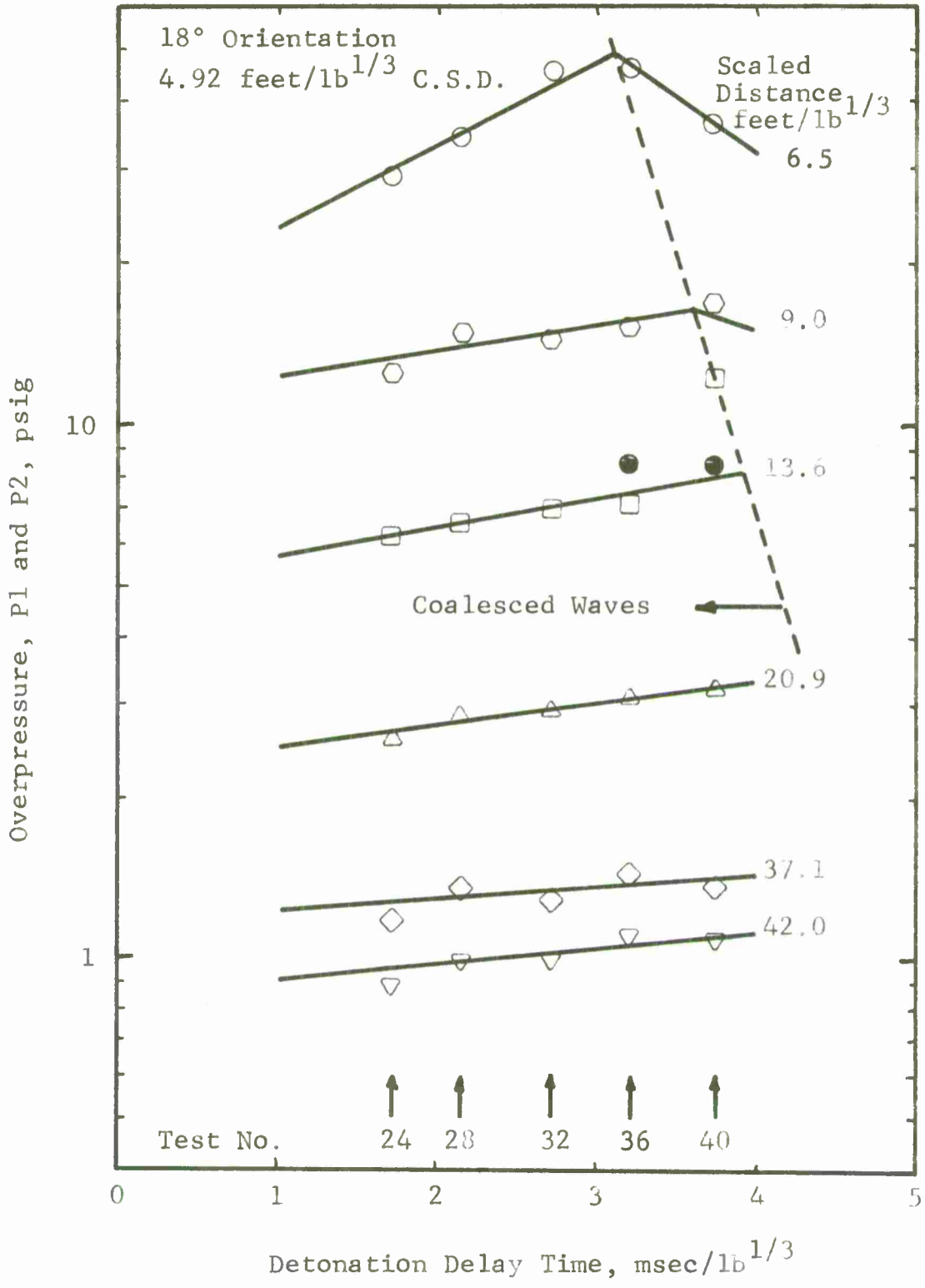

Figure A21 Pressure (18°, 4.92 feet/lb$^{1/3}$)

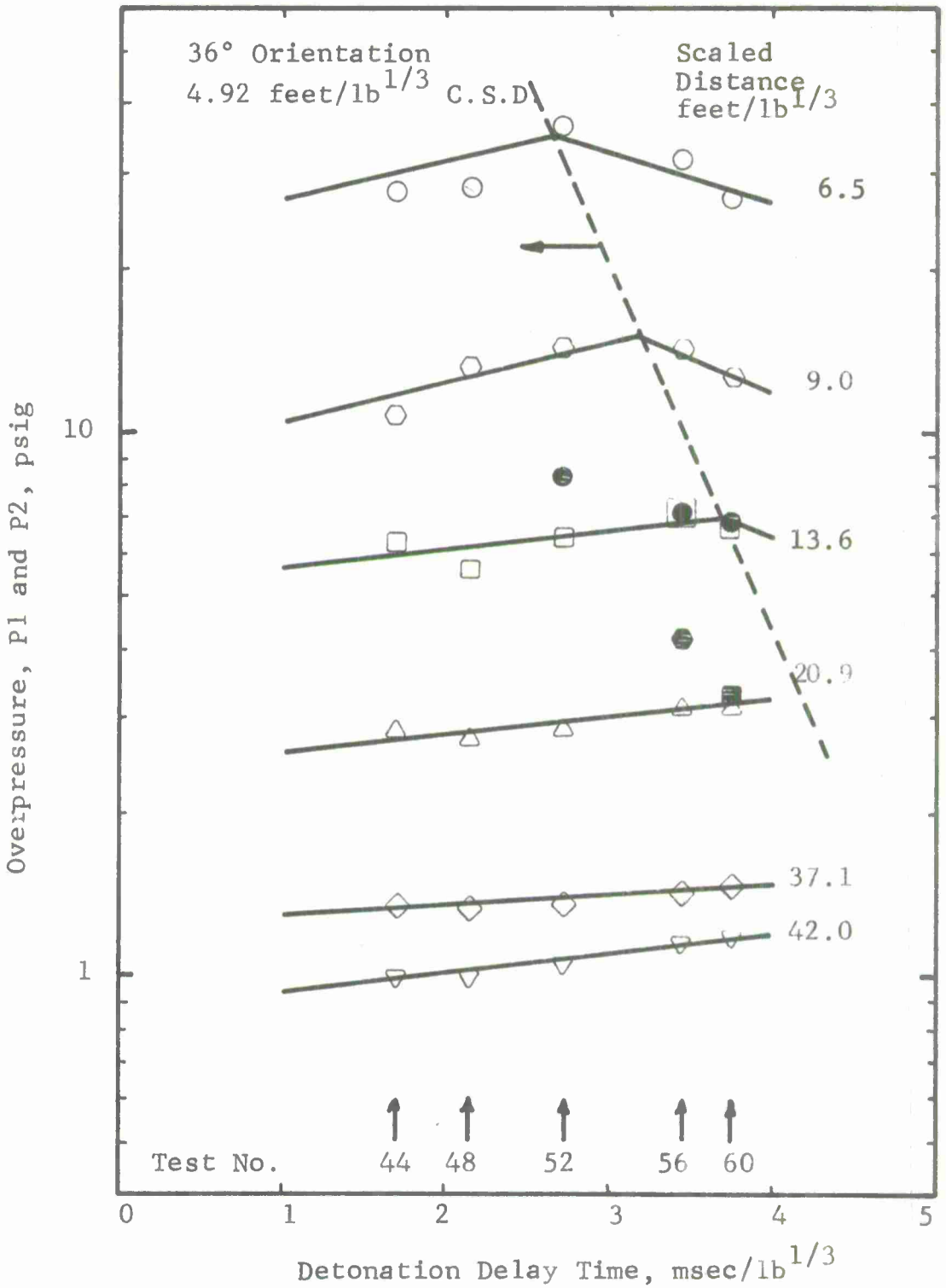

Figure A22 Pressure (36°, 4.92 feet/lb$^{1/3}$)

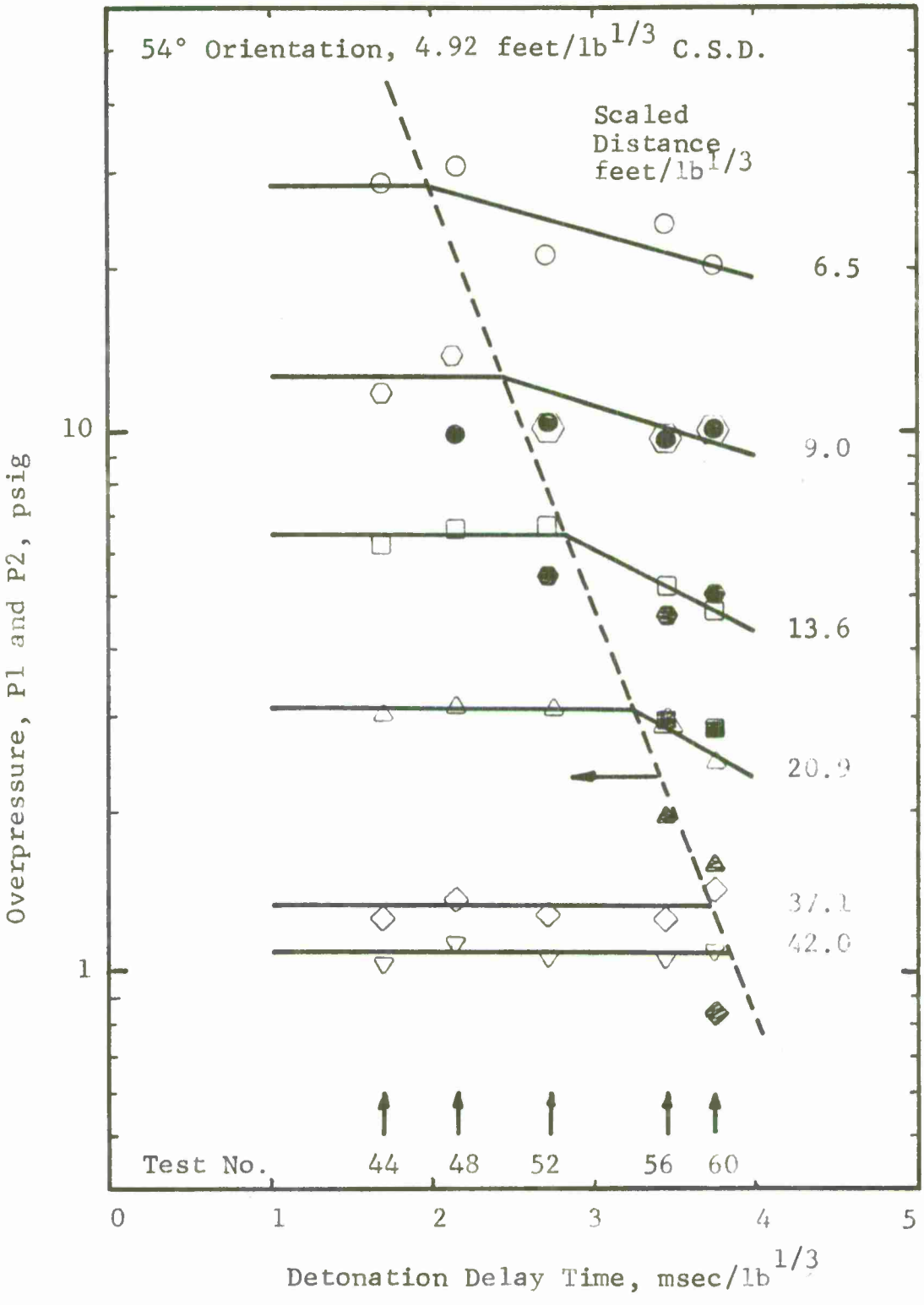

Figure A23 Pressure (54°, 4.92 feet/lb$^{1/3}$)

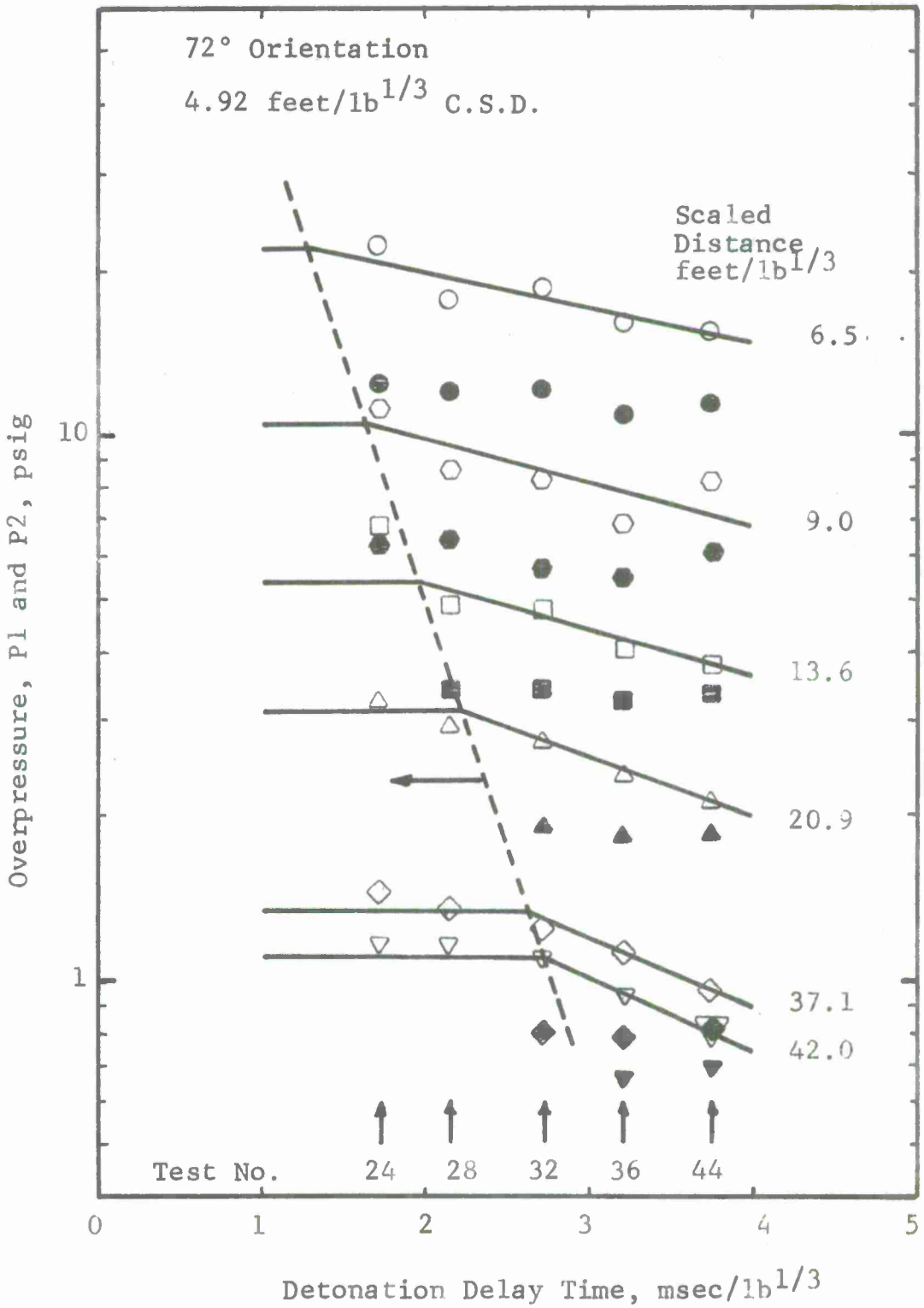

Figure A24 Pressure (72°, 4.92 feet/lb$^{1/3}$)

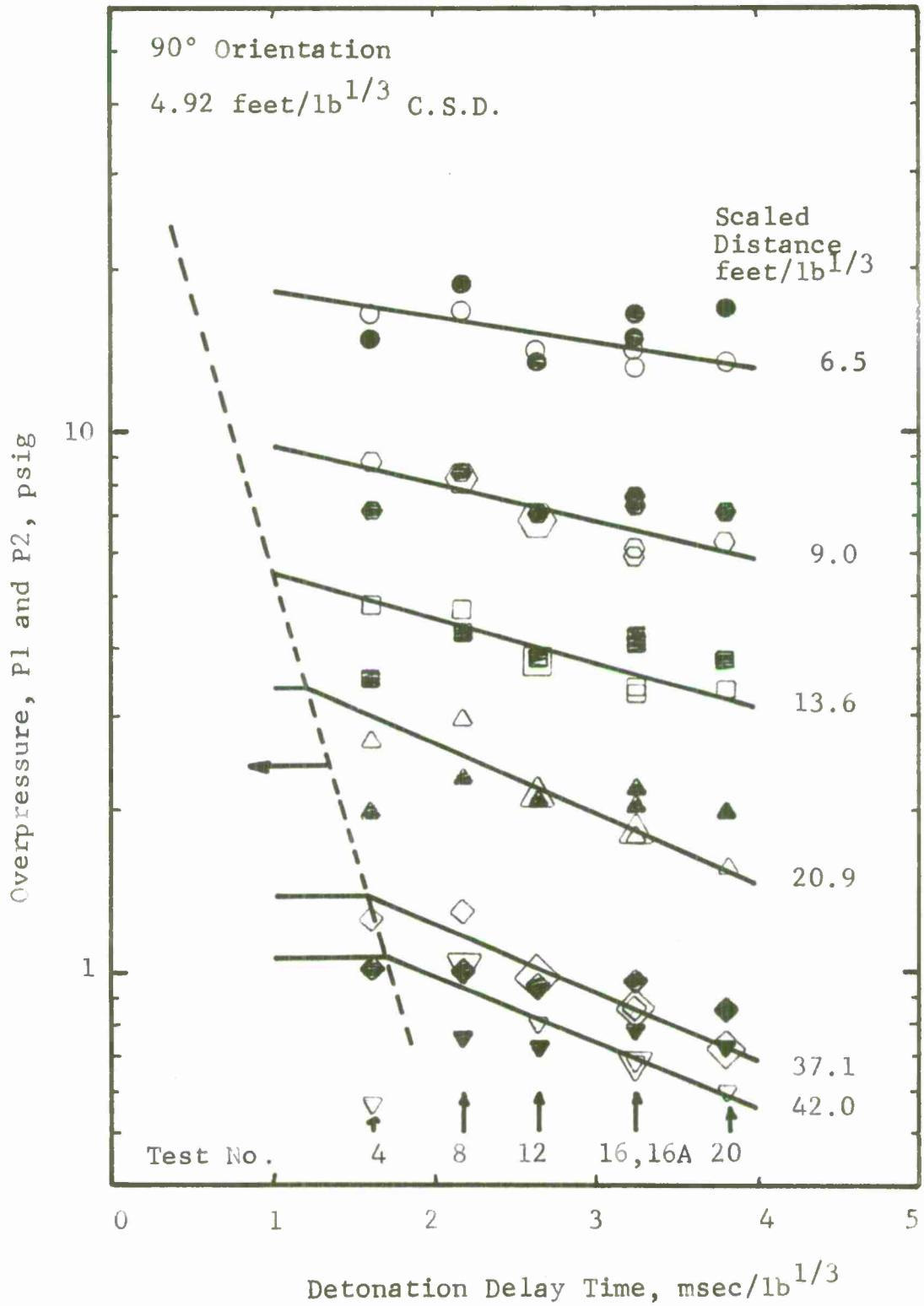

Figure A25 Pressure (90°, 4.92 feet/lb$^{1/3}$)

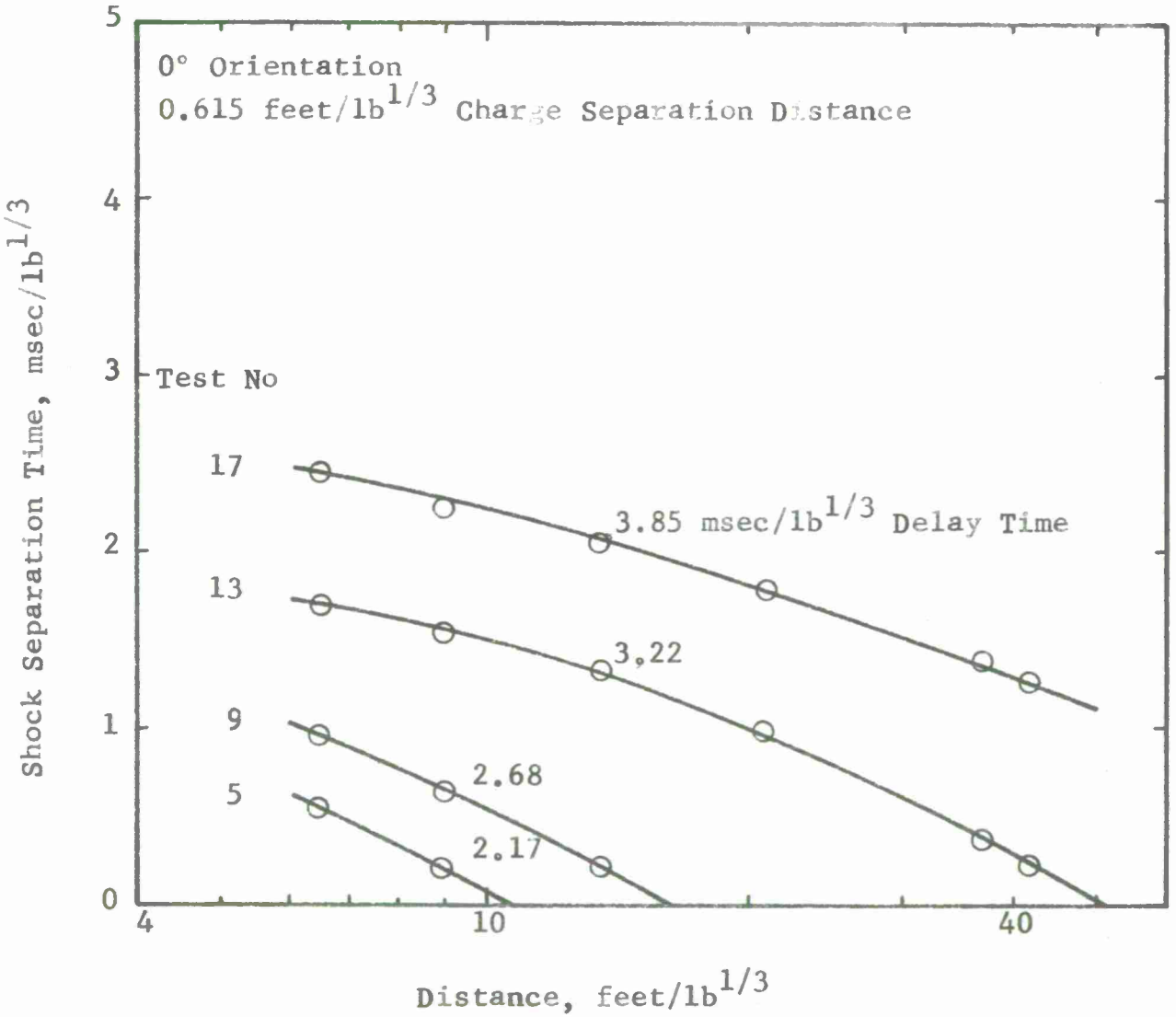

Figure A26 Shock Separation Time Data (0°-0.615 feet/lb$^{1/3}$)

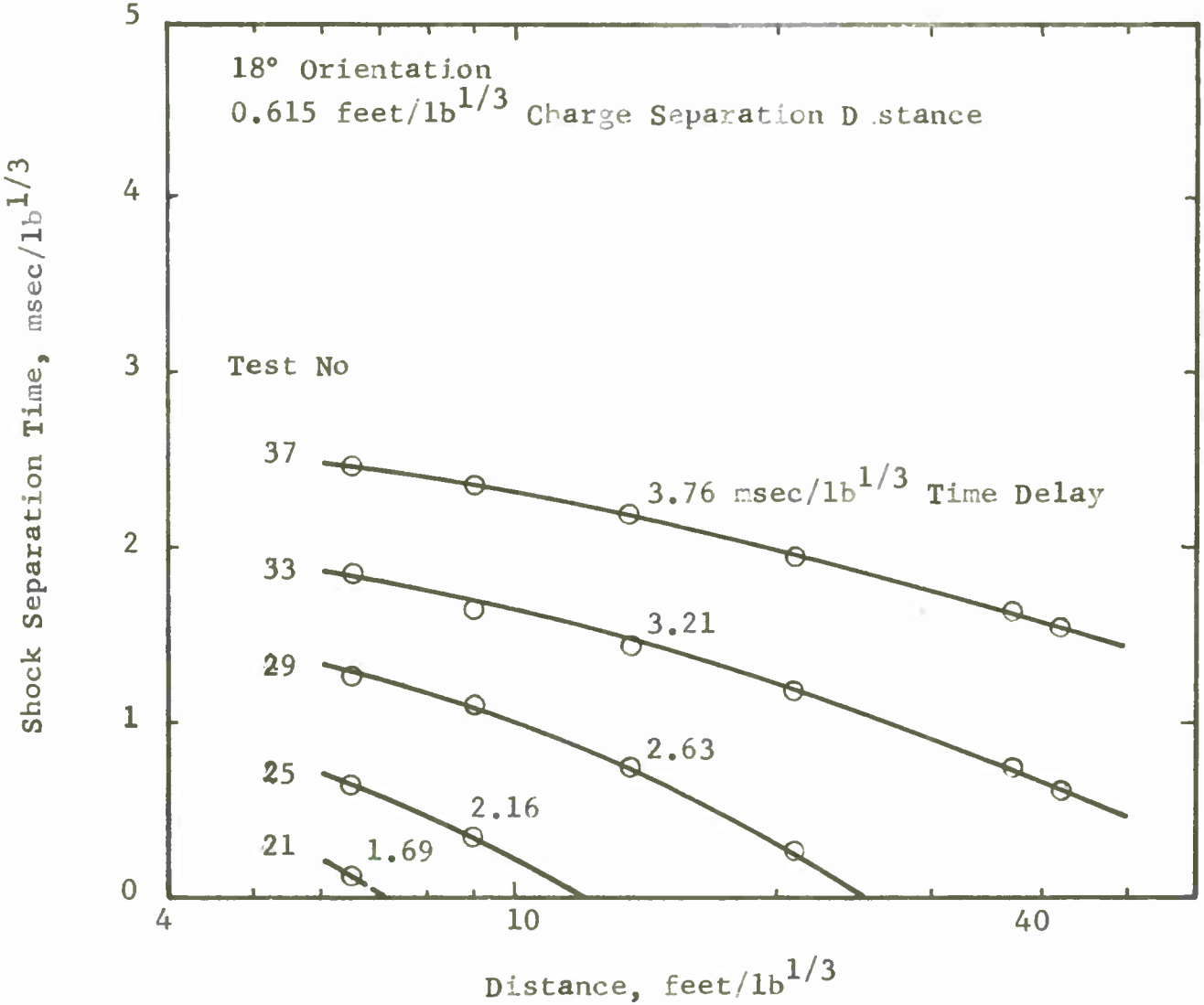

Figure A27 Shock Separation Time Data (18°-0.615 feet/lb$^{1/3}$)

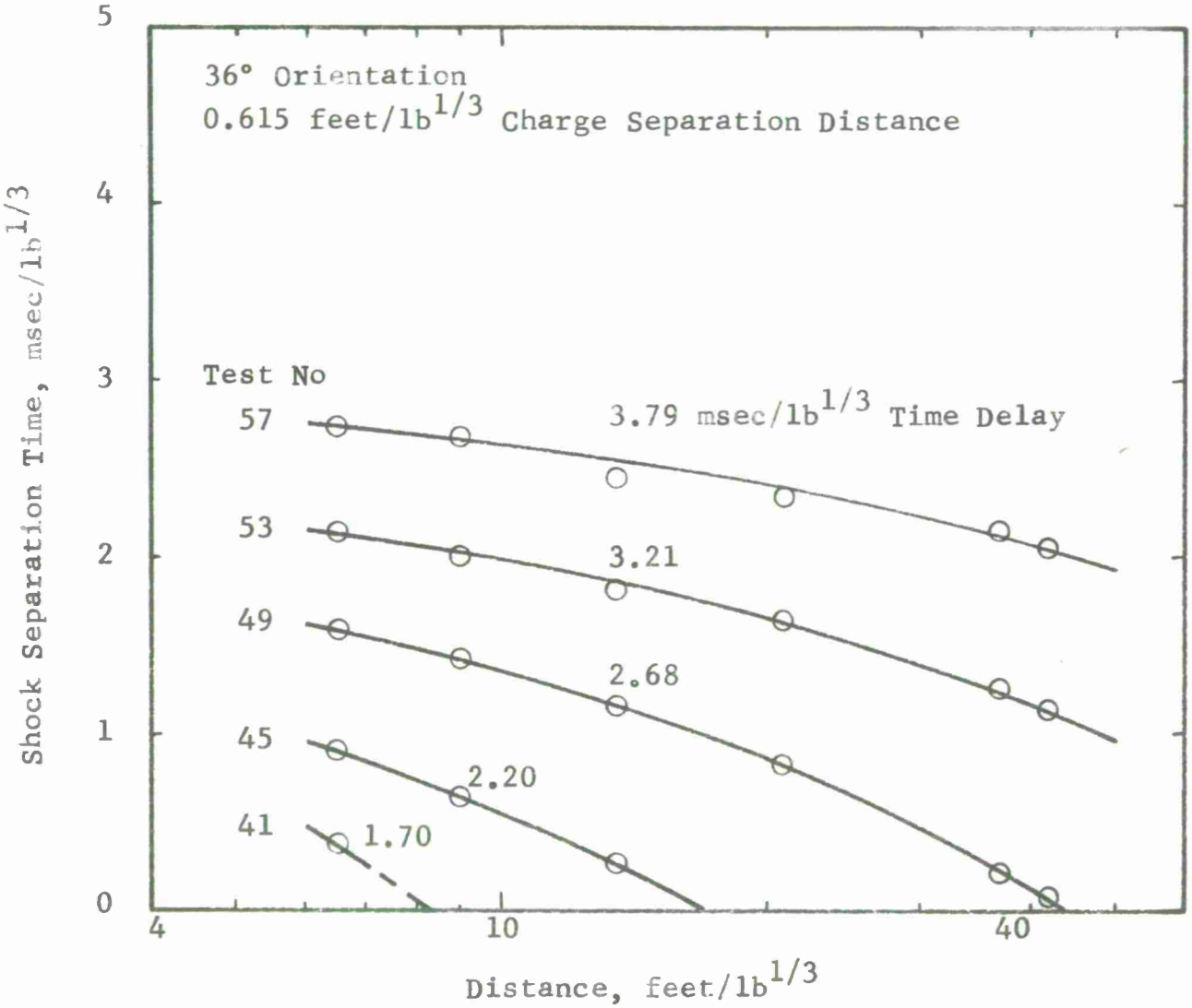

Figure A28 Shock Separation Time Data (36°-0.615 feet/lb$^{1/3}$)

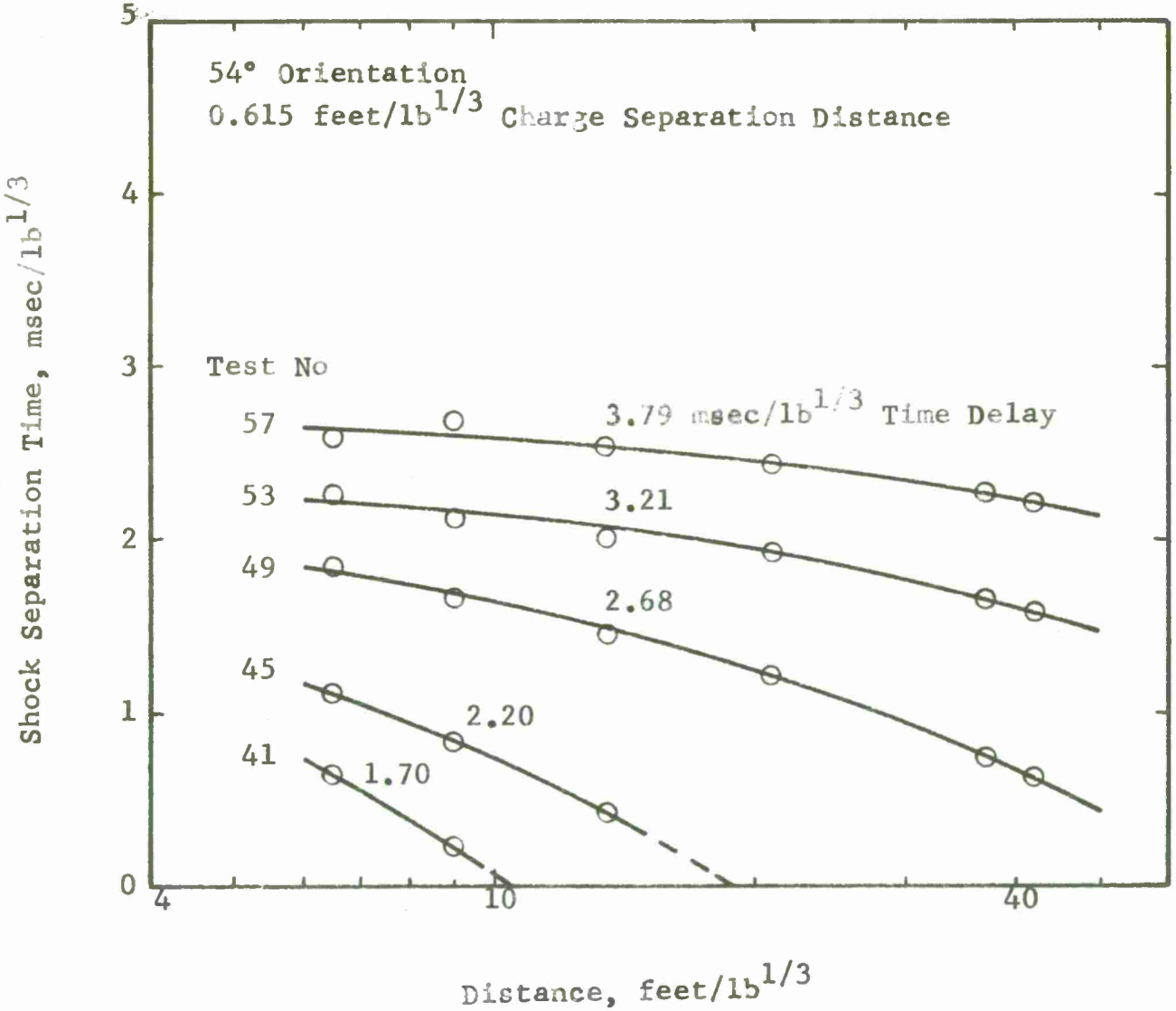

Figure A29 Shock Separation Time Data (54°-0.615 feet/lb$^{1/3}$)

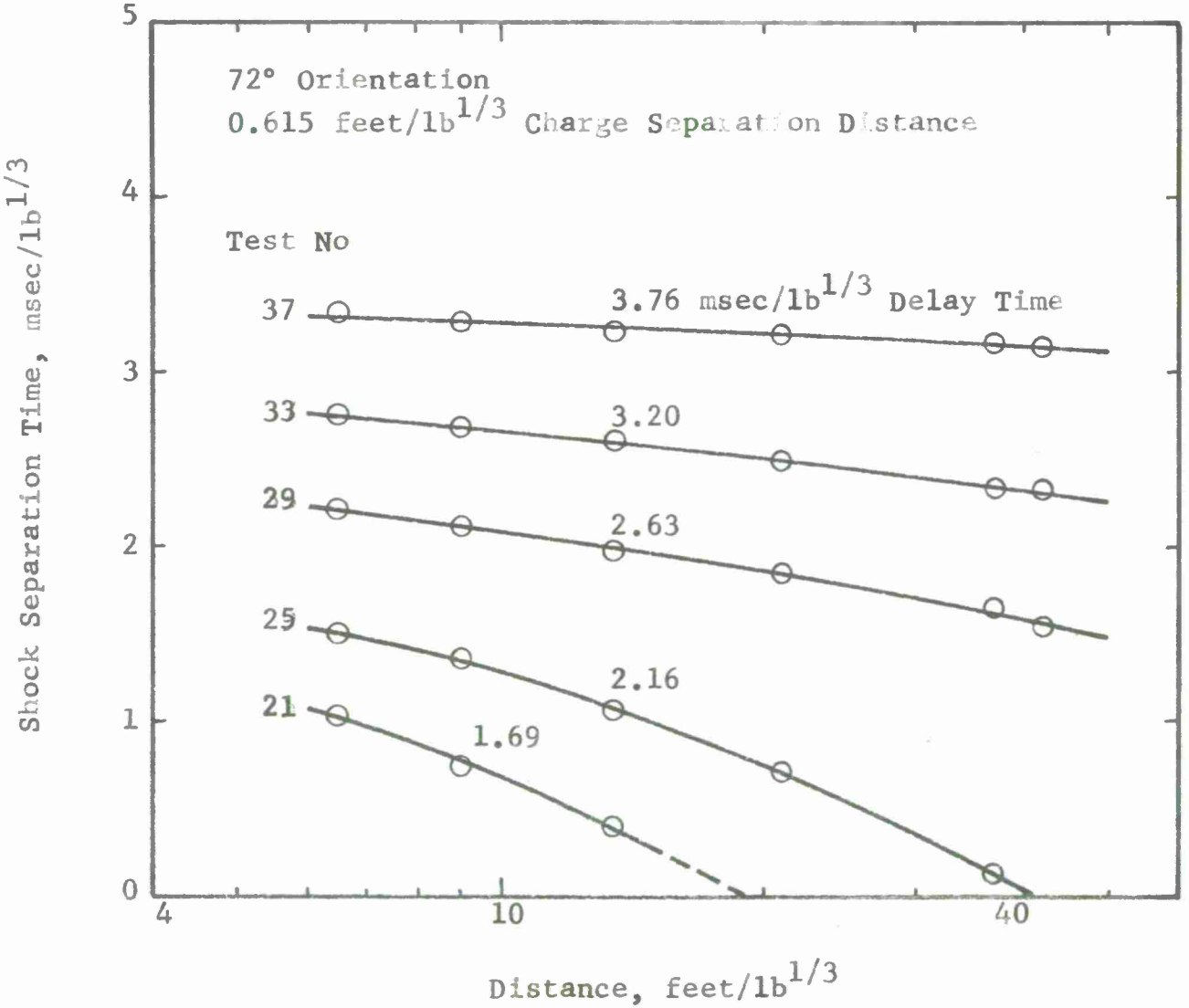

Figure A30 Shock Separation Time Data (72°-0.615 feet/lb$^{1/3}$)

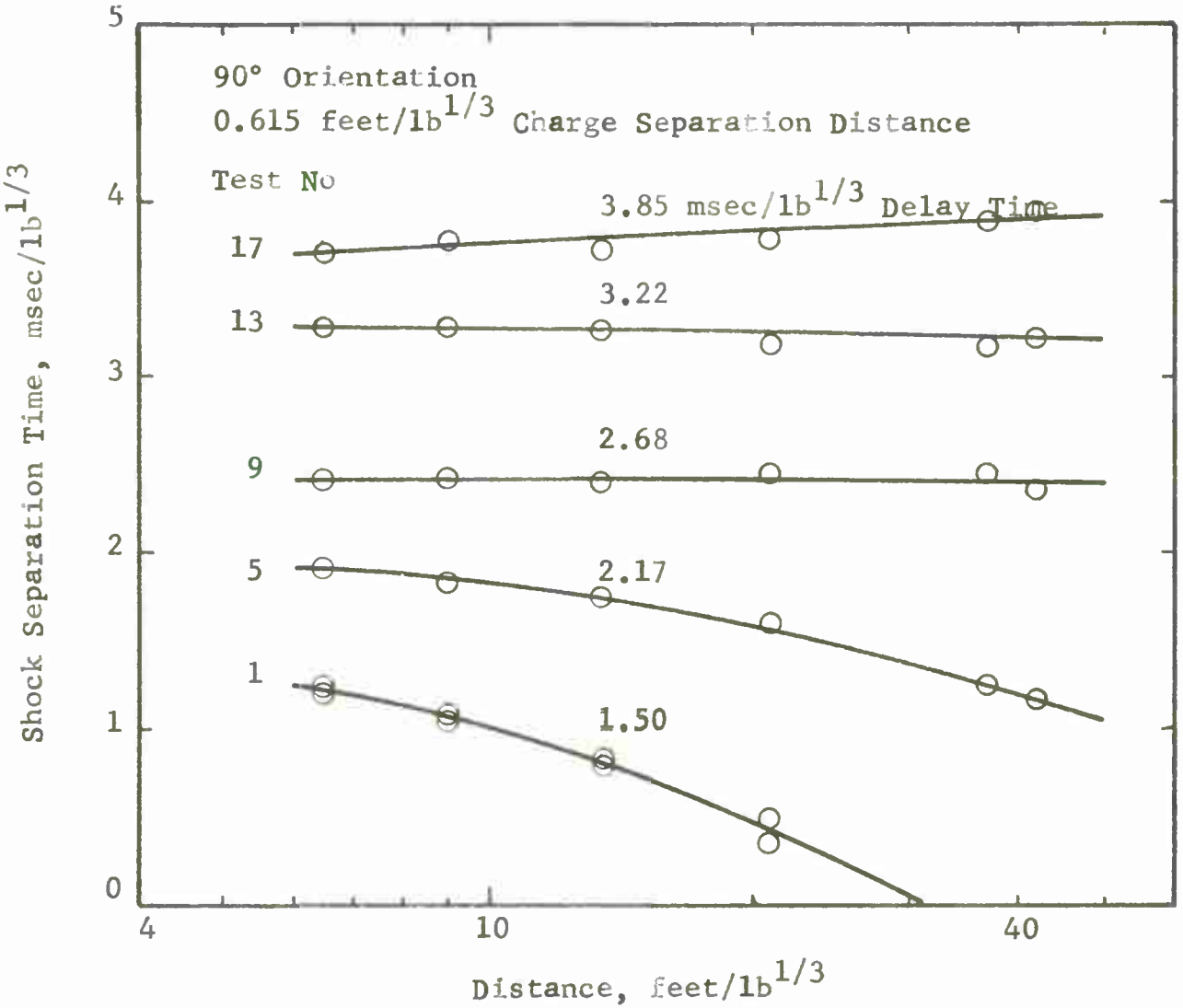

Figure A31 Shock Separation Time Data (90°-0.615 feet/lb$^{1/3}$)

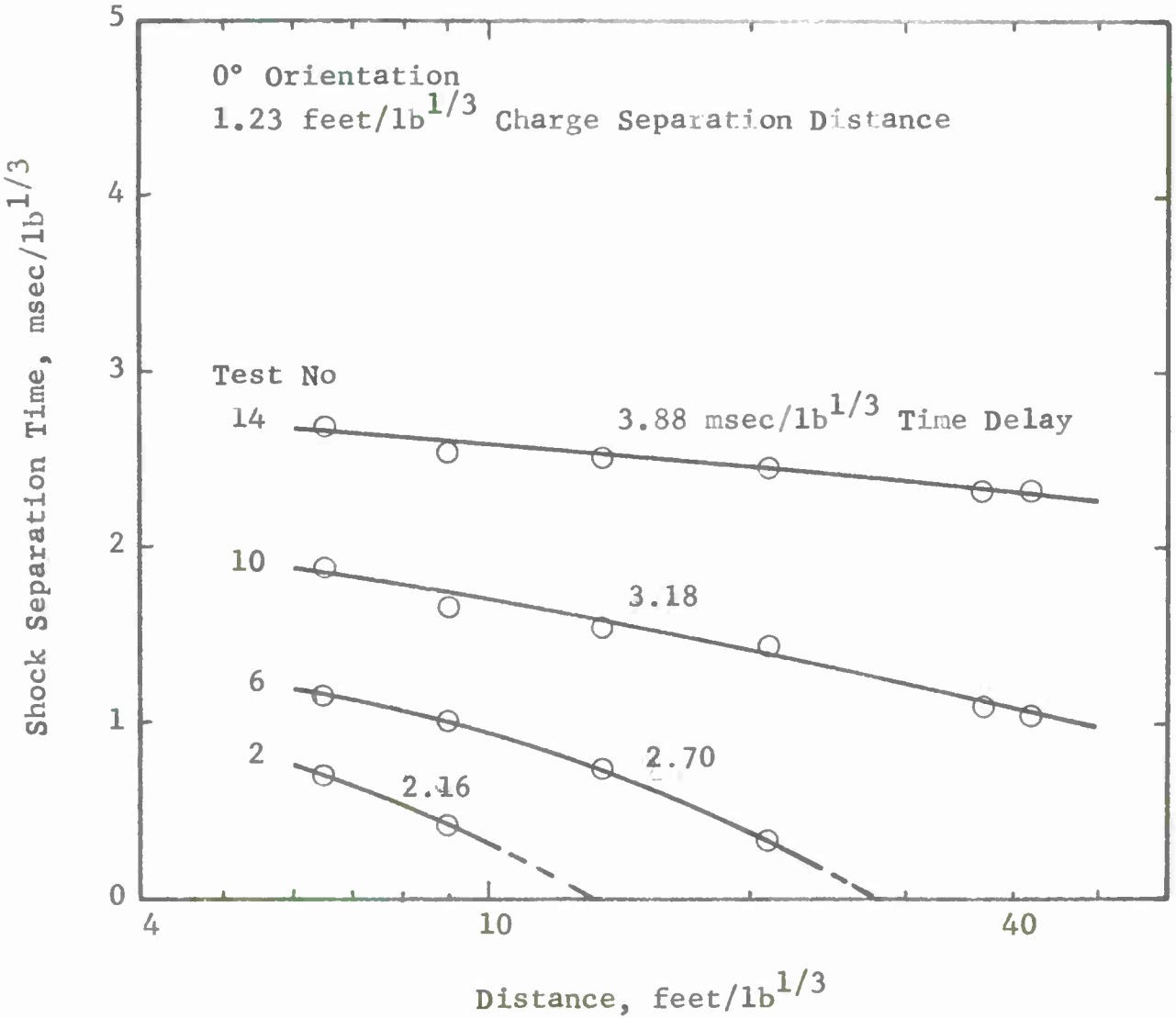

Figure A32 Shock Separation Time Data (0°-1.23 feet/lb$^{1/3}$)

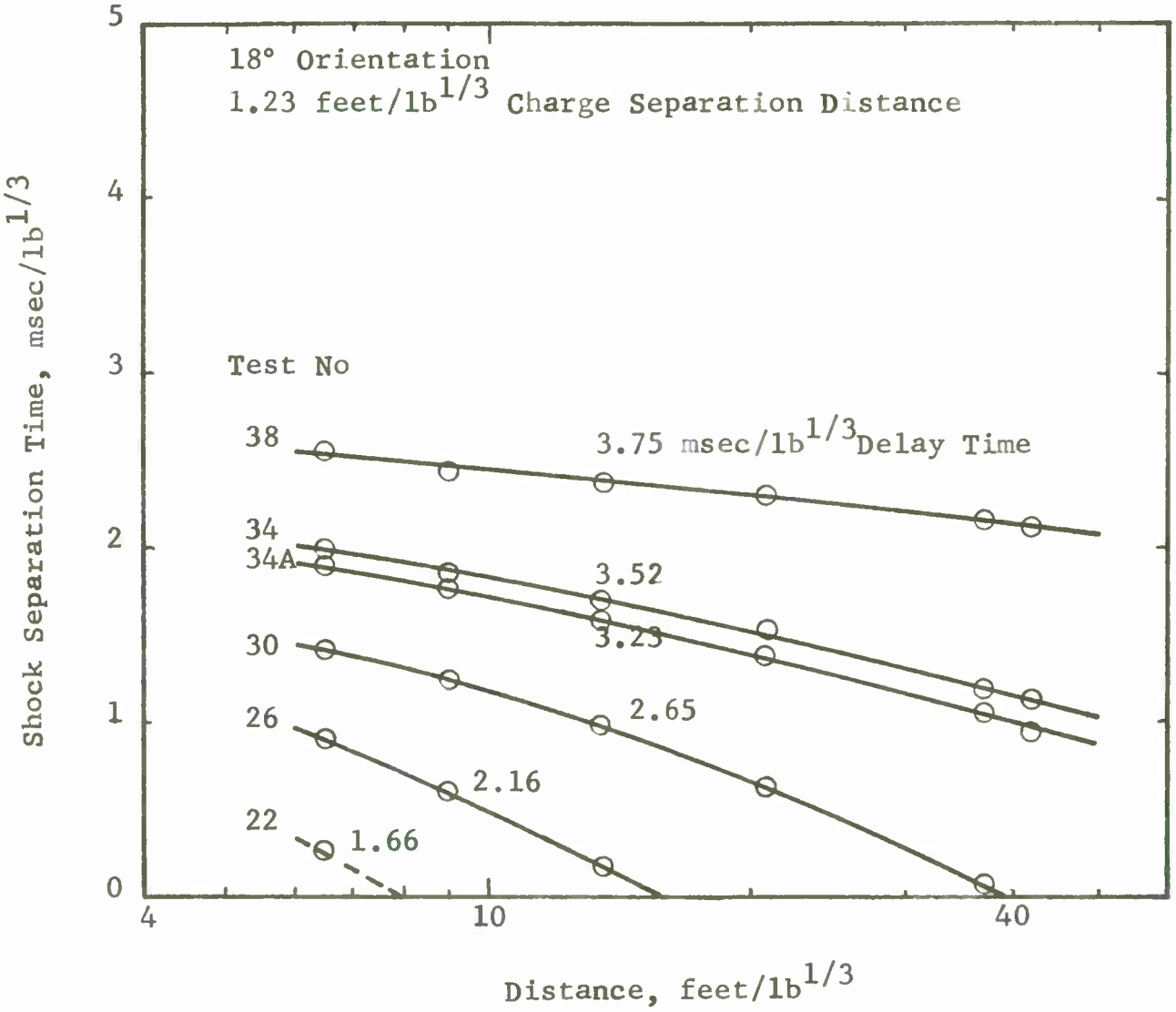

Figure A33 Shock Separation Time Data (18°-1.23 feet/lb$^{1/3}$)

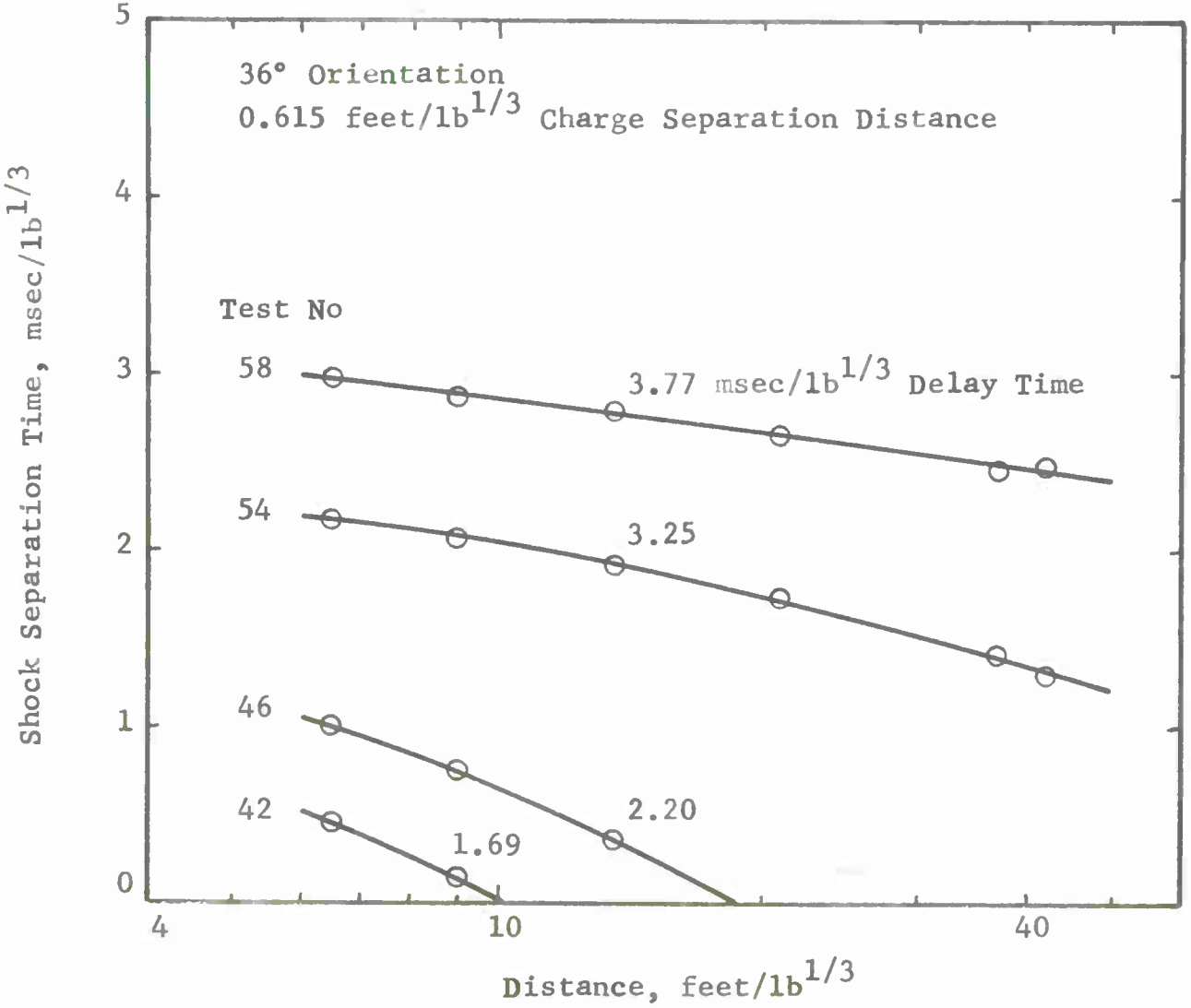

Figure A34 Shock Separation Time Data (36°-1.23 feet/lb$^{1/3}$)

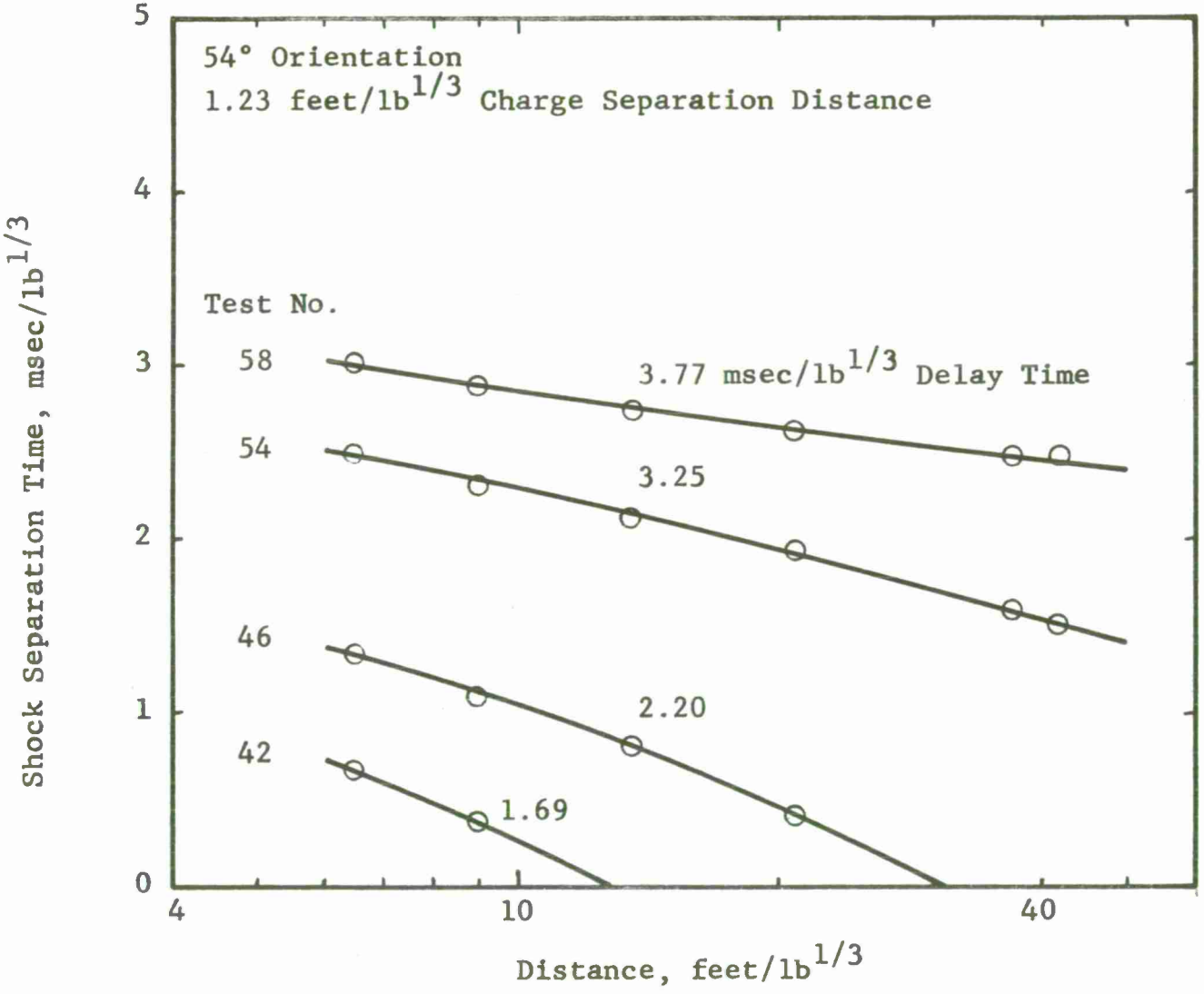

Figure A35 Shock Separation Time Data (54°, 1.23 feet/lb$^{1/3}$)

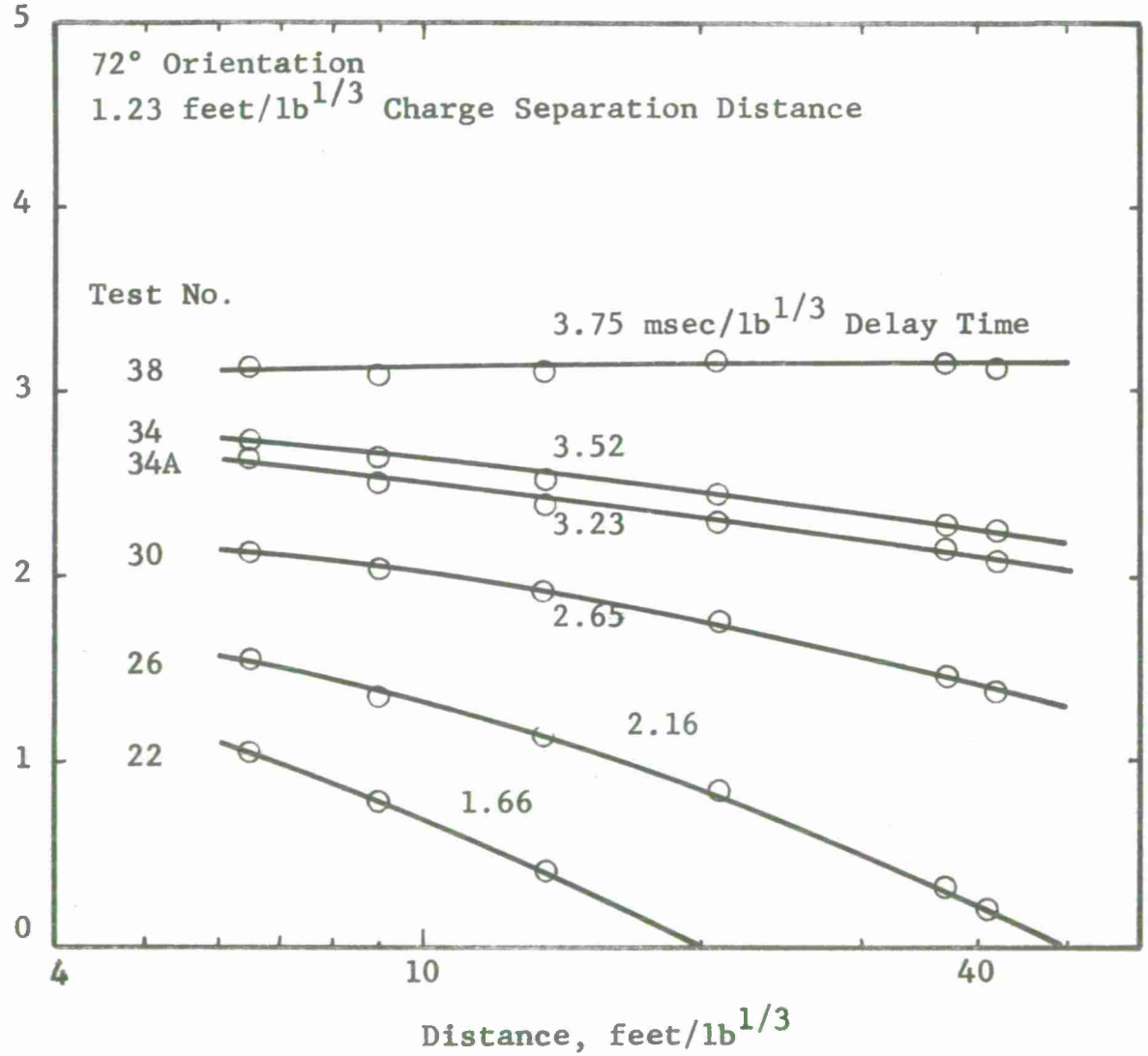

Figure A36 Shock Separation Time Data (72°, 1.23 feet/lb$^{1/3}$)

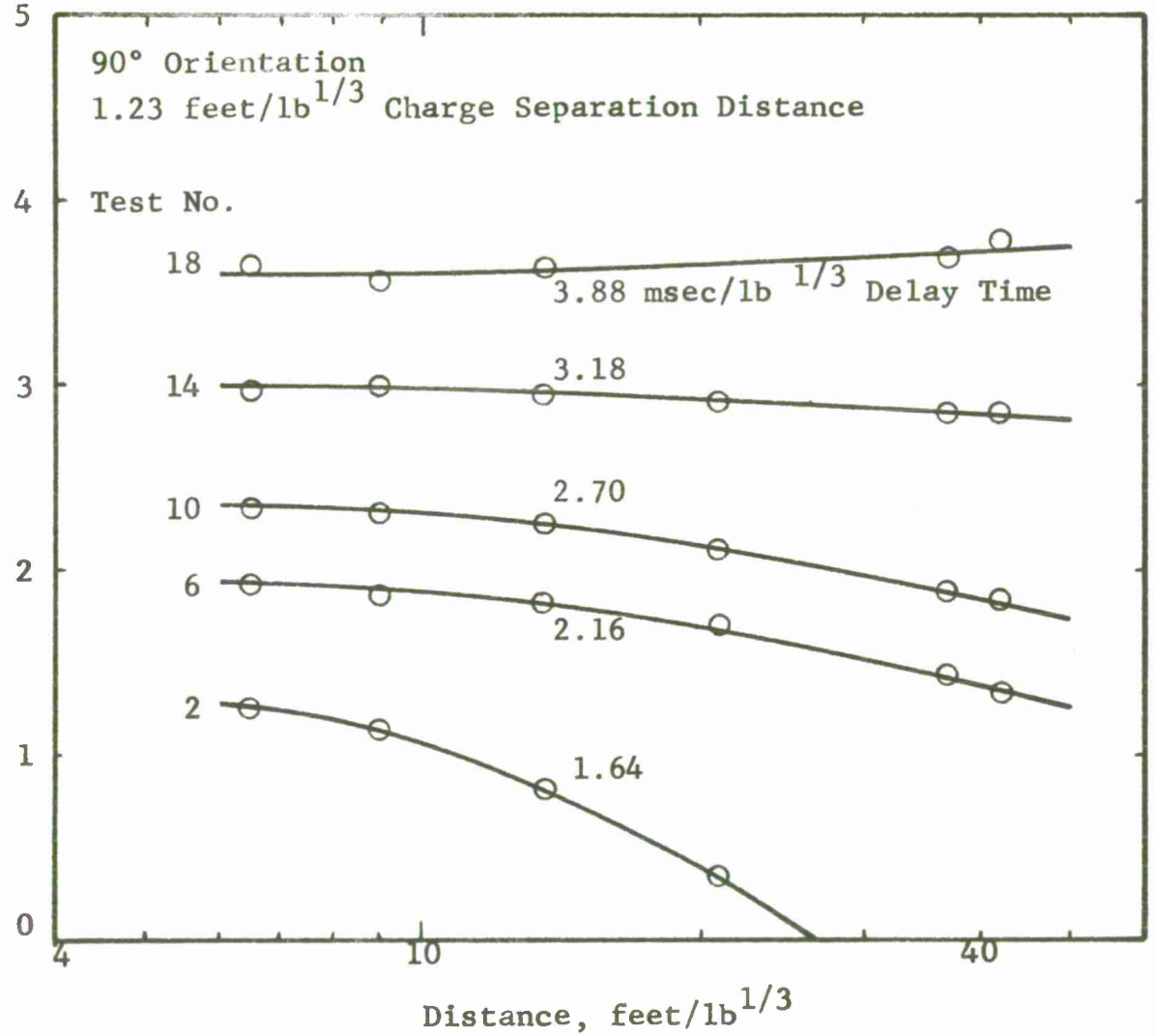

Figure A37 Shock Separation Time Data (90°, 1.23 feet/lb$^{1/3}$)

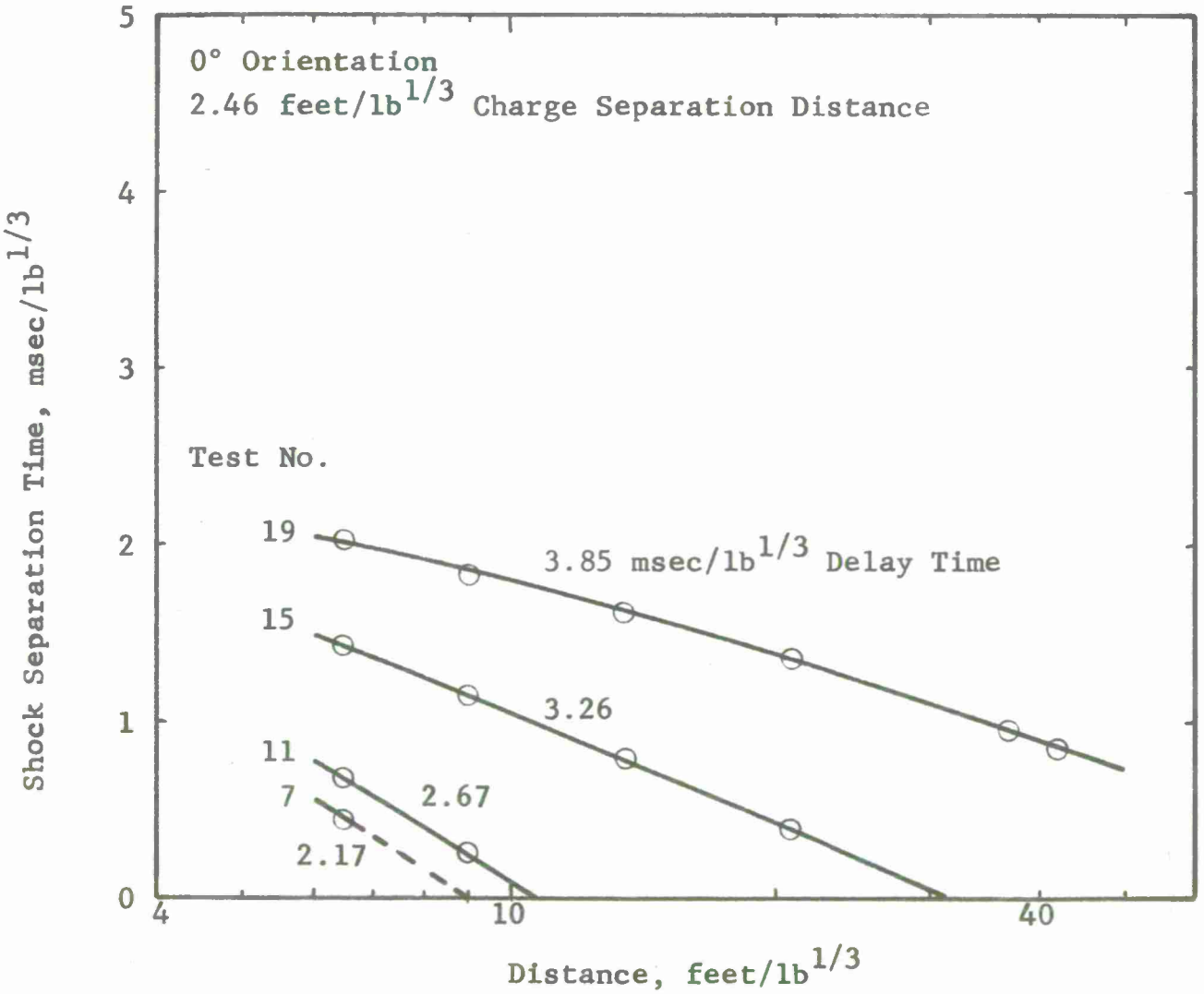

Figure A38 Shock Separation Time Data (0°, 2.46 feet/lb$^{1/3}$)

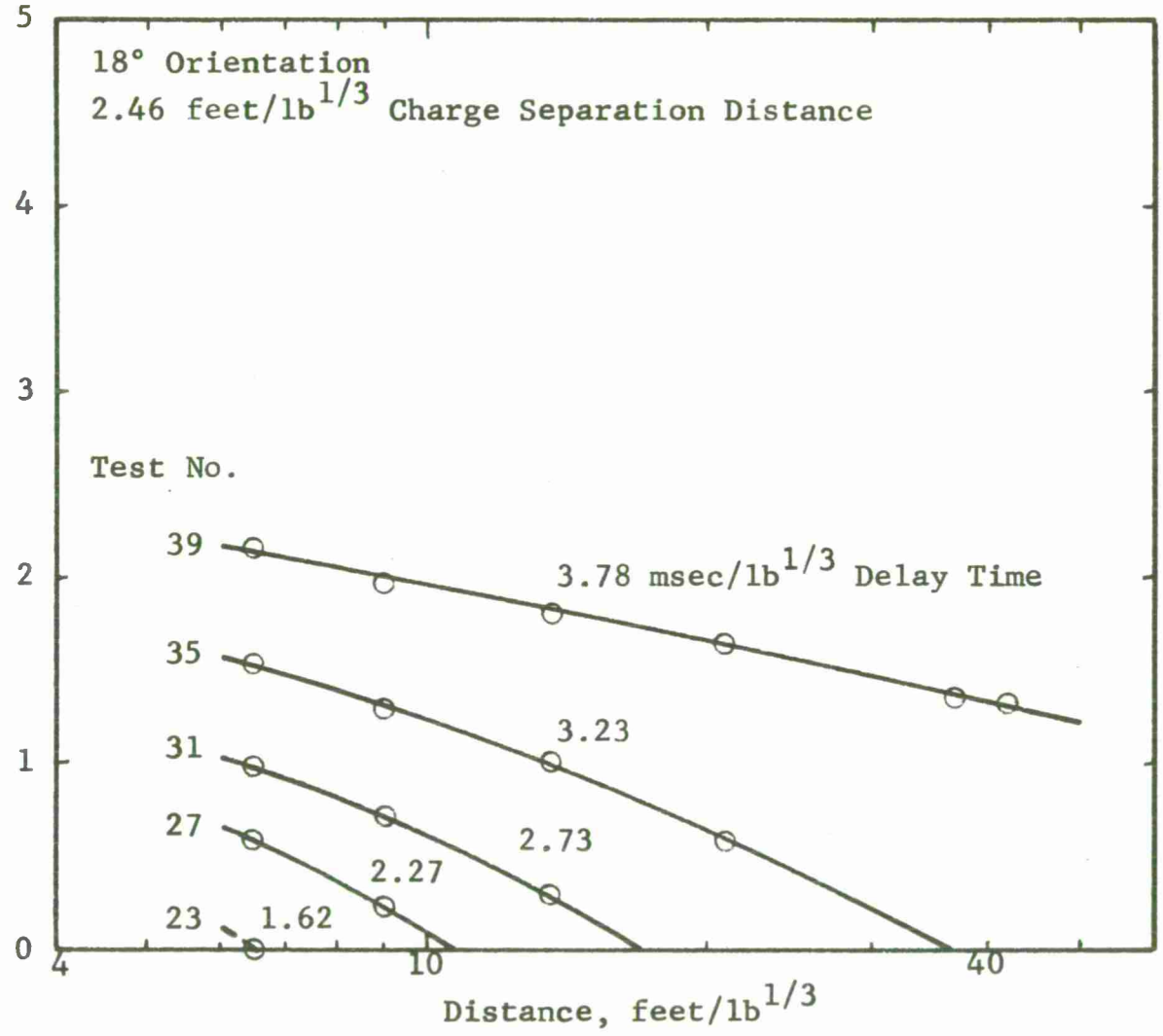

Figure A39 Shock Separation Time Data (18°, 2.46 feet/lb$^{1/3}$)

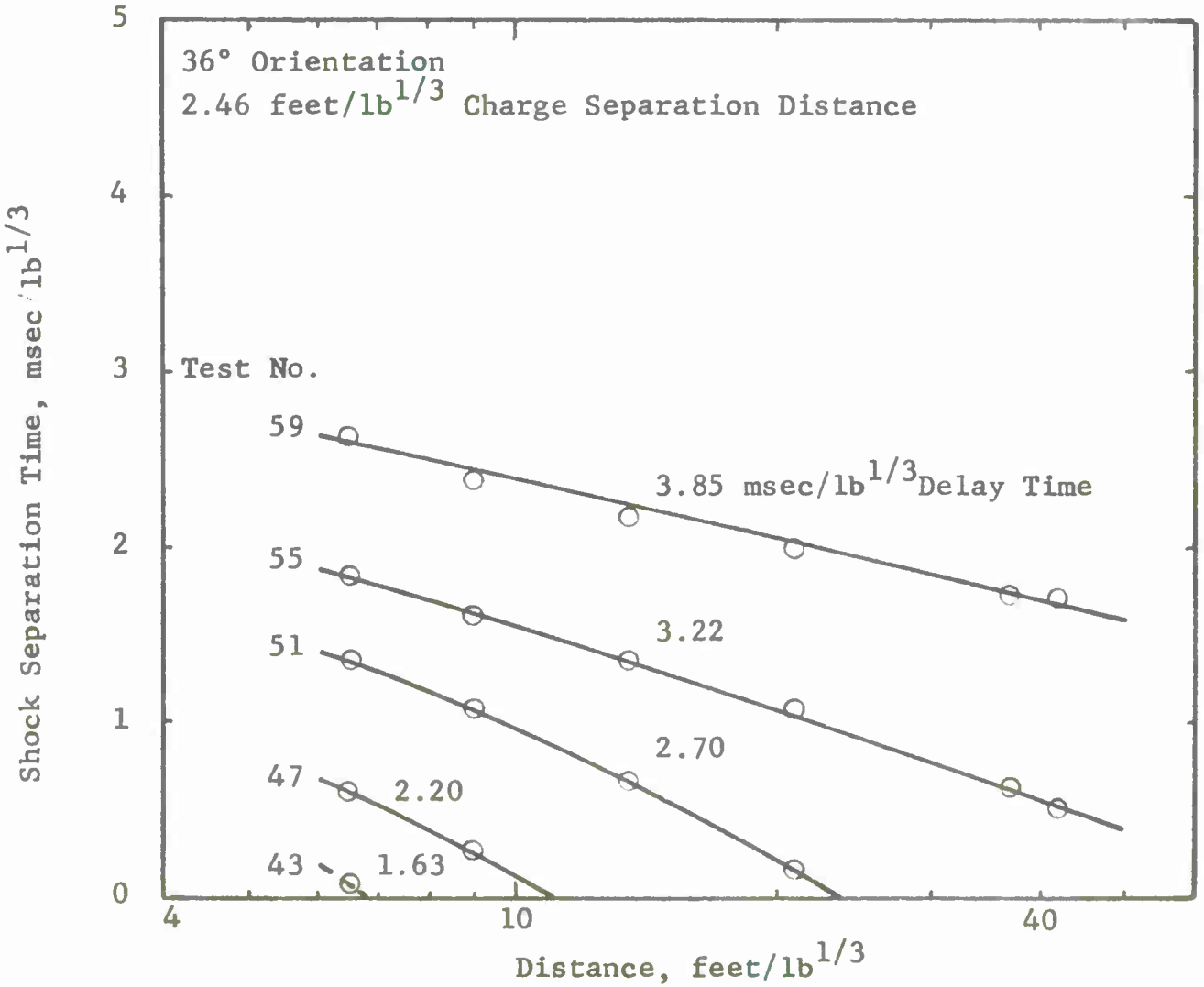

Figure A40 Shock Separation Time Data (36°, 2.46 feet/lb$^{1/3}$)

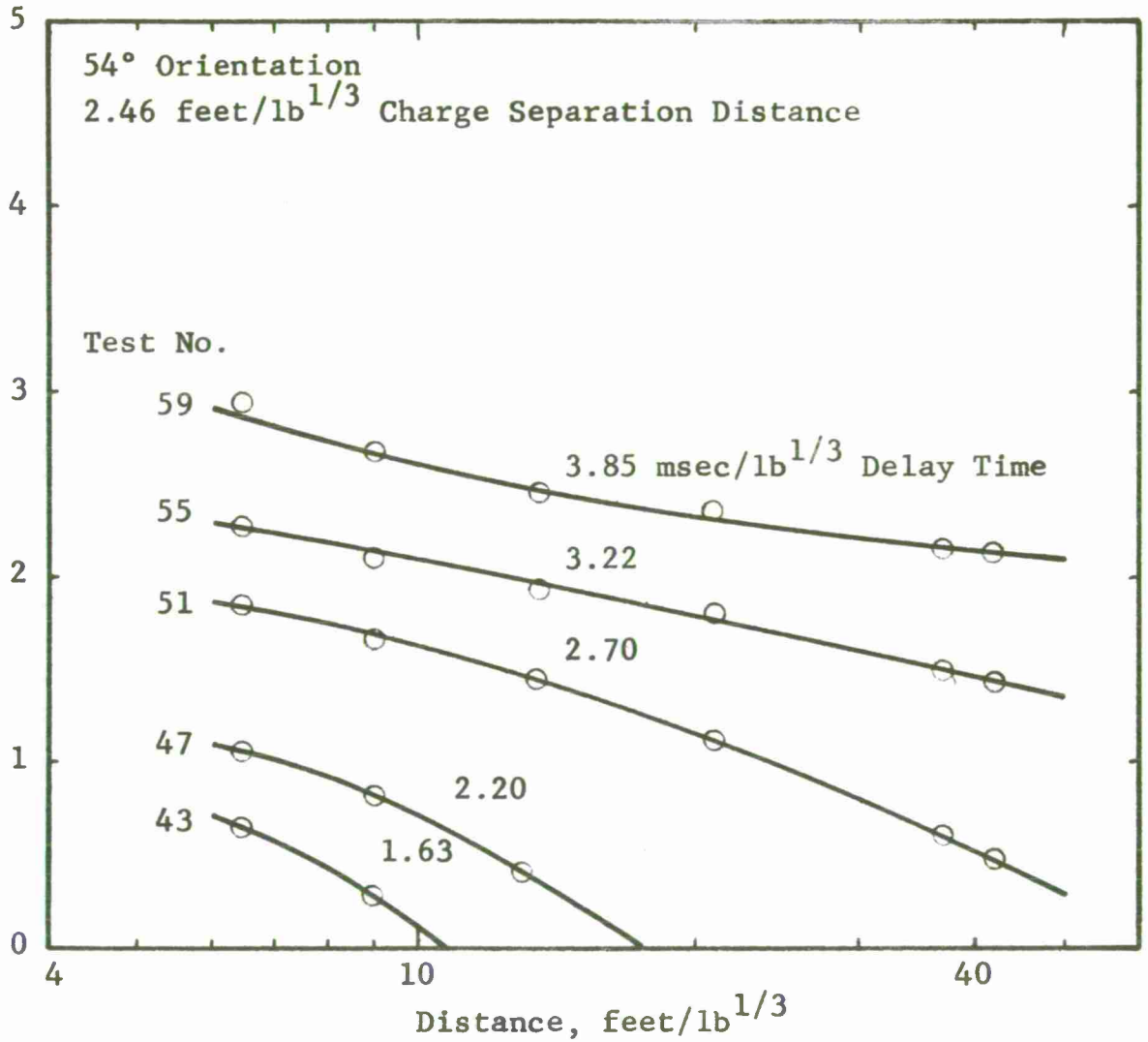

Figure A41 Shock Separation Time Data (54°, 2.46 feet/lb$^{1/3}$)

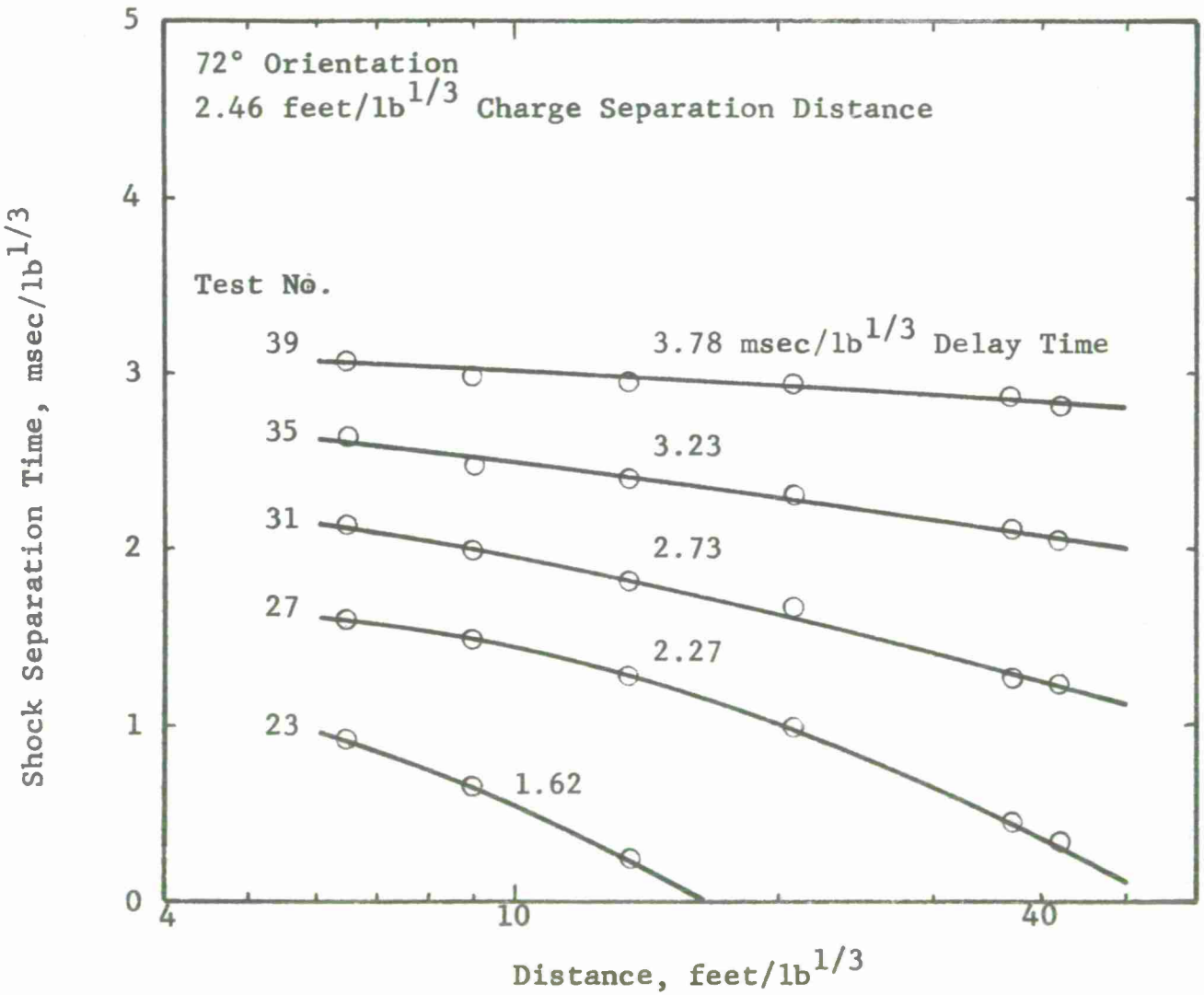

Figure A42 Shock Separation Time Data (72°, 2.46 feet/lb$^{1/3}$)

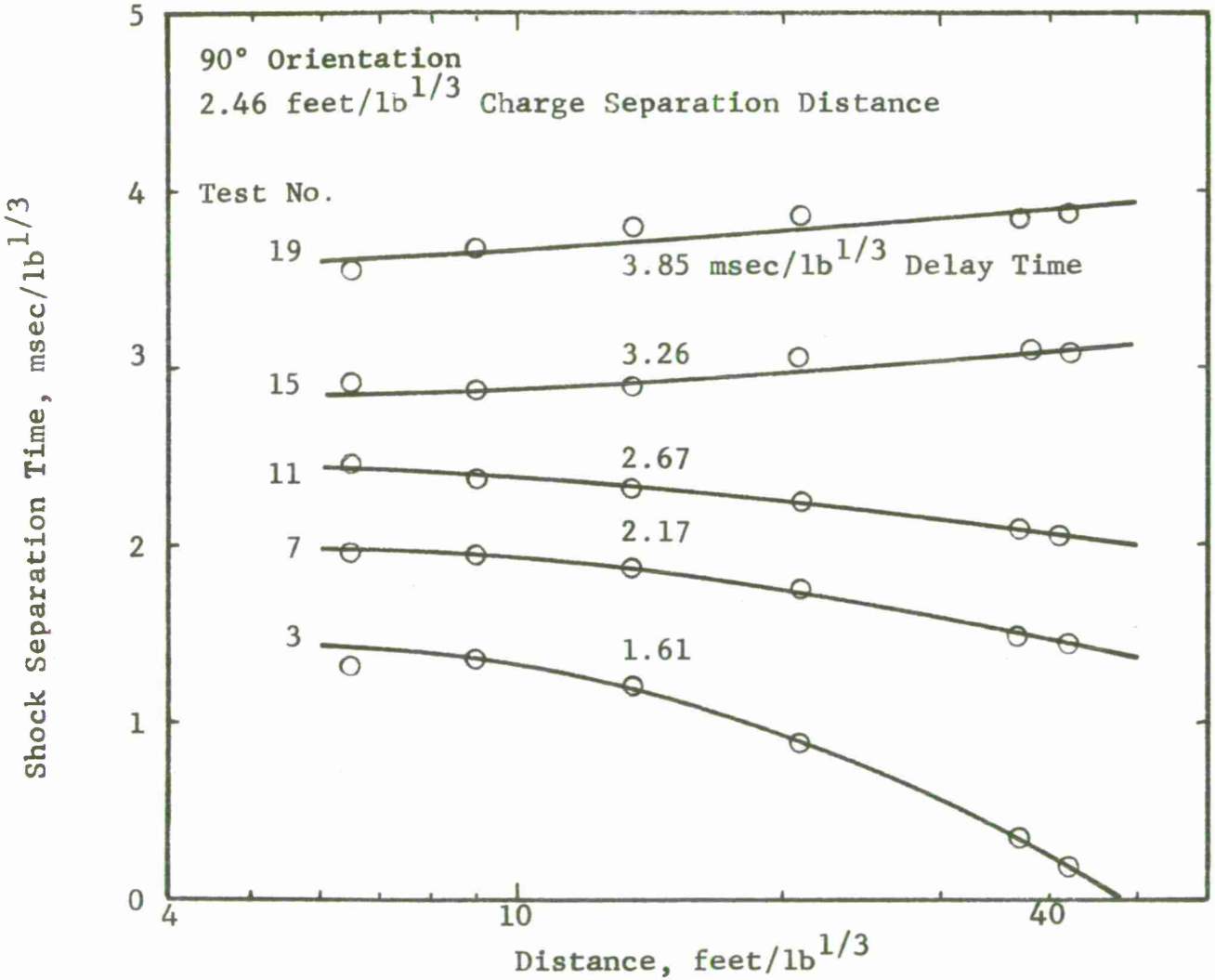

Figure A43 Shock Separation Time Data (90°, 2.46 feet/lb$^{1/3}$)

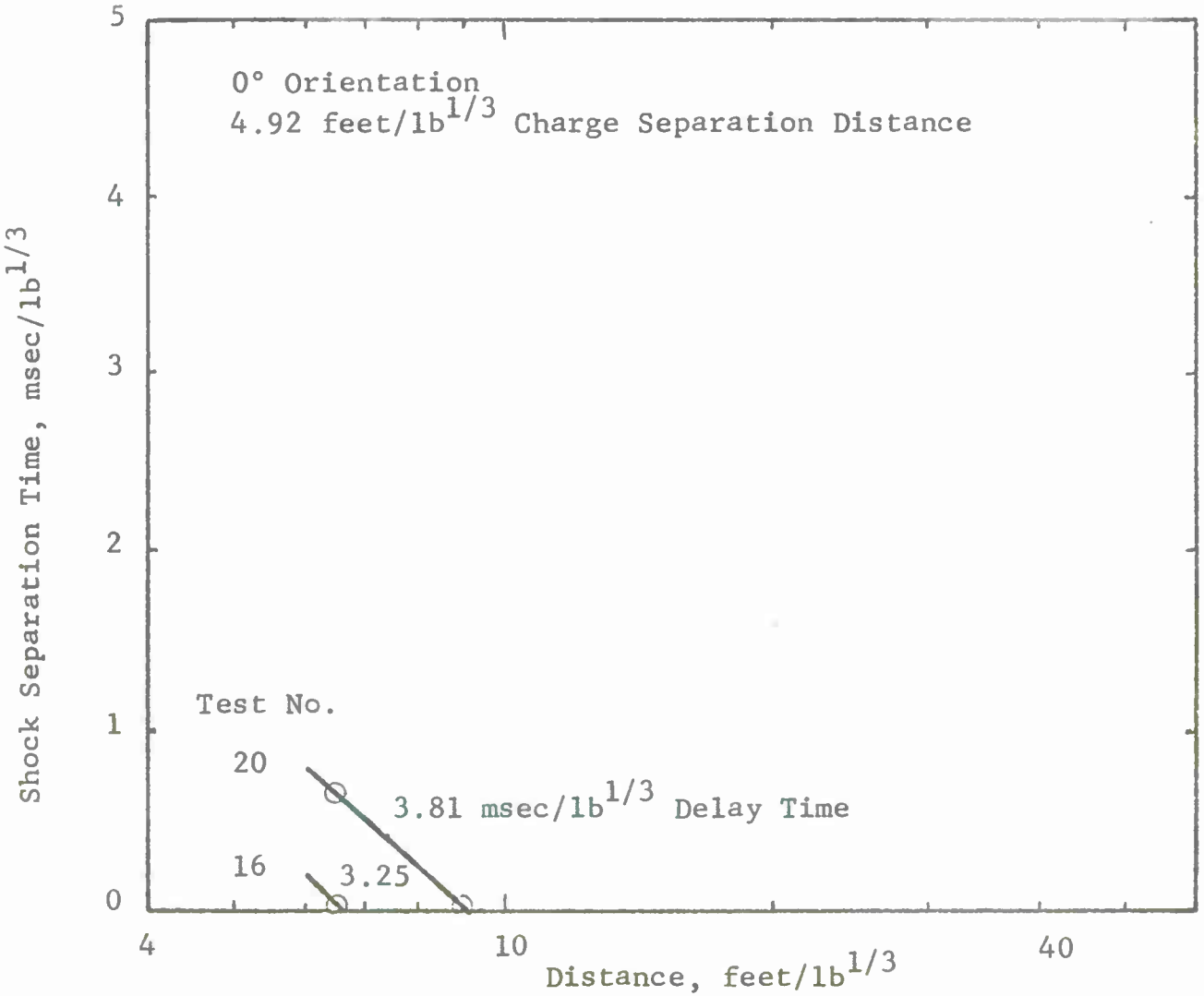

Figure A44 Shock Separation Time Data (0°, 4.92 feet/lb$^{1/3}$)

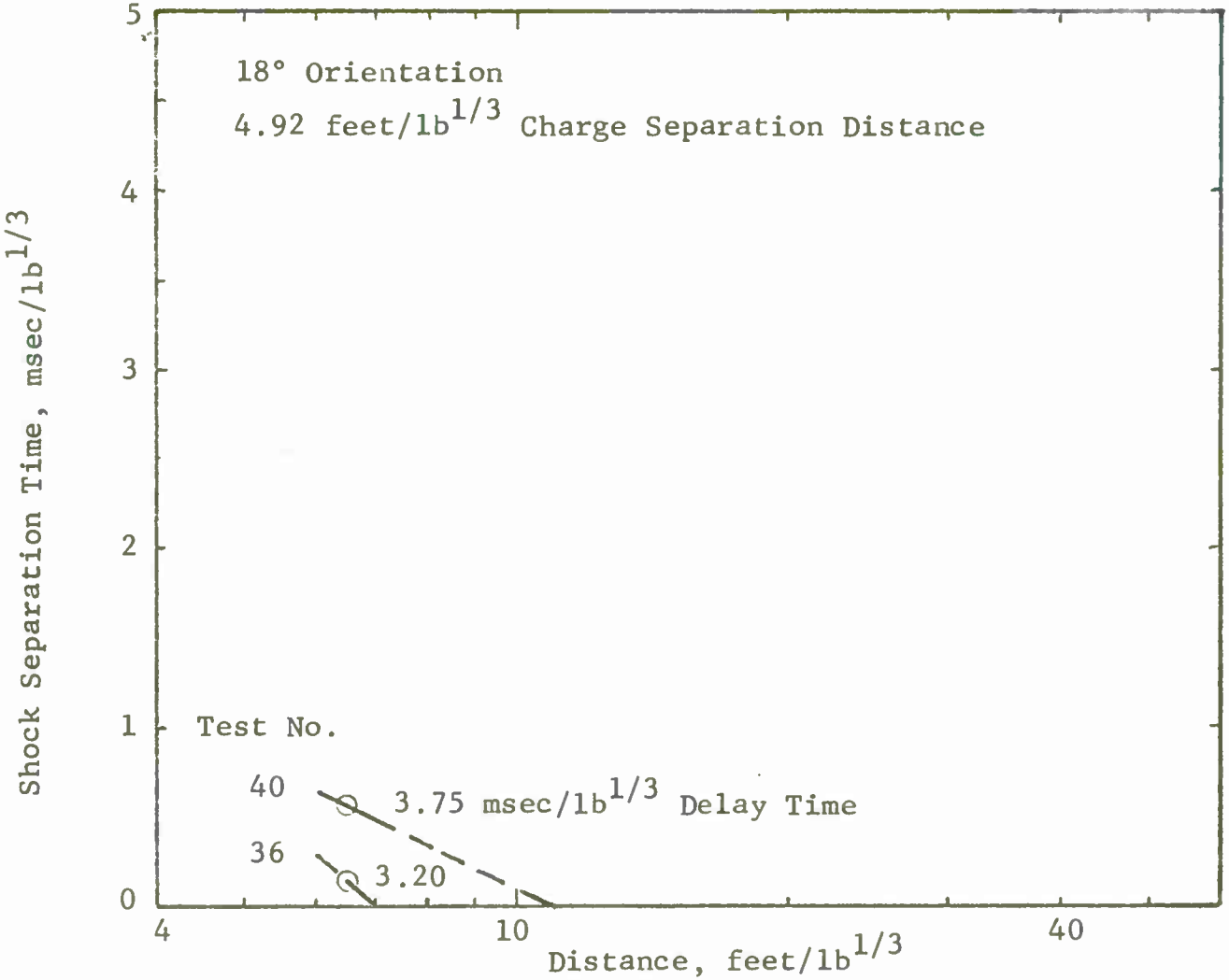

Figure A45 Shock Separation Time Data (18°, 4.92 feet/lb$^{1/3}$)

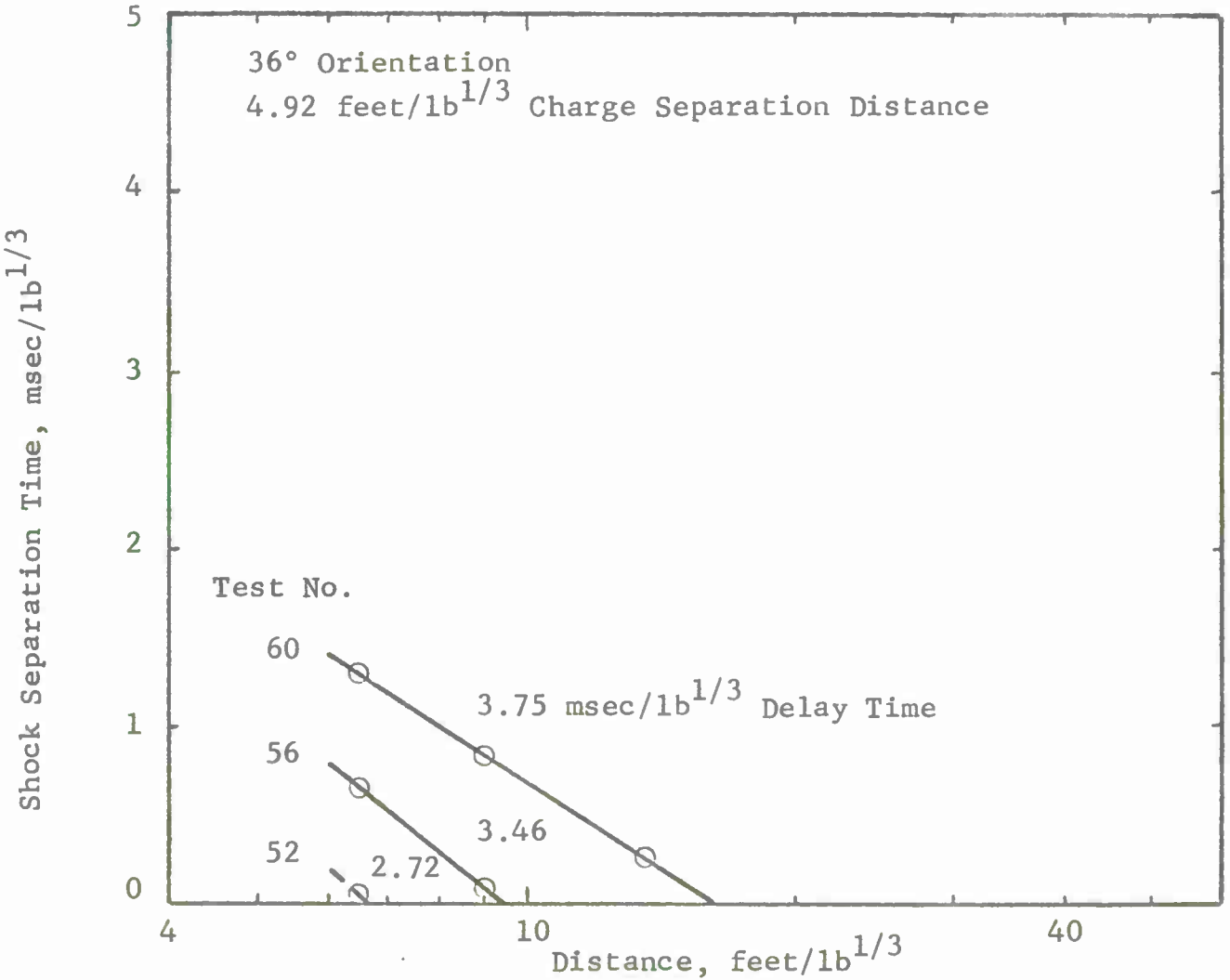

Figure A46 Shock Separation Time Data (36°, 4.92 feet/lb$^{1/3}$)

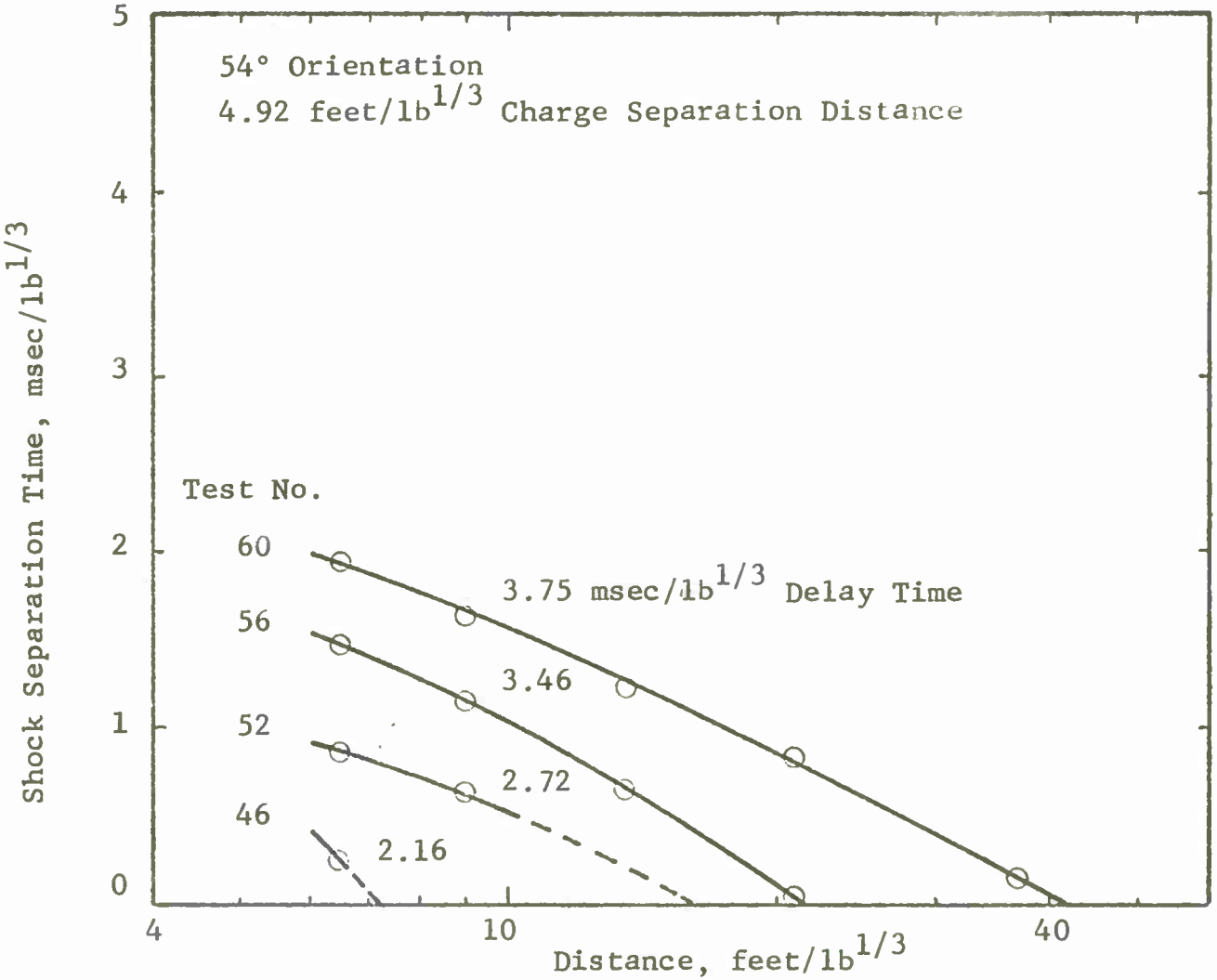

Figure A47 Shock Separation Time Data (54°, 4.92 feet/lb$^{1/3}$)

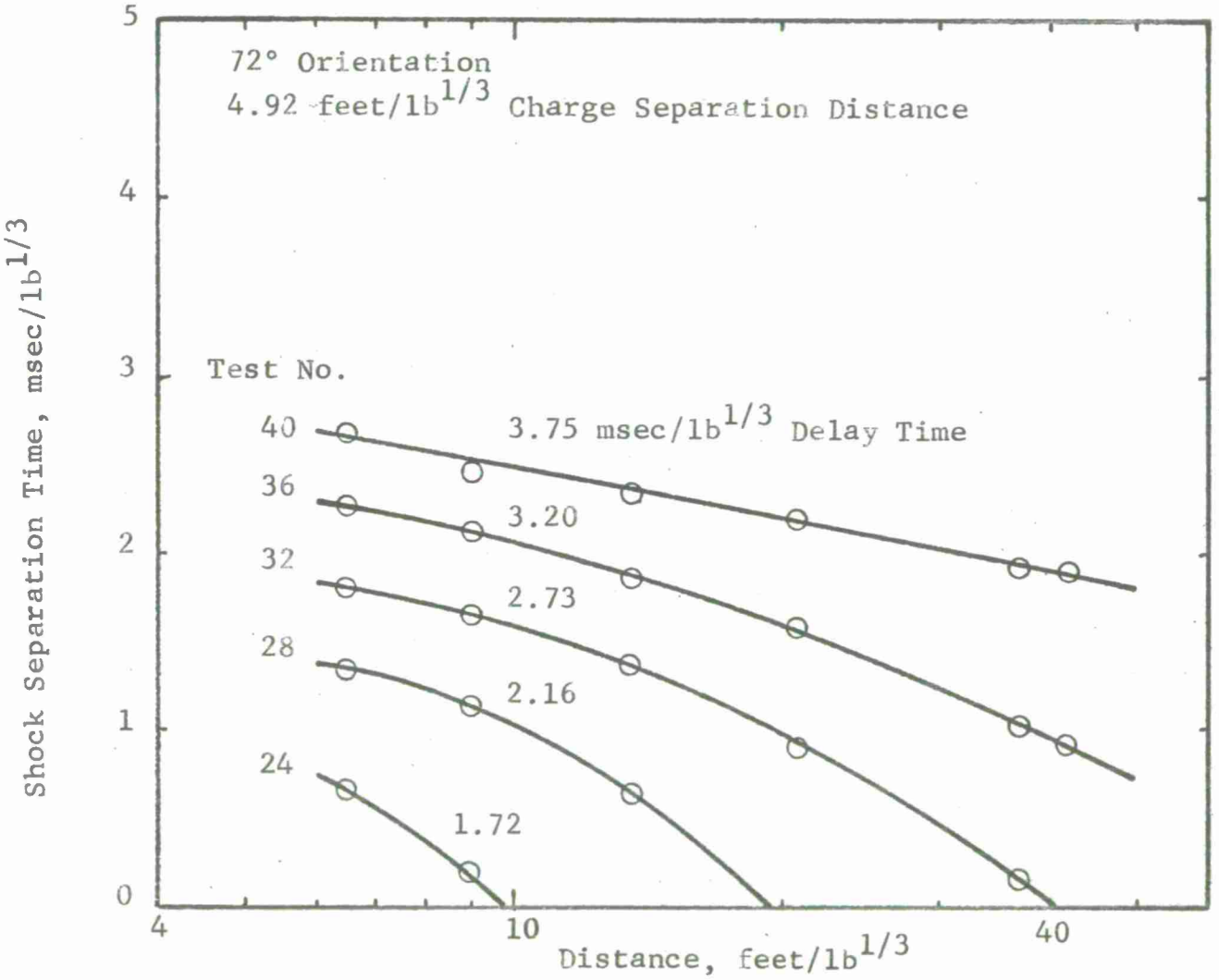

Figure A48 Shock Separation Time Data (72°, 4.92 feet/lb$^{1/3}$)

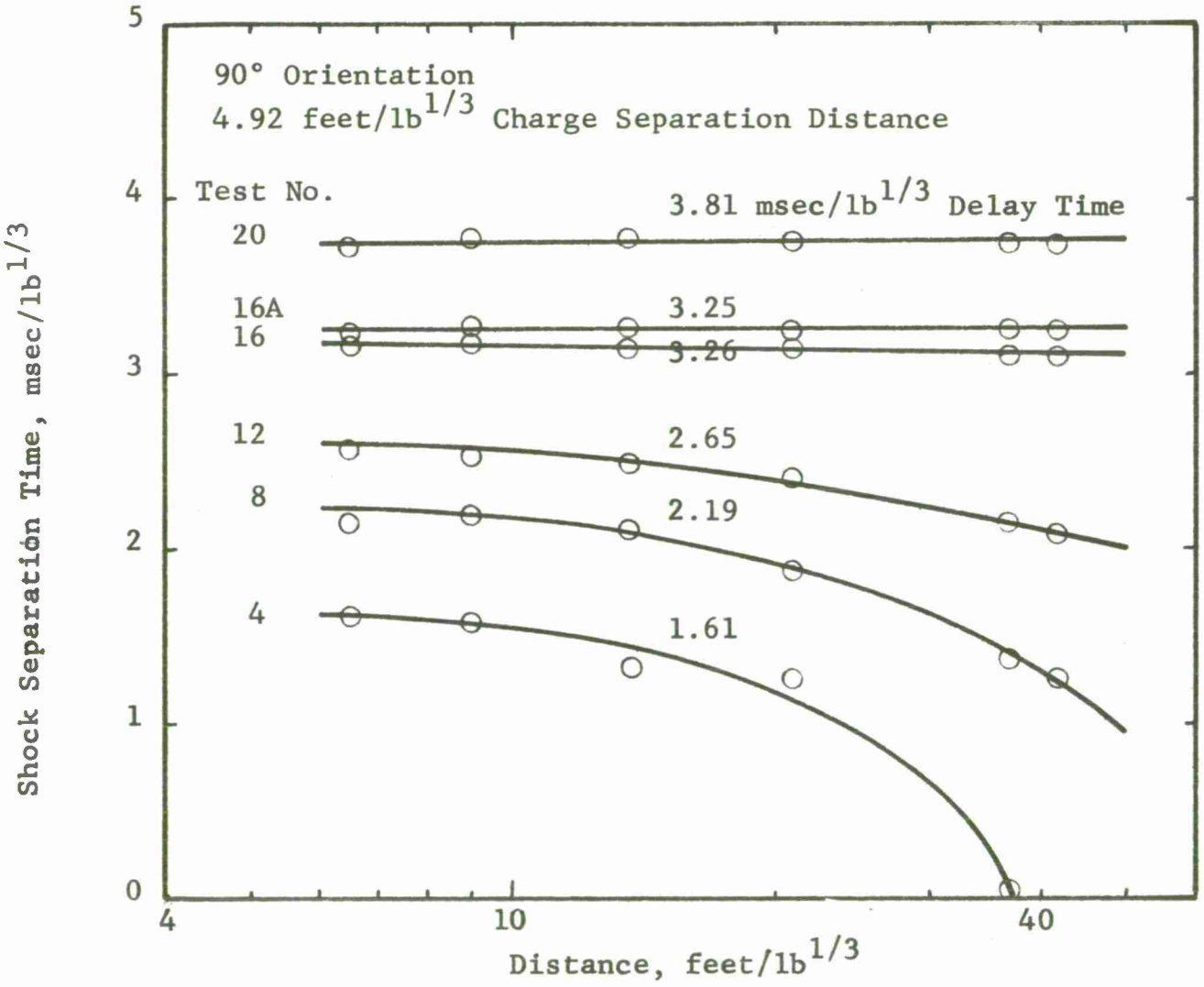

Figure A49 Shock Separation Time Data (90°, 4.92 feet/lb$^{1/3}$)

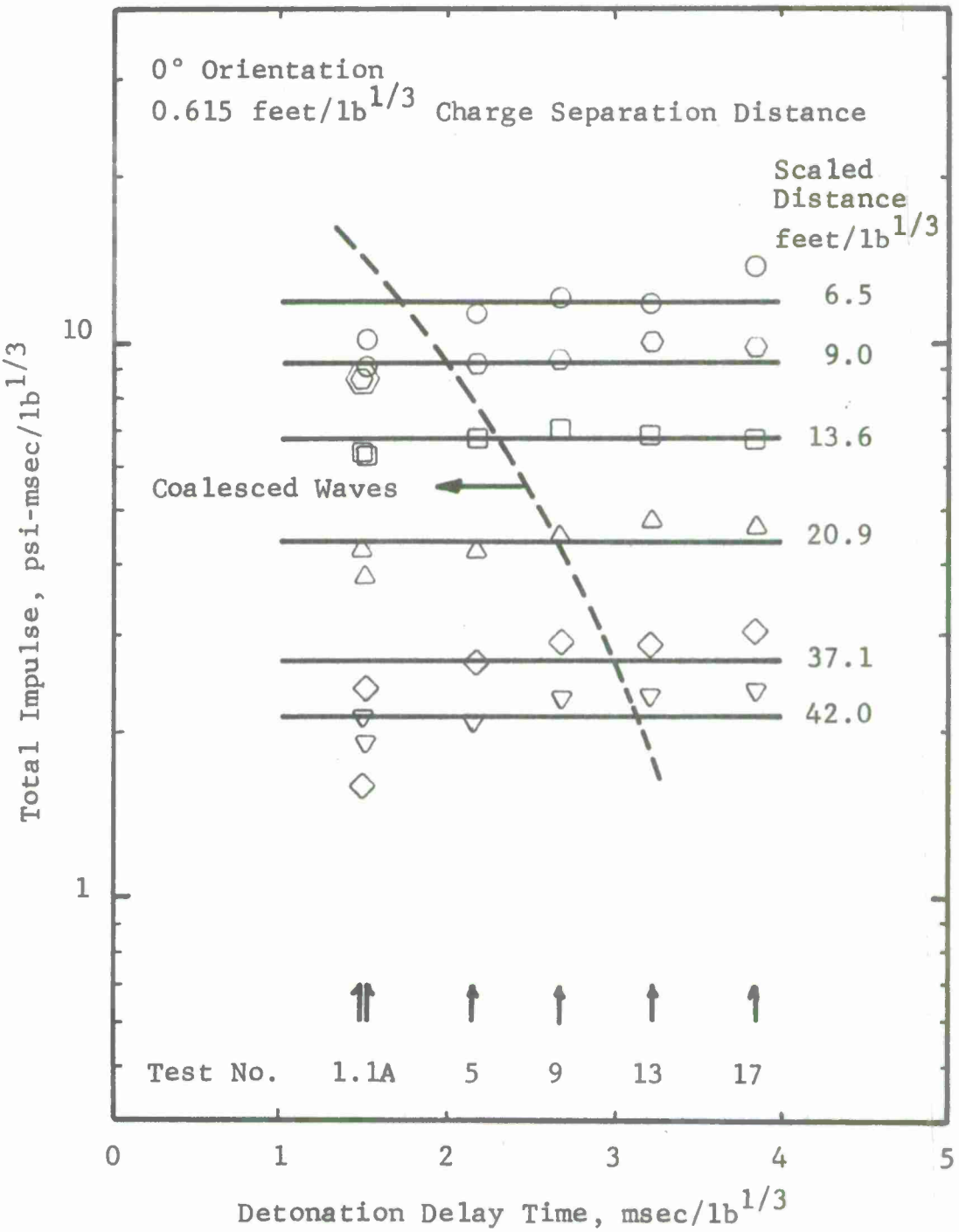

Figure A50 Total Impulse (0°,0.615 feet/lb$^{1/3}$)

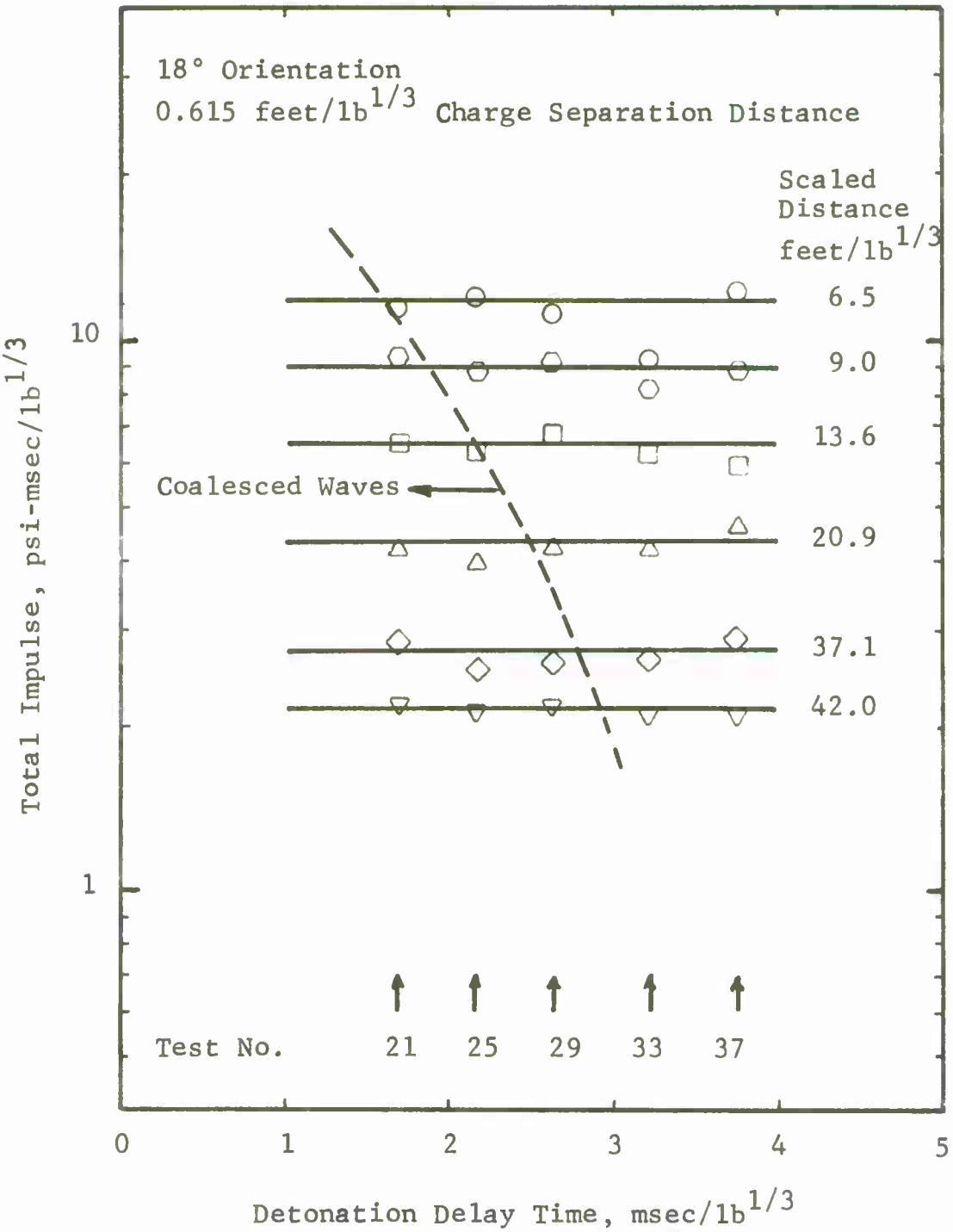

Figure A51 Total Impulse (18°,0.615 feet/lb$^{1/3}$)

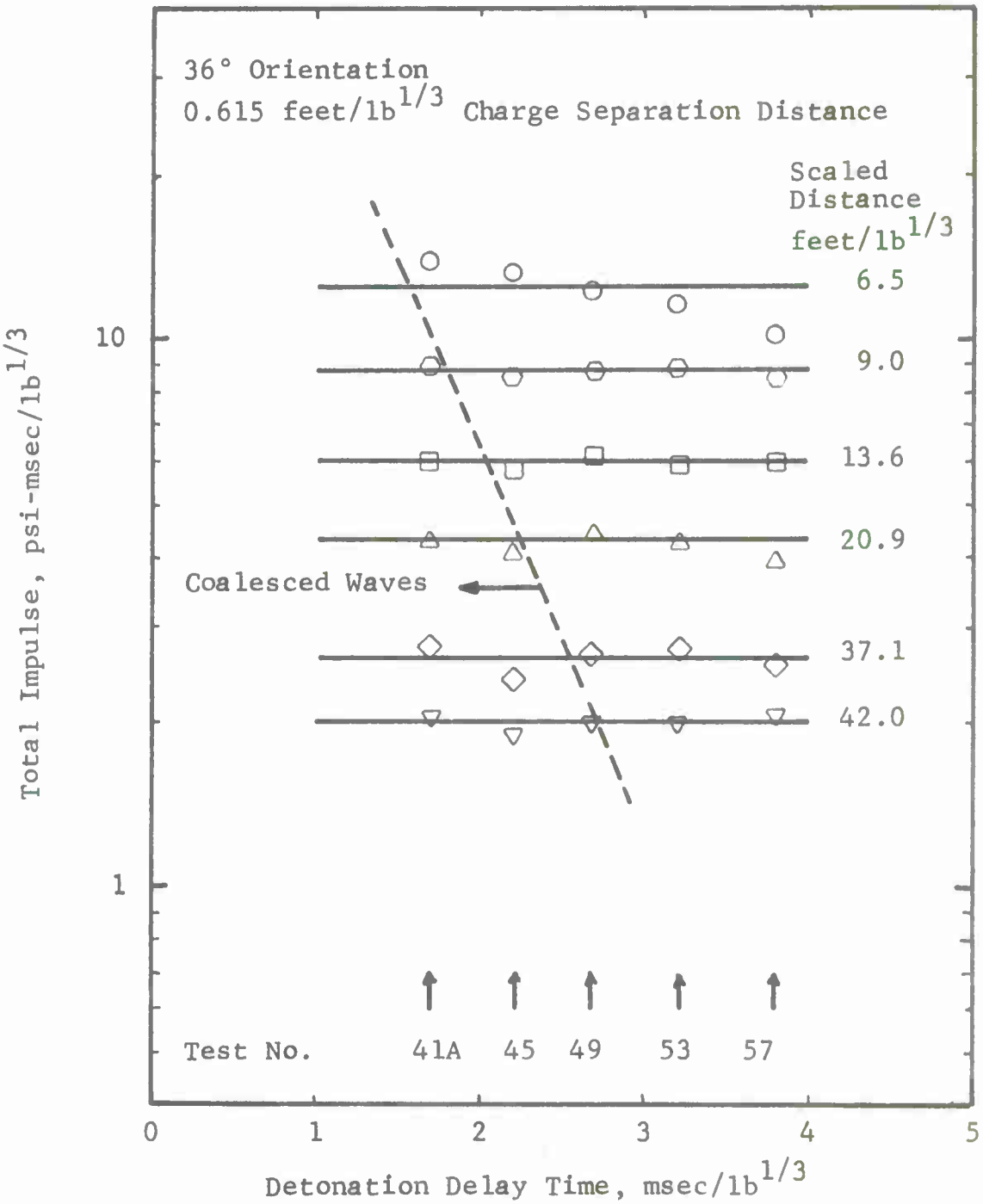

Figure A52 Total Impulse (36°,0.615 feet/lb$^{1/3}$)

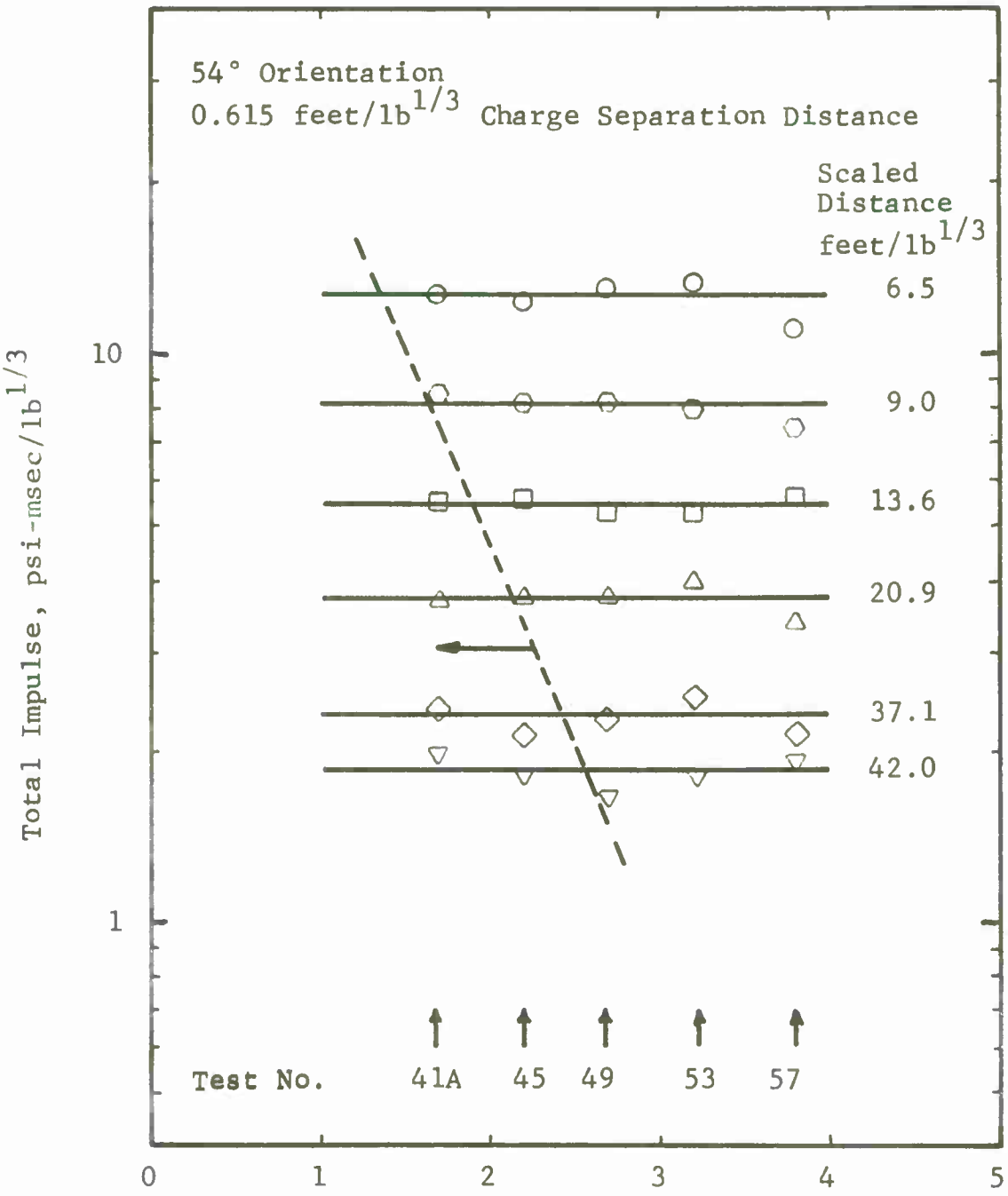

Figure A53 Total Impulse (54°, 0.615 feet/lb$^{1/3}$)

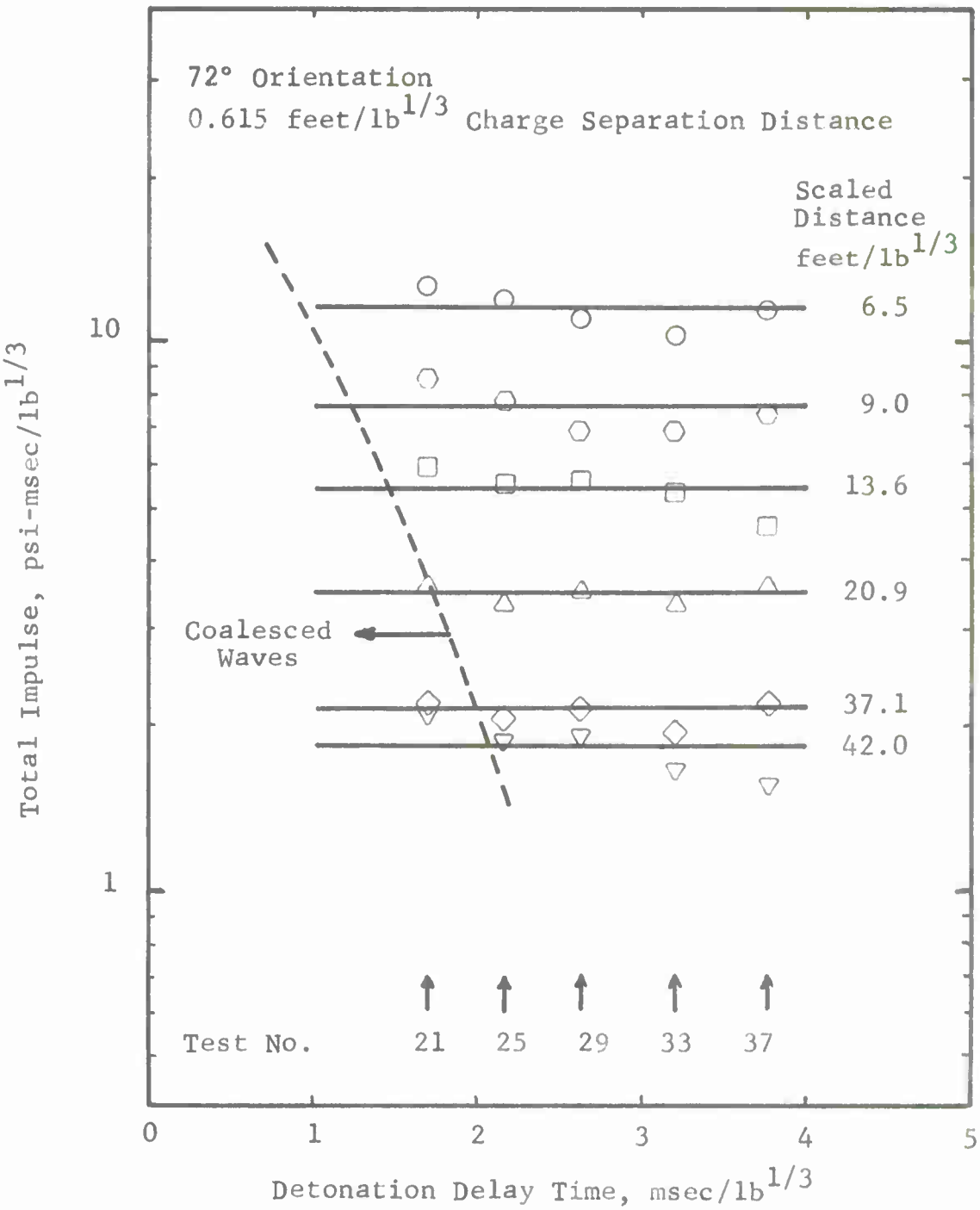

Figure A54 Total Impulse (72°, 0.615 feet/lb$^{1/3}$)

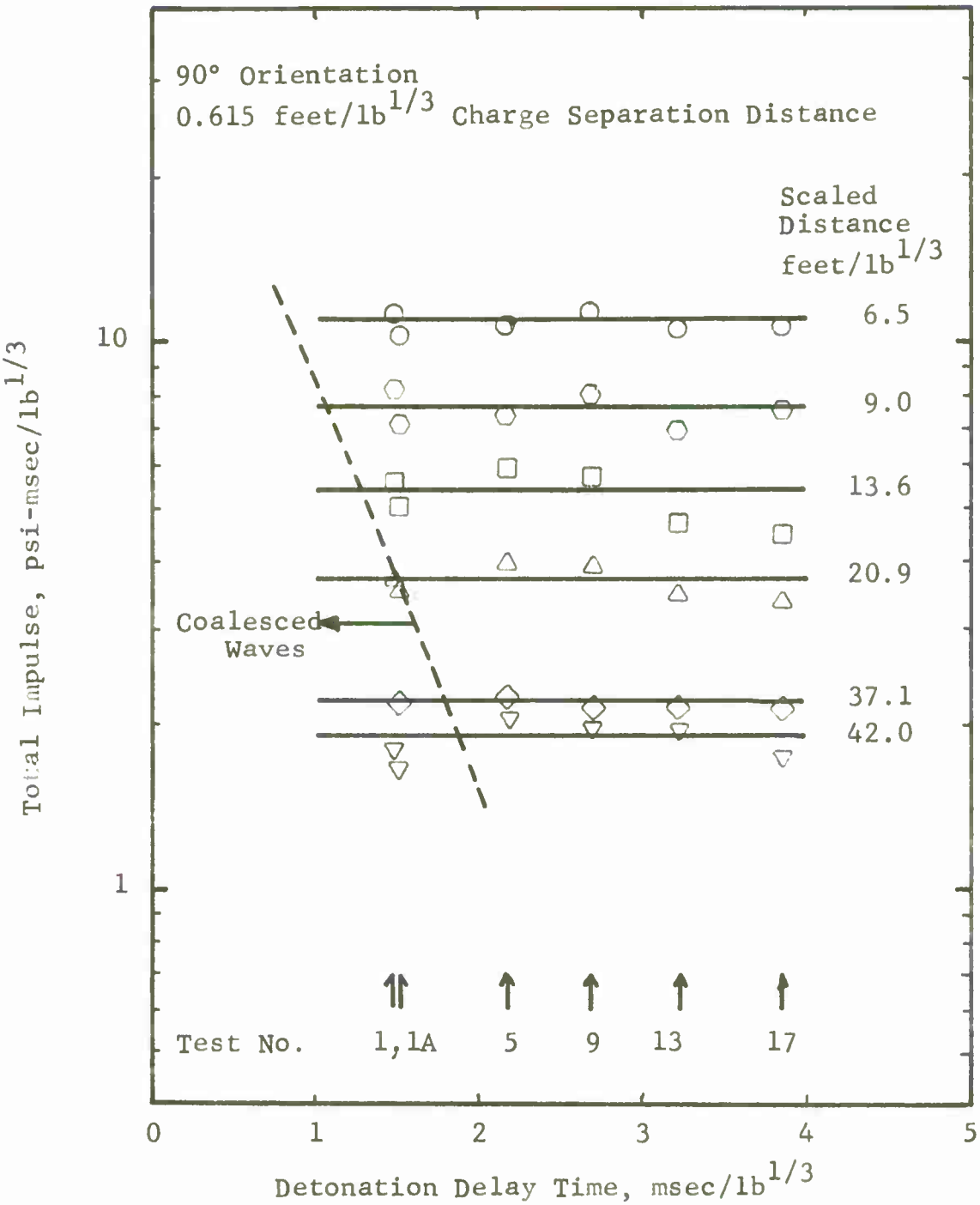

Figure A55 Total Impulse (90°,0.615 feet/lb$^{1/3}$)

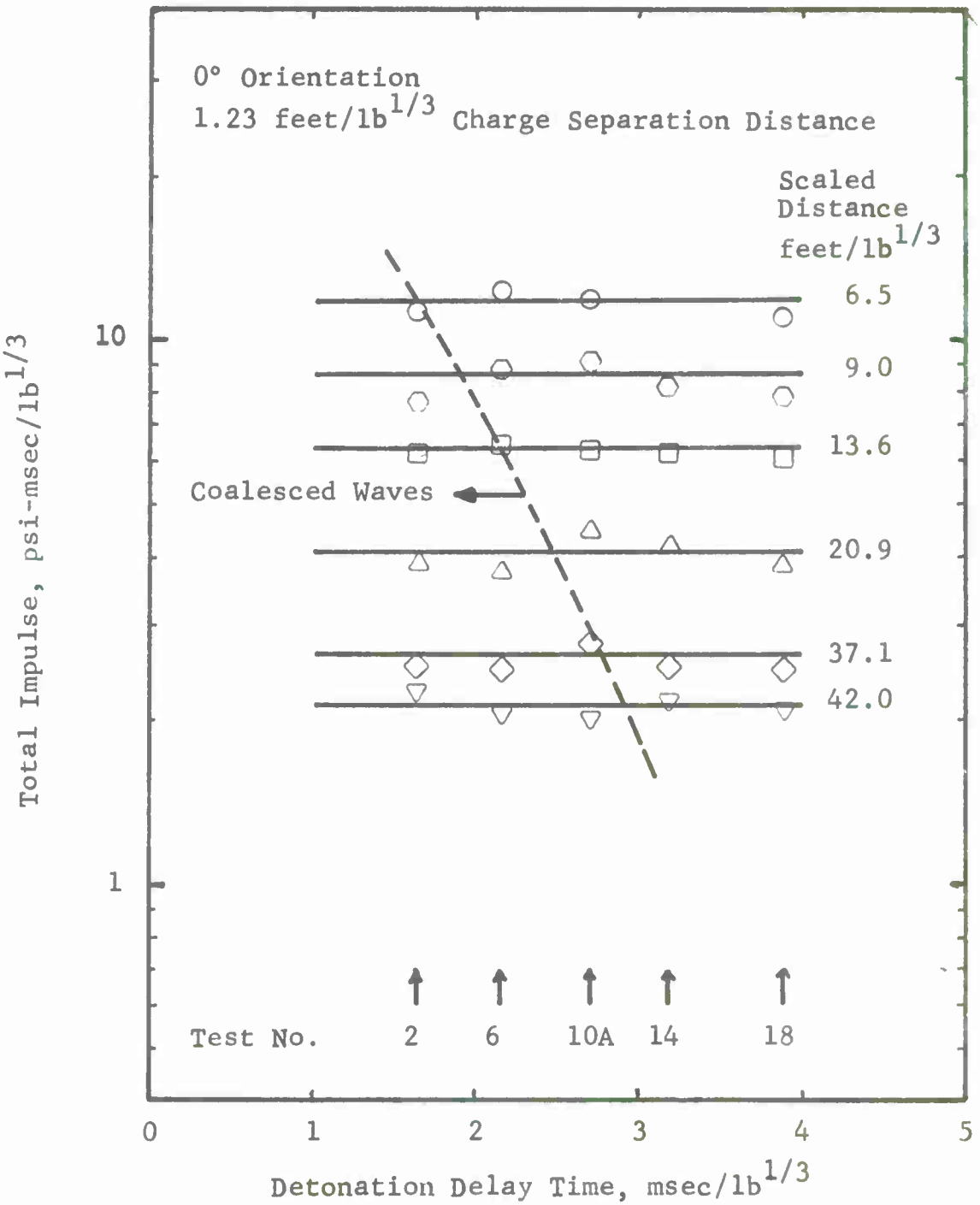

Figure A56 Total Impulse (0°, 1.23 feet/lb$^{1/3}$)

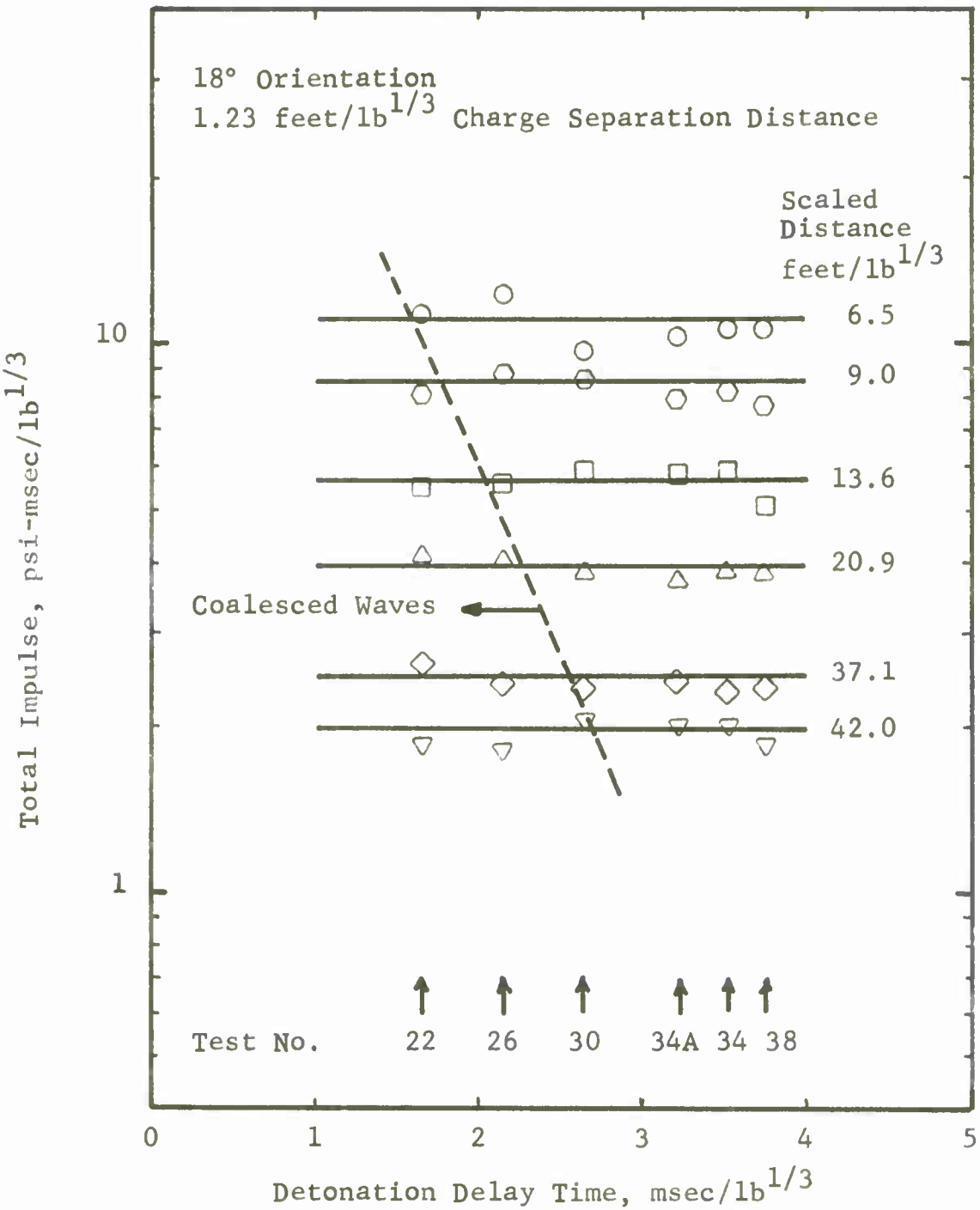

Figure A57 Total Impulse (18°, 1.23 feet/lb$^{1/3}$)

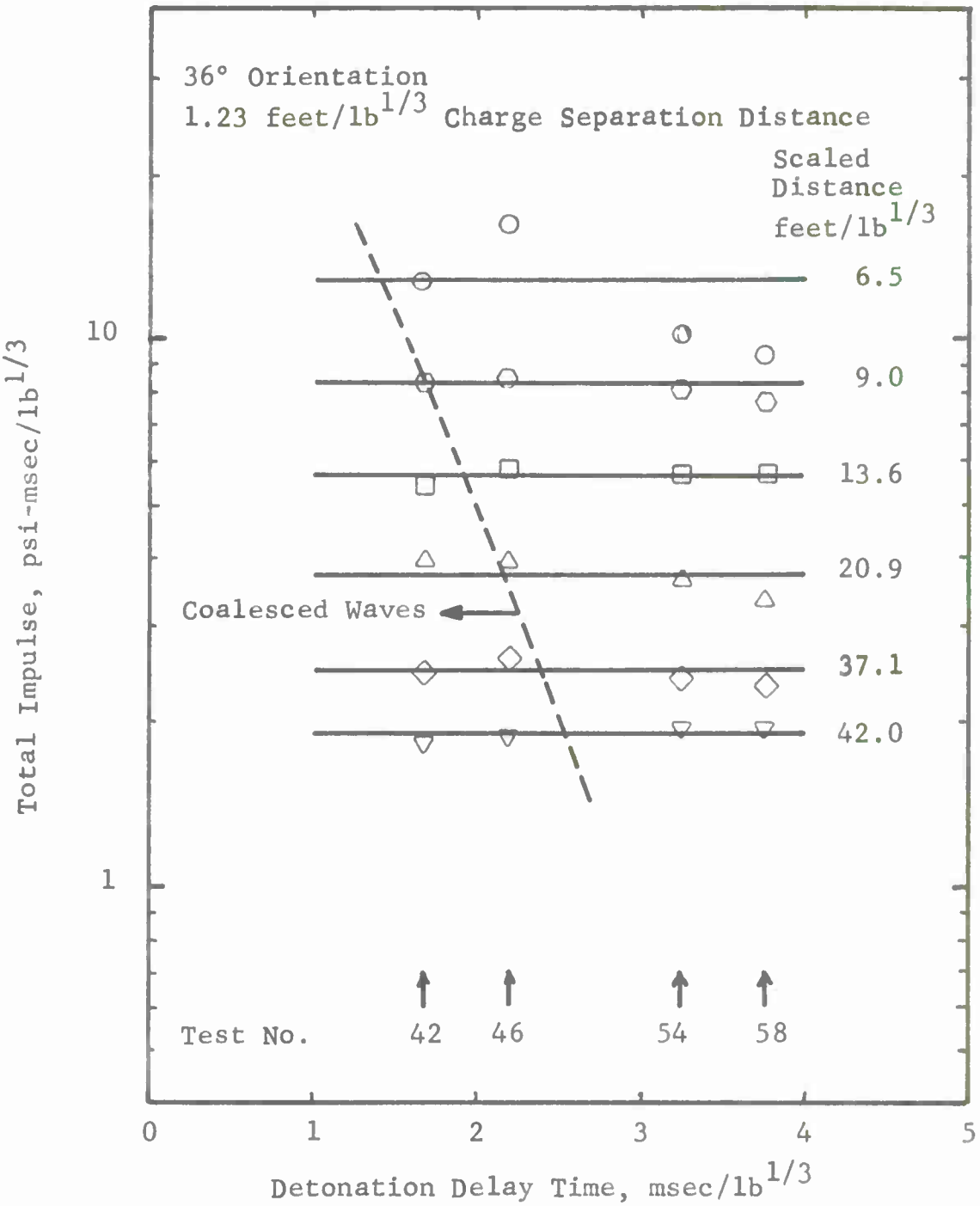

Figure A58 Total Impulse (36°, 1.23 feet/lb$^{1/3}$)

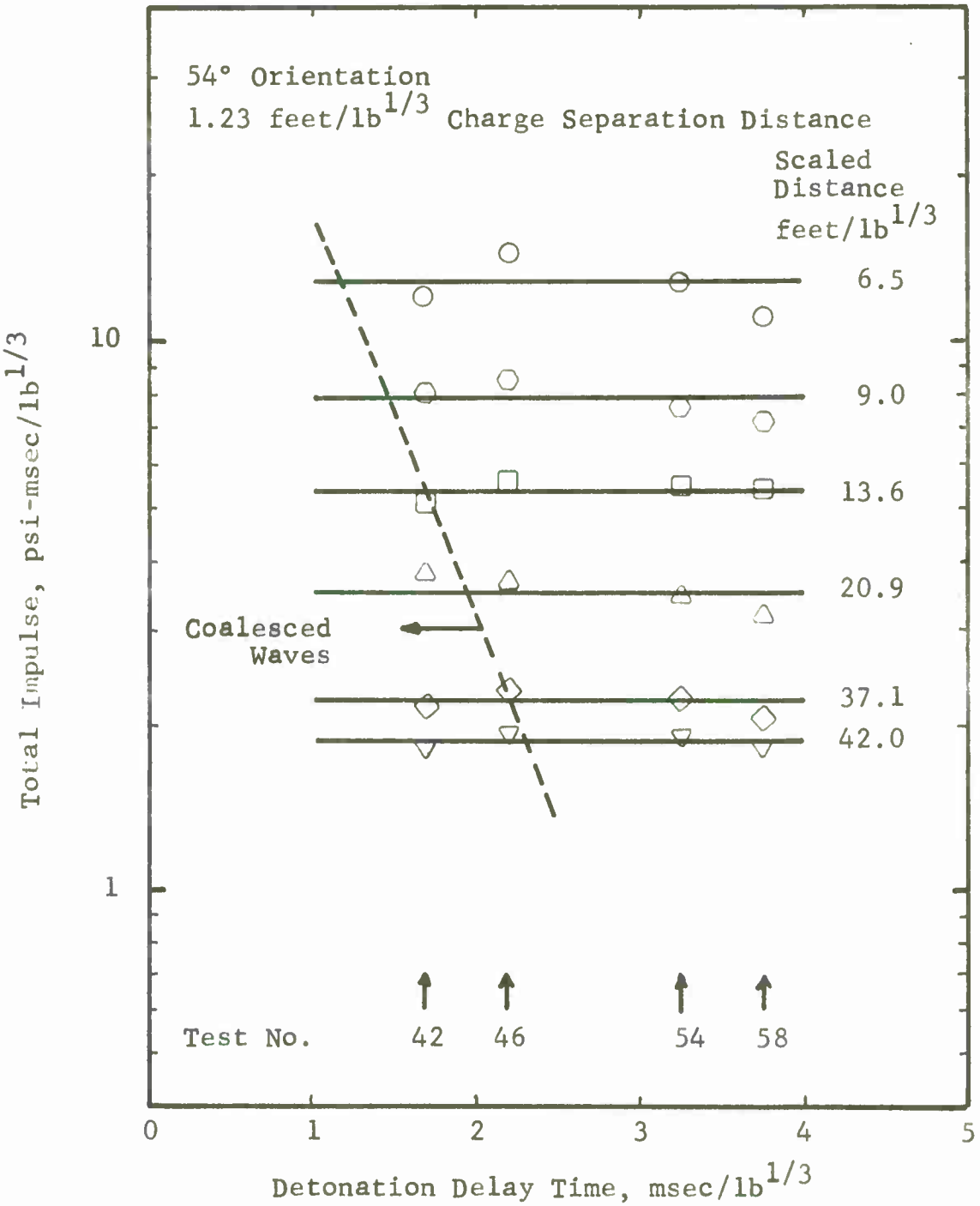

Figure A59 Total Impulse (54°, 1.23 feet/lb$^{1/3}$)

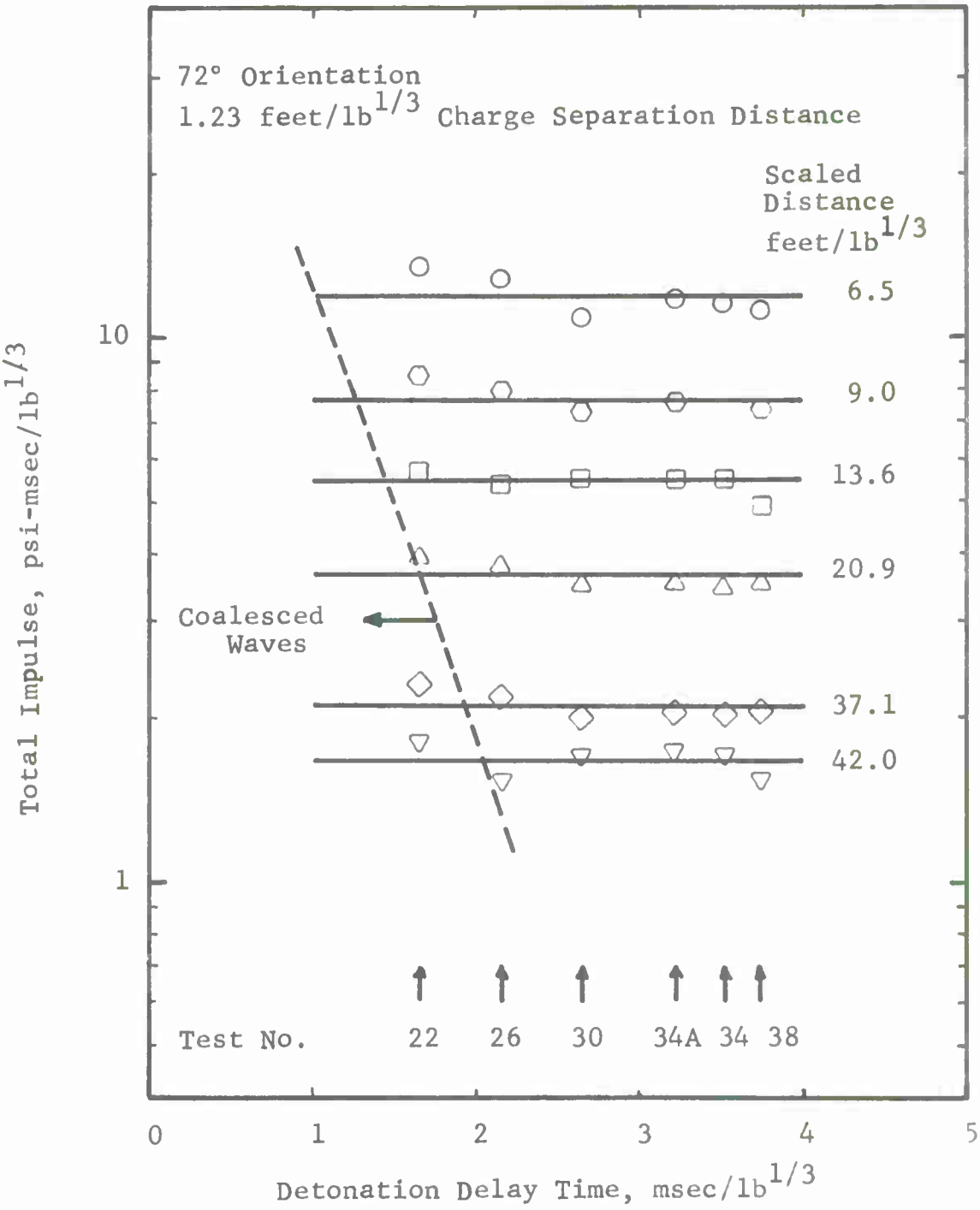

Figure A60 Total Impulse (72°, 1.23 feet/lb$^{1/3}$)

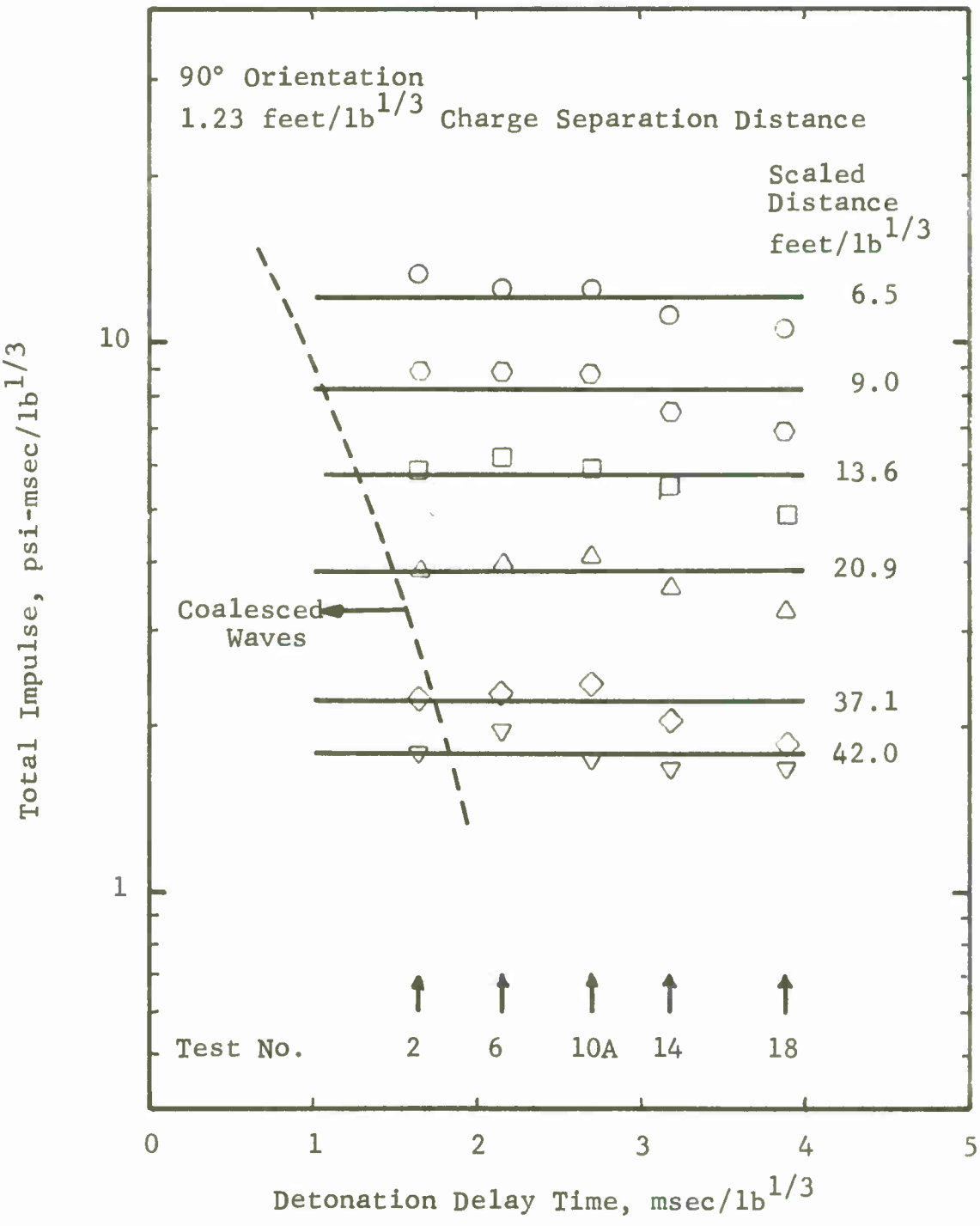

Figure A61 Total Impulse (90°, 1.23 feet/lb$^{1/3}$)

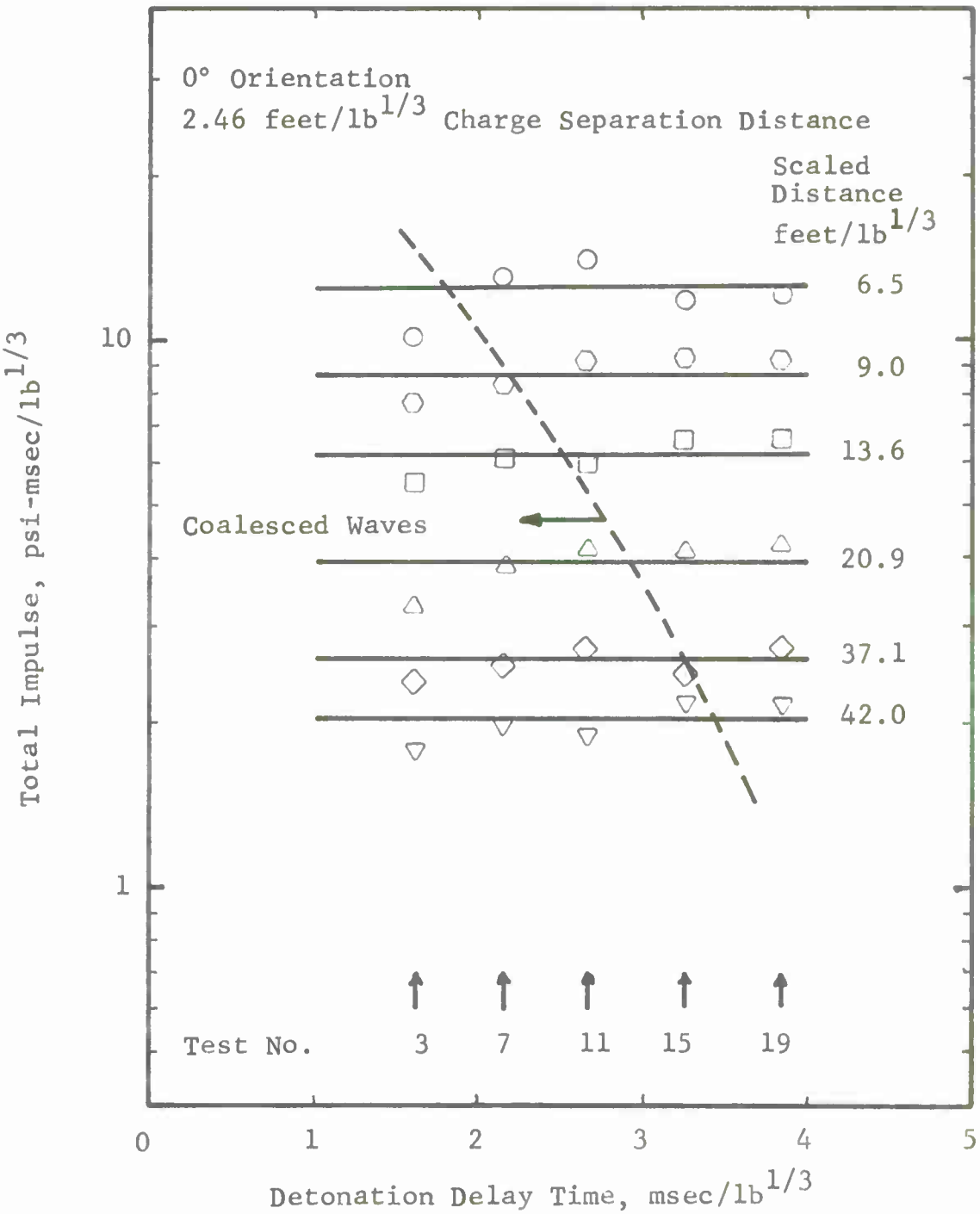

Figure A62 Total Impulse (0°, 2.46 feet/lb$^{1/3}$)

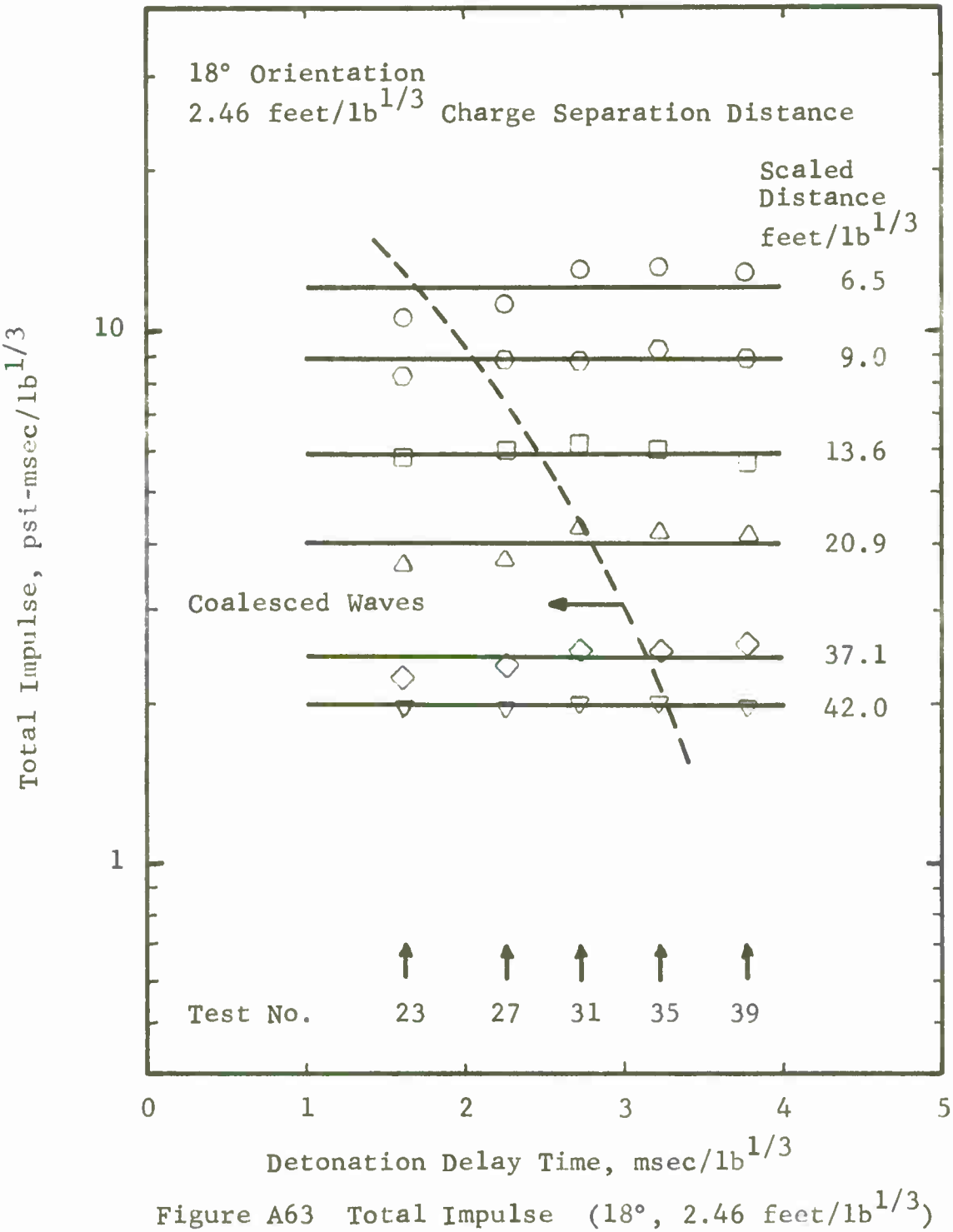

Figure A63 Total Impulse (18°, 2.46 feet/lb$^{1/3}$)

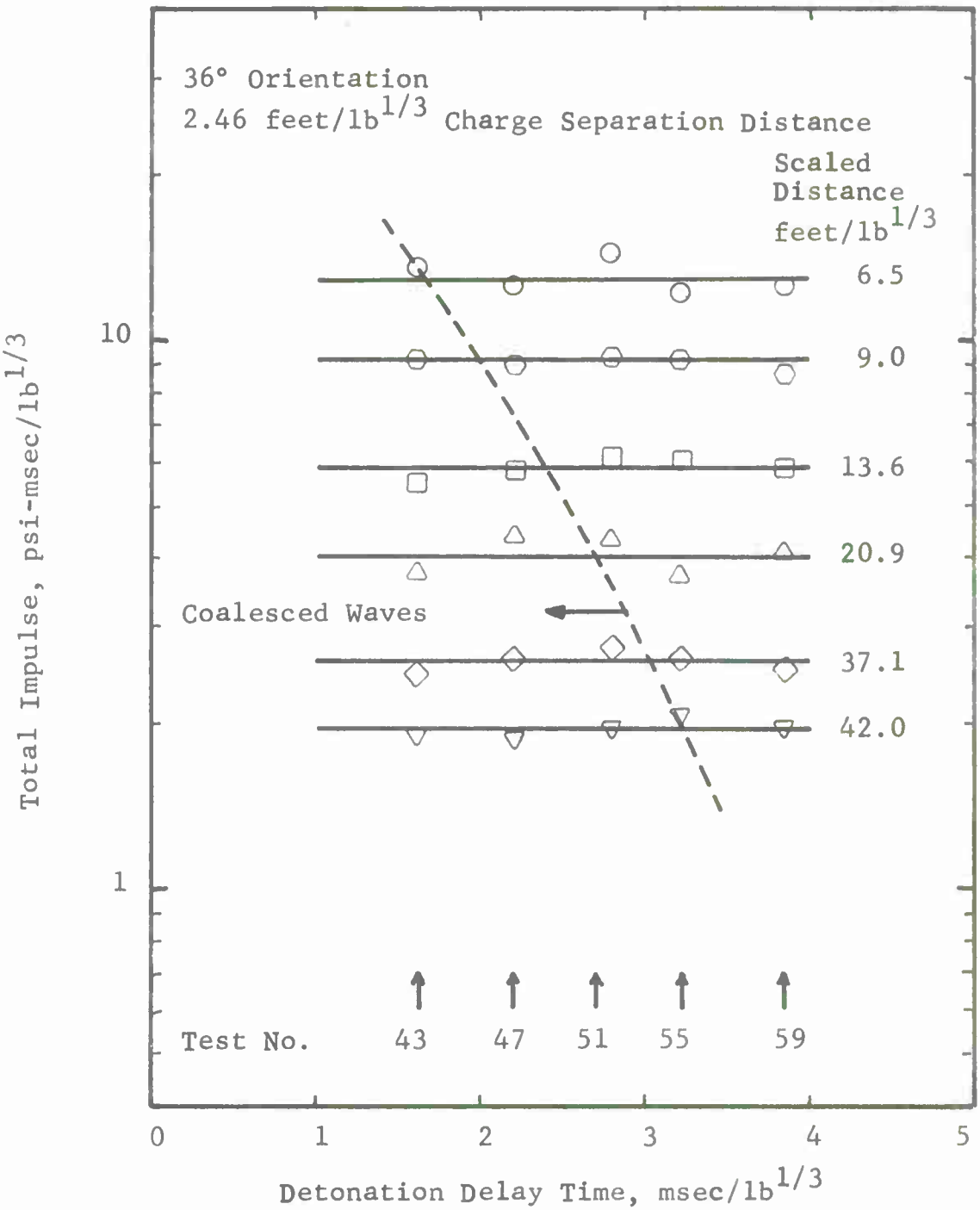

Figure A64 Total Impulse (36°, 2.46 feet/lb$^{1/3}$)

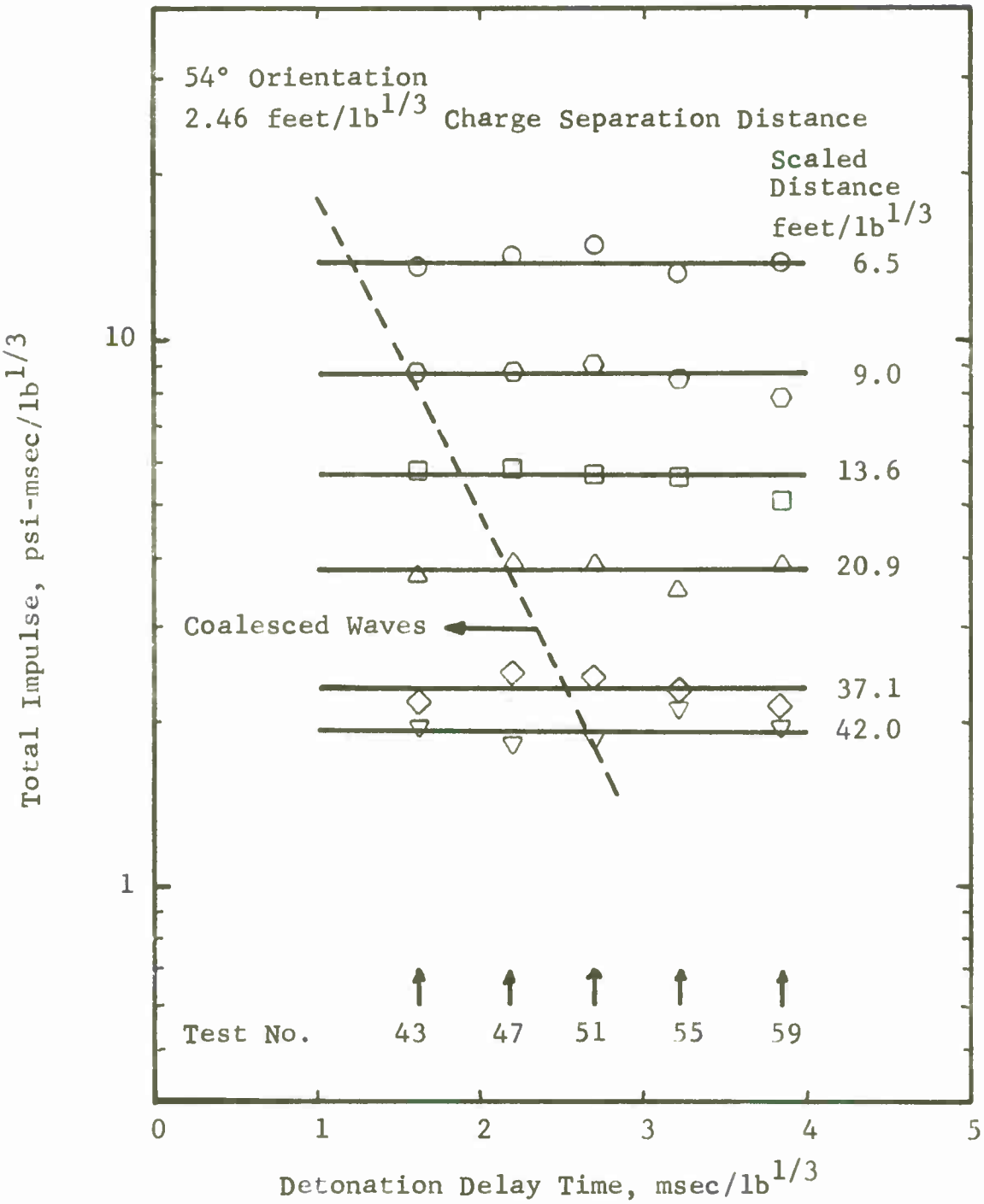

Figure A65 Total Impulse (54°, 2.46 feet/lb$^{1/3}$)

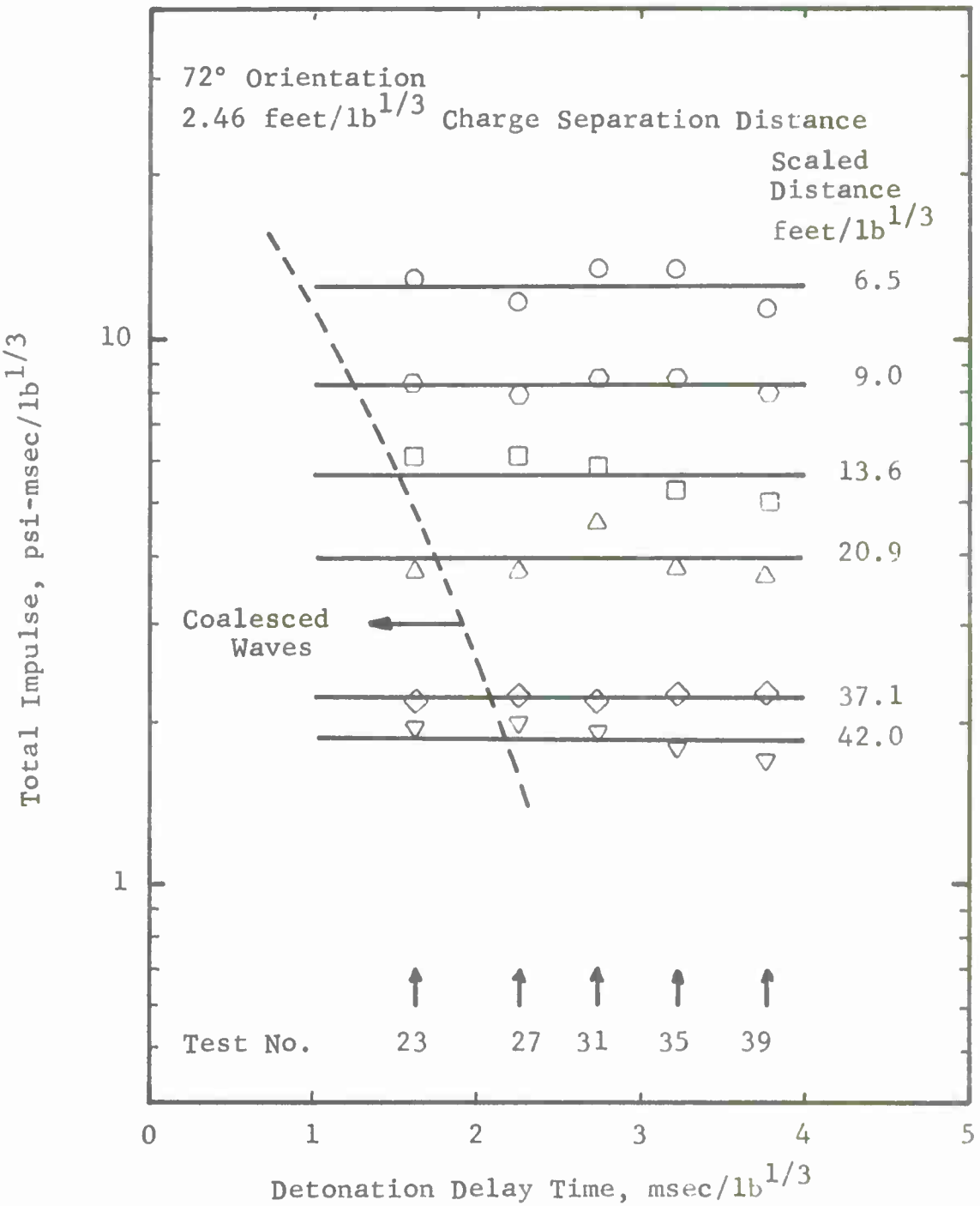

Figure A66 Total Impulse (72°, 2.46 feet/lb$^{1/3}$)

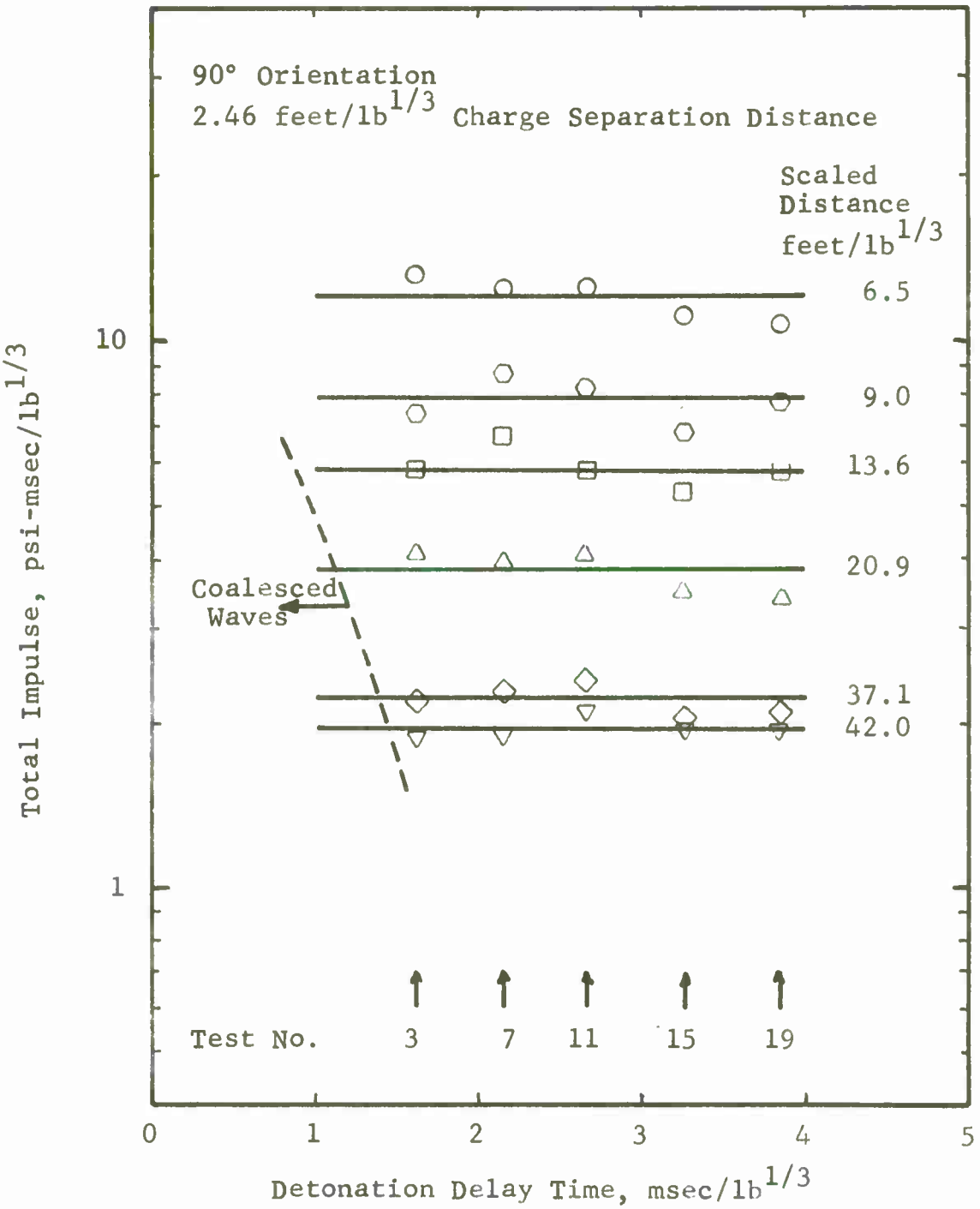

Figure A67 Total Impulse (90°, 2.46 feet/lb$^{1/3}$)

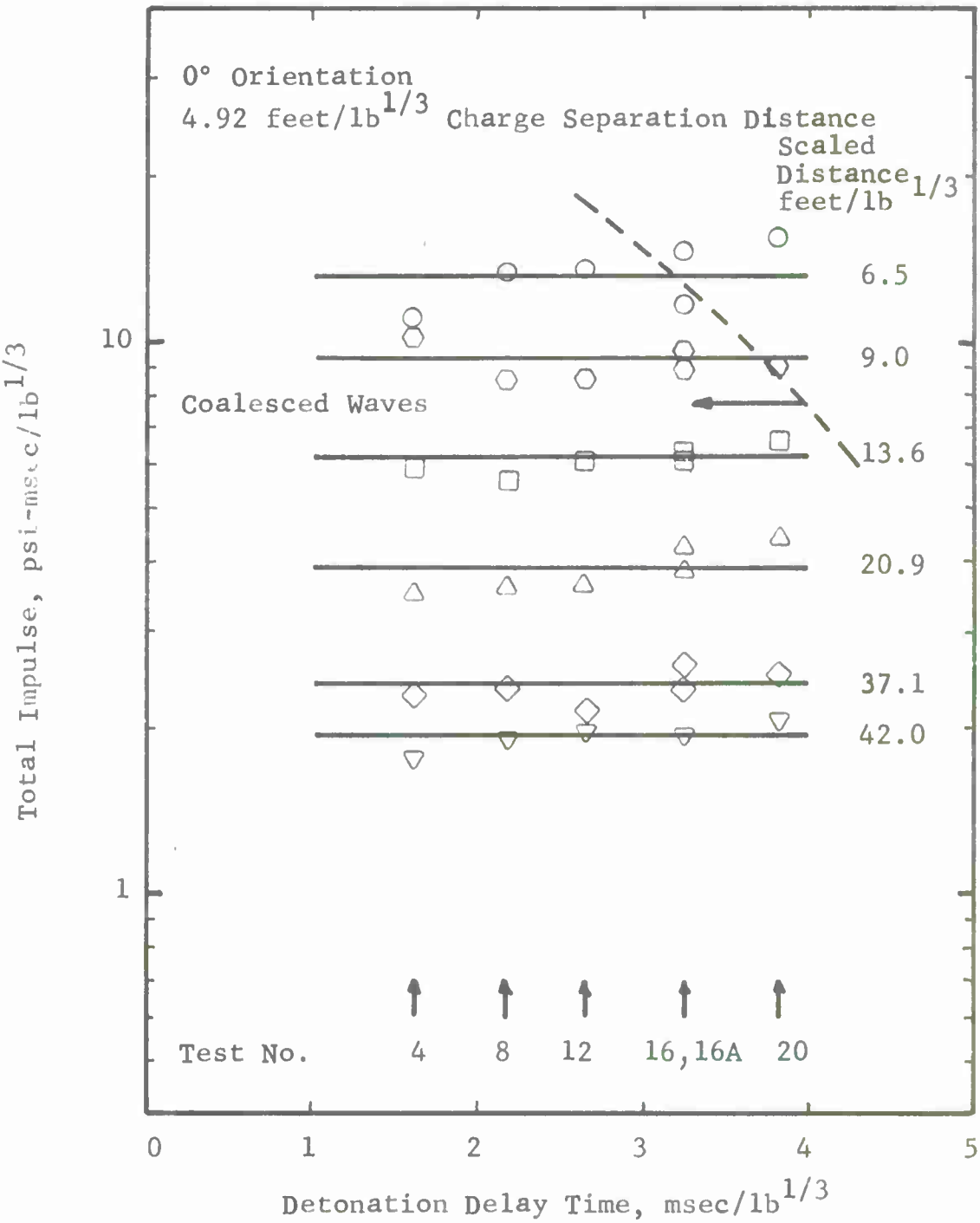

Figure A68 Total Impulse (0°, 4.92 feet/lb$^{1/3}$)

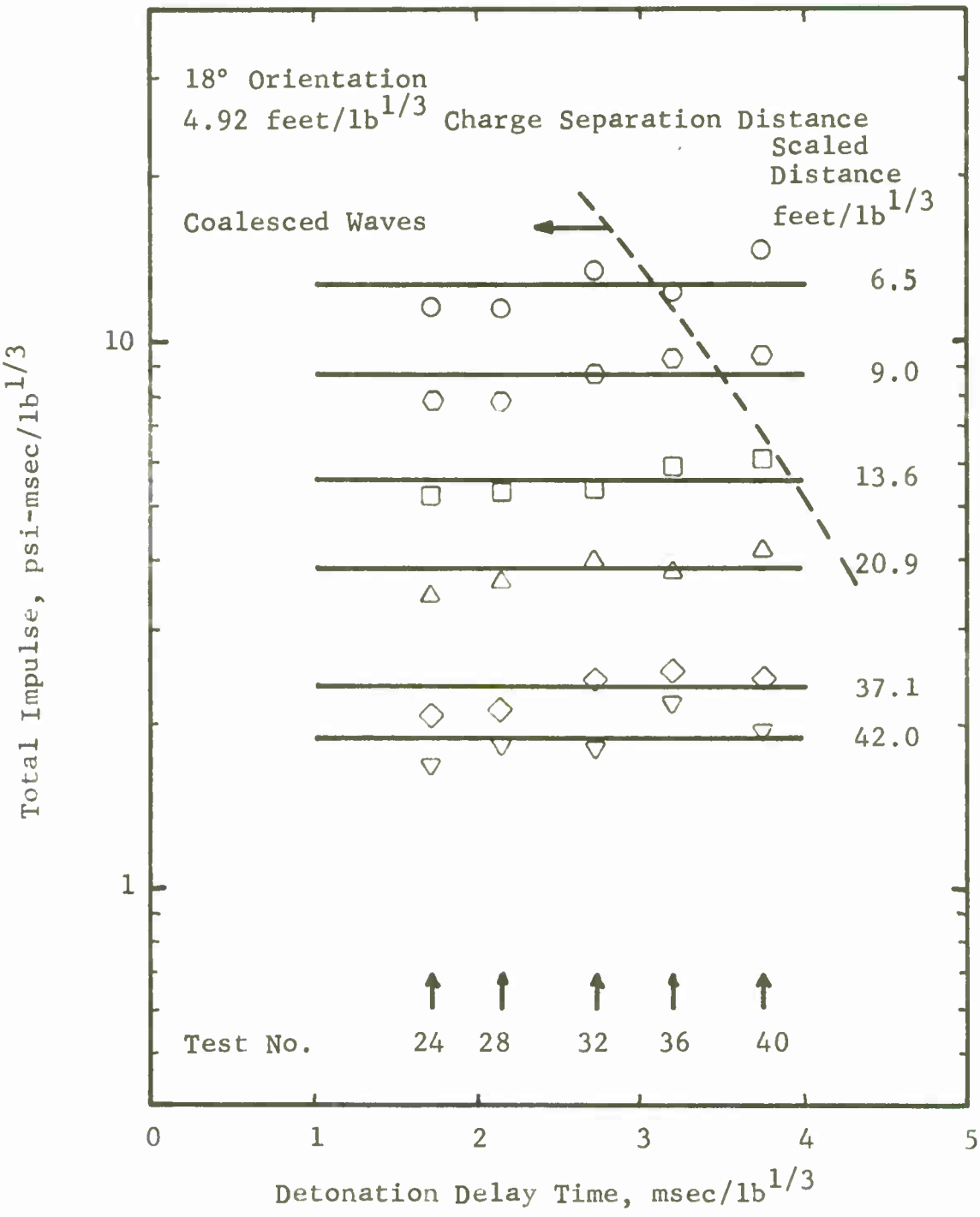

Figure A69 Total Impulse (18°, 4.92 feet/lb$^{1/3}$)

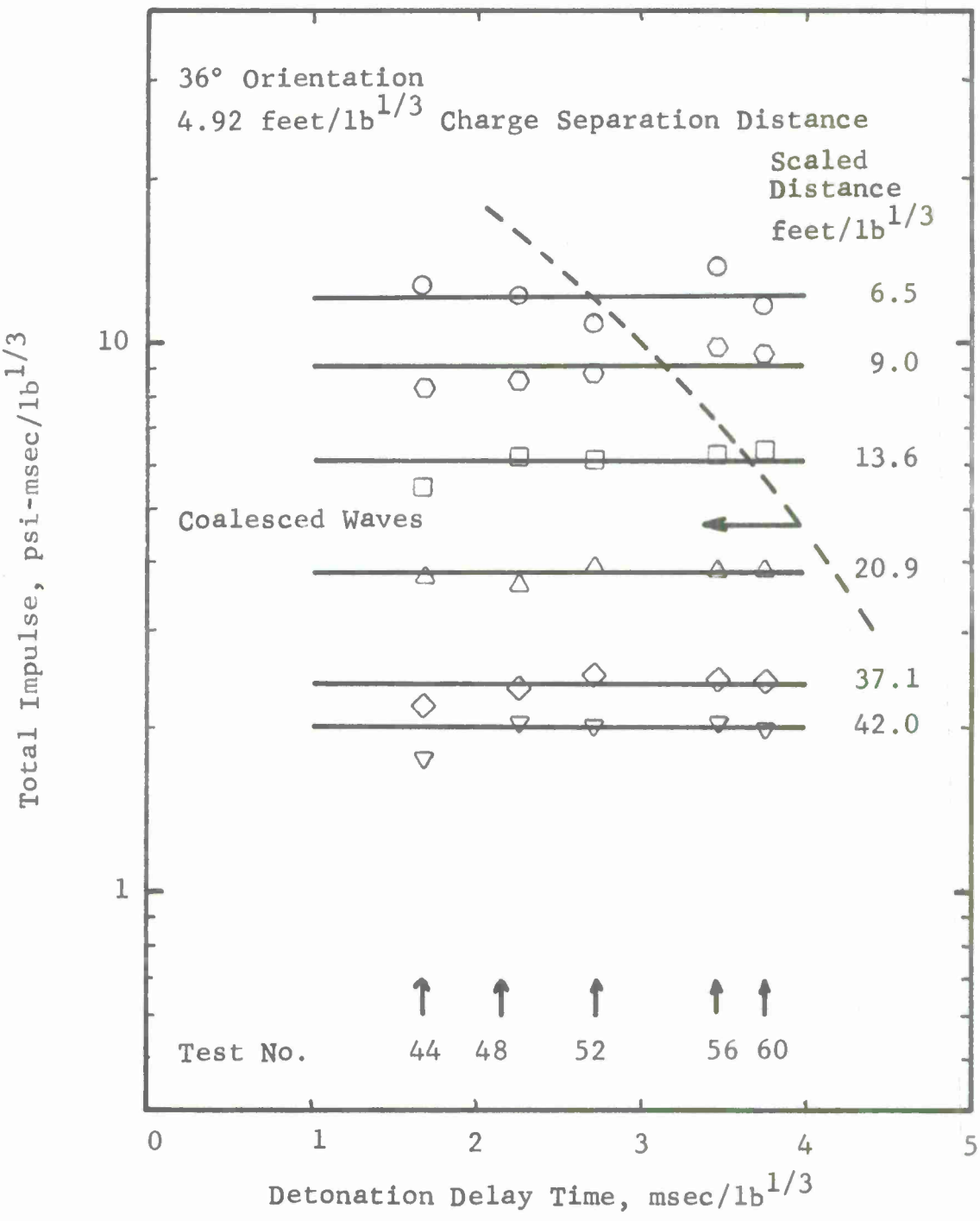

Figure A70 Total Impulse (36°, 4.92 feet/lb$^{1/3}$)

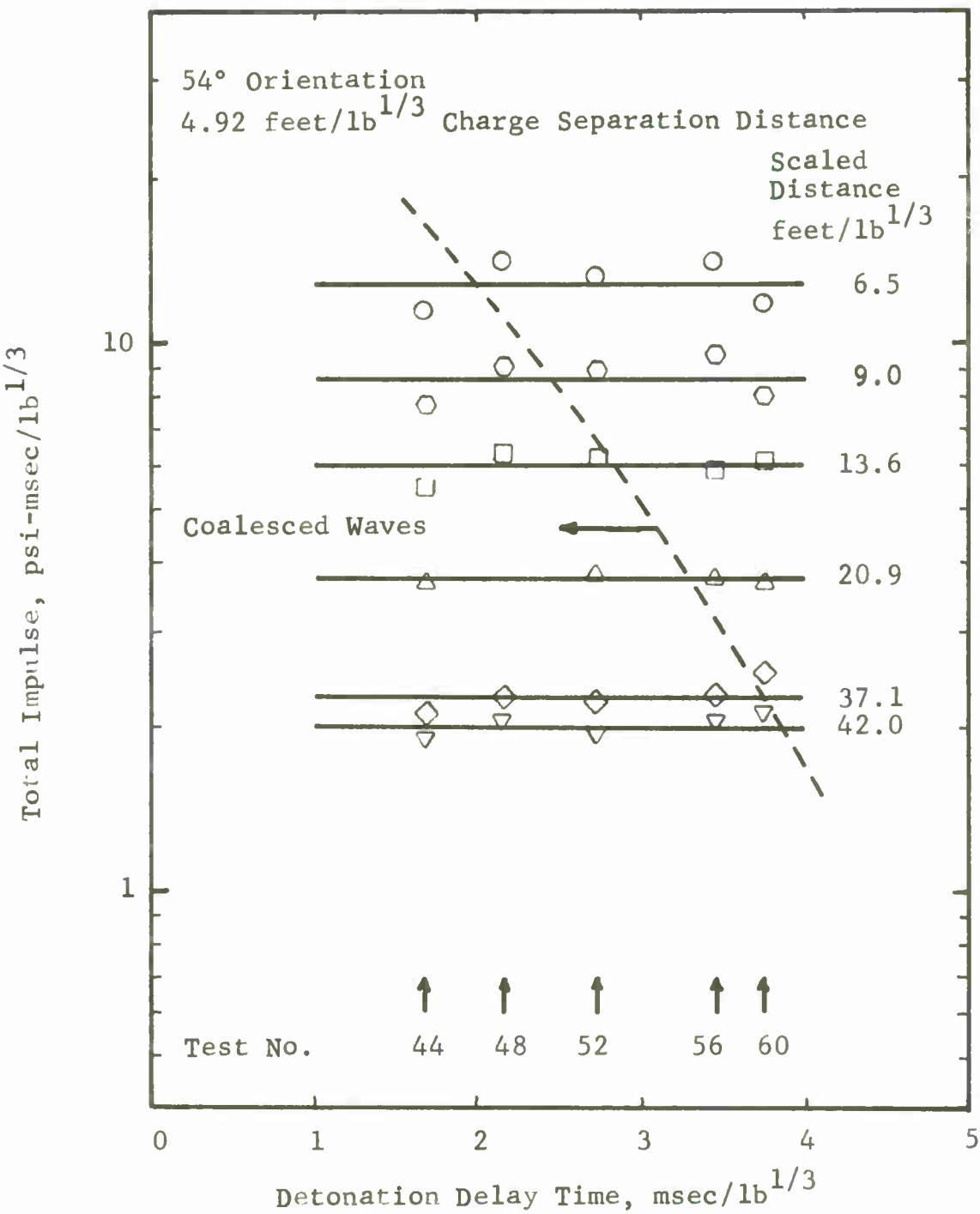

Figure A71 Total Impulse (54°, 4.92 feet/lb$^{1/3}$)

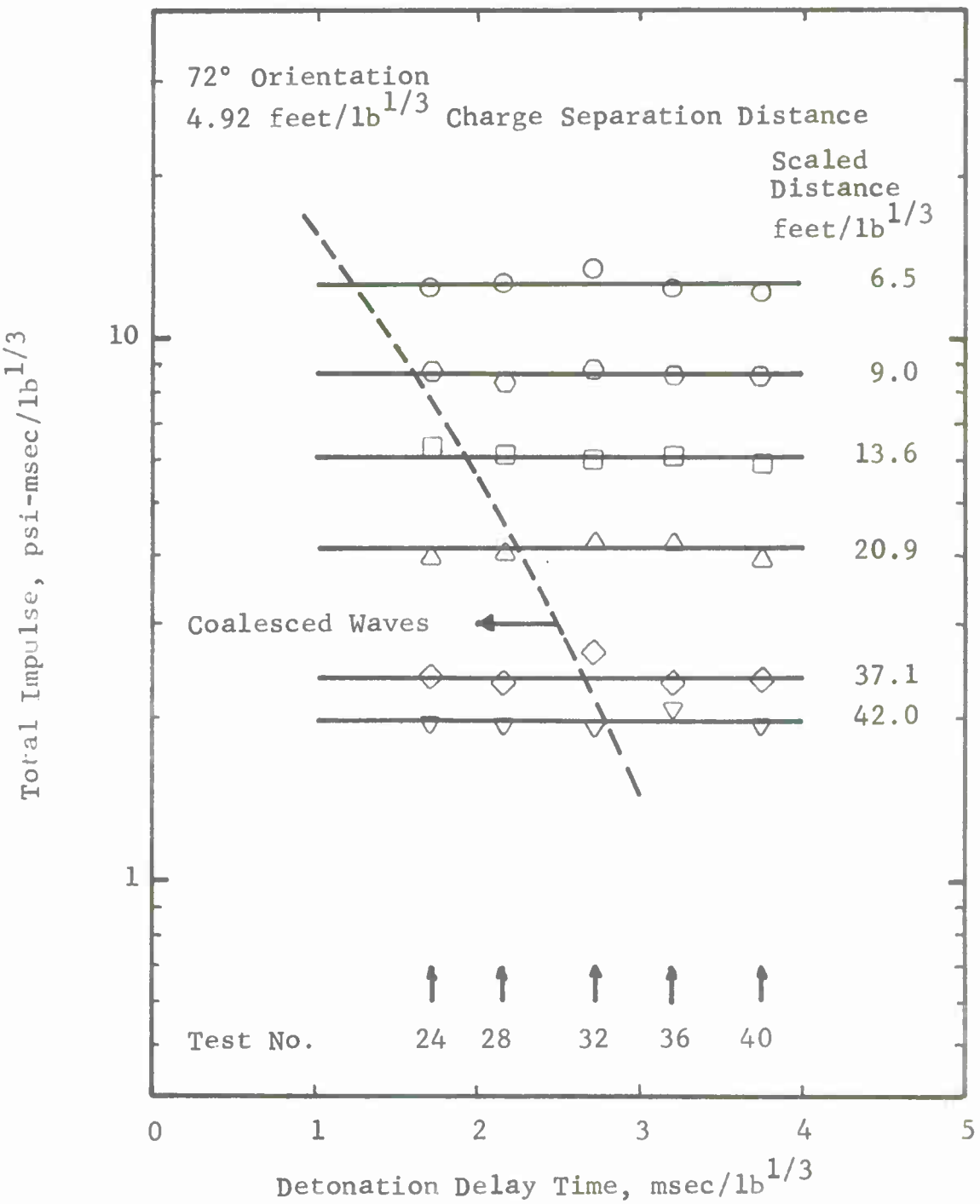

Figure A72 Total Impulse (72°, 4.92 feet/lb$^{1/3}$)

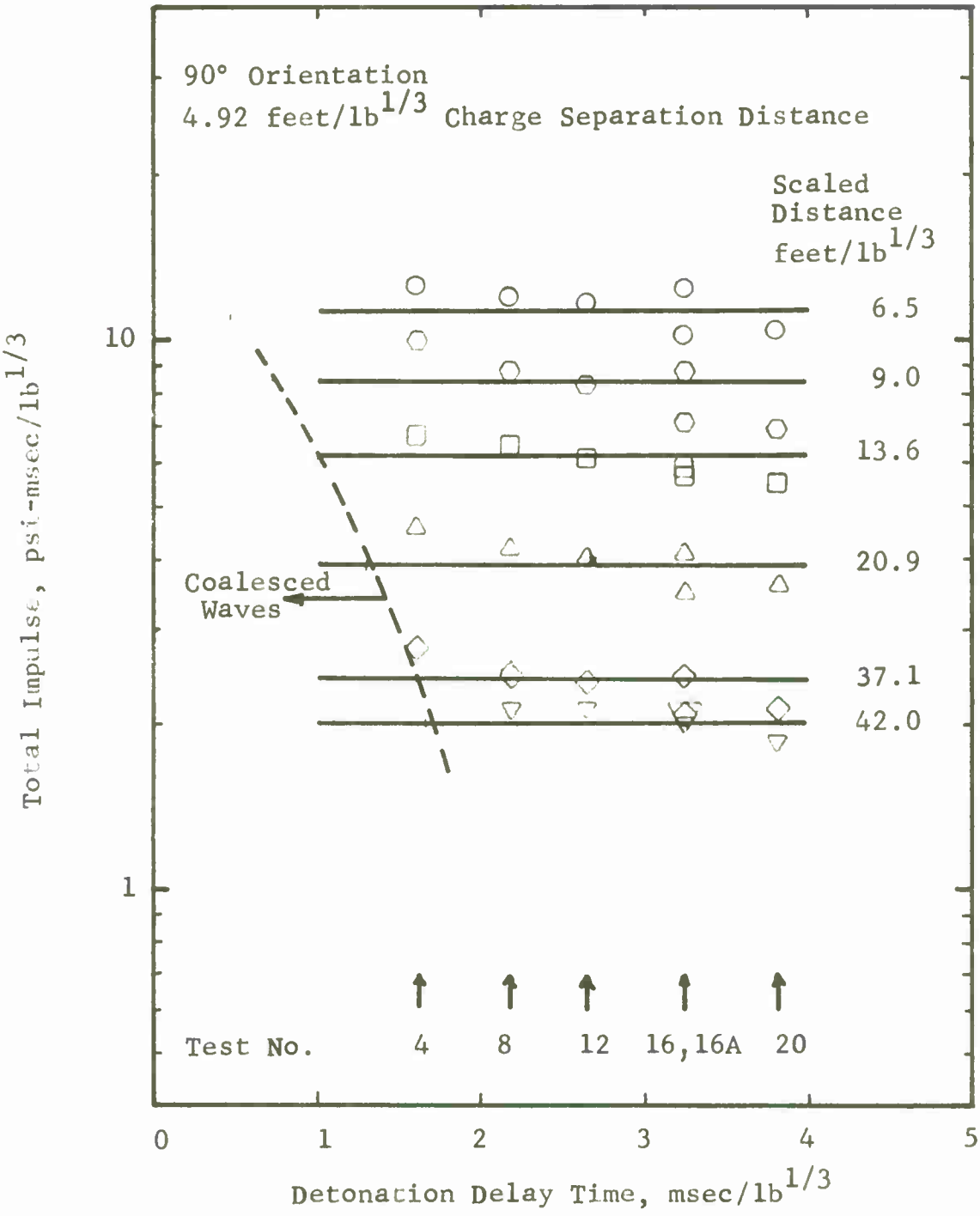

Figure A73 Total Impulse (90°, 4.92 feet/lb$^{1/3}$)

APPENDIX B

INSTRUMENTATION

by Richard P. Joyce

Pressure-time functions were monitored at locations as previously described. The pressure-time signals were integrated to produce impulse-time functions. Data signals were recorded on magnetic tape and reproduced on an oscillograph recorder. The following subsections contain a description of the instrumentation equipment, calibration technique and computational procedure employed on the test program.

B.1 Pressure Measuring Systems

The pressure measuring systems employed in the test program were manufactured by Photocon Research Products (PRP). These systems consist of three elements: the Dynagage (DG605D), a transmission line, and the pressure transducer (Type 752A).

The Photocon Type 752-40 psig transducer has a dynamic range of 0 to 40 psig and frequency response of 0 to 10 kHz. The diaphragm of the transducer, in conjunction with an insulated stationary electrode, forms an electrical capacitor. The pressure to be measured is applied to the diaphragm, causing a change in capacitance proportional to the applied pressure. The transducer capacitance and a built-in inductance form a tuned radio-frequency circuit. The tuned circuit is line-coupled, by means of a low impedance cable, to a Dynagage system consisting of an oscillator-detector circuit and a cathode-follower amplifier. The changes in capacitance produce changes in the diode detector impedance, and thereby produce a signal voltage proportional to the applied pressure.

The transducers were removed from their water-cooled flame shields and placed in an electrical insulated mounting adapter. The adapter was designed to provide flush mounting of the diaphragm. The electrical insulation material was used to break ground loops, thus reducing interference caused by stray pickup and intercarrier beats.

As previously stated, the transducers were installed flush with the ground surface in mechanically isolated steel mounting plates on the centerlines of two 75-ft-long by 10-ft-wide concrete slabs. Pressure measurements were made at six stations on each of two blast gage lines. The transmission line was run, in conduit in the near-field and aboveground in the farfield, to the instrumentation trailer.

B.2 Recording Instrument

Hewlett Packard (HP) Model 8875A differential amplifiers were used to condition the data signals for magnetic tape recording. These units were used to provide a voltage gain and impedance match between the pressure measuring system and magnetic tape recorder.

The data signals were recorded on an Ampex series CP-100 magnetic tape recorder. This unit is equipped with 13 FM recording tracks for data recording, and a single channel of direct recording for time base signals. The tape recorder conforms to specifications for the IRIG intermediate band.

B.3 Pressure Impulse Measurements

The pressure impulse is defined as the area under the pressure time history

$$I(t) = \int_{t_o}^{t} P(t)\, dt$$

where P is the pressure and t is the time.

The signal voltage at the output of the Model 8875A amplifier is an electrical analog of the pressure-time history. This signal was used as input to a Tektronix Type O operational amplifier, where the electrical integration was performed. The integrated signal was amplified and in turn, recorded on a CP100 magnetic tape recorder.

B.4 Data Reproduction

Oscillograph reproductions of the magnetic tape recordings were made by employing Consolidated Electrodynamics Corp. (CEC) Type 1-172 Driver Amplifiers to drive a CEC Type 5-124 Recording Oscillograph. The oscillograph was equipped with CEC Type 7-363 galvanometers.

The pressure data were recorded at a tape speed of 60 ips and reproduced at a tape speed of 1-7/8 ips, resulting in a frequency division of 32. The oscillograph paper speed was 32 ips. For these conditions, the oscillograph has a horizontal resolution of 976 μsec/in. and an effective frequency response from dc to 20kHz, referred to real time.

B.5 Block Diagram

A simplified block diagram of the record/reproduce instrumentation system is shown as Figure B1. A single data channel is shown here. In the test program, 12 identical channels were used.

In addition to the equipment described, the monitoring and signal control equipment is shown. The data channels were monitored and an electrical calibration signal was recorded on each data track immediately preceding each test run. The electrical calibration signal is a voltage simulation of a predetermined impulse or pressure level. This signal is used in data reduction and to verify the integrity of the record/reproduce system.

B.6 Calibration Procedures

The primary purpose of the calibration series is to establish sensitivity factors for each pressure measuring system. A precisely known pressure is applied to the transducer. The applied pressure causes a voltage rise at the output of the Dynagage Amplifier. The sensitivity factor (k) is the output voltage from the Dynagage (V) divided by the applied pressure P

$$K = \frac{V}{P} \text{ (Volts/psi)}$$

The Photocon systems were calibrated at five points in the range 0 to 50 psi. The quantity K for the range is the arithmetic mean of the values of K determined at all the points.

B.7 Computational Procedure

This subsection contains the equations used to determine the relationship between signal amplitude on the oscillograph recording and applied pressure and impulse. The symbols and units are:

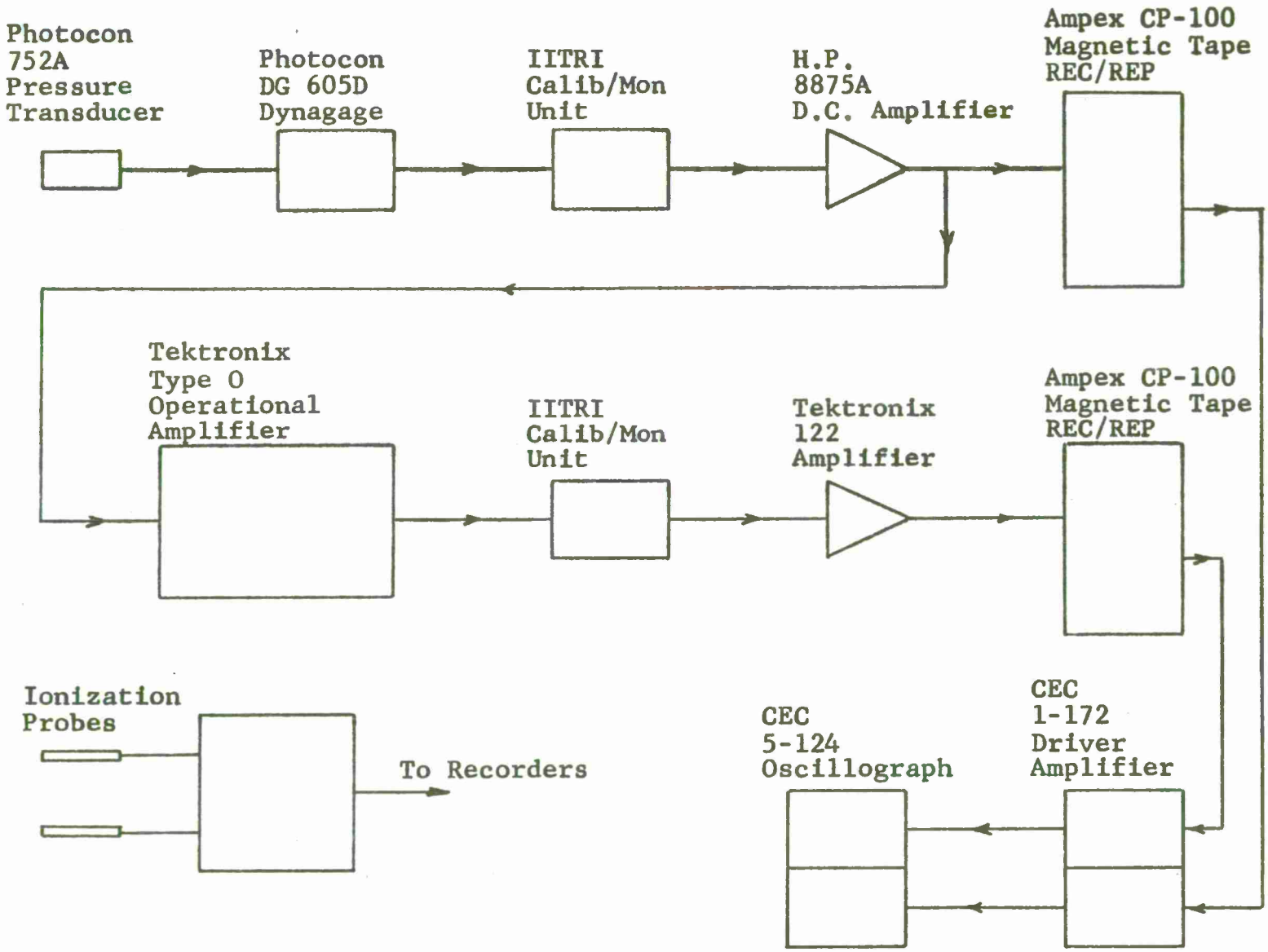

Figure B1 BLOCK DIAGRAM OF RECORD/REPRODUCE INSTRUMENTATION

$p(t)$ = Applied pressure (psi)

K = Sensitivity factor of pressure sensing system (volts/psi)

$I(t)$ = Pressure impulse (psi-sec)

t_o = Initial time (sec)

t_d = Time of positive duration of the second pressure pulse (sec)

E_{c1} = Calibration voltage for the pressure channel (volts)

E_{c2} = Calibration voltage for the impulse channel (volts)

D_{c1} = Deflection of trace due to pressure calibration signal (in.)

D_{c2} = Deflection of trace due to impulse calibration signal (in.)

$D_{t1}(t)$ = Deflection of trace due to the applied pressure (in.)

$D_{t2}(t)$ = Deflection of the trace due to the applied impulse (in.)

A_1 = Voltage gain of Sanborn 8875A Amplifier

A_2 = Voltage gain of Tektronix 122 Amplifier

A_s = Combined voltage gain of record/reproduce system and galvanometer sensitivity (in./volt)

B.8 Pressure Measurements

The deflection of the trace on the oscillograph trace due to the calibration signal is

$$D_{c1} = E_{c1} A_1 A_s$$

The deflection of the trace due to the applied pressure is

$$D_{t1}(t) = K P(t) A_1 A_s$$

Combining the above equations

$$P(t) = \frac{E_{c1}\, D_{t1}\ (t)}{K\, D_{c1}}$$

B.9 Impulse Measurements

Referring to the block diagram (Figure B1), and assuming the validity of the ideal gain of the generalized operational amplifier

$$\frac{E_o}{E_i} = -\frac{Z_o}{Z_i}$$

where E_i and E_o are the input and output voltages of the operational amplifier respectively, and Z_i and Z_o are the input and feedback impedances.

For the integrator configuration

$$Z_i = R \text{ and } Z_o = \frac{1}{Cp}$$

where p is the operator, $\frac{d}{dt}$.

The gain expression in terms of the circuit parameters is

$$E_o = -\frac{Z_o}{Z_i} E_i = -\frac{E_i}{RCp} = -\frac{1}{RC} \int E_i\, dt$$

Writing the gain expression in terms of the applied pressure

$$E_o = -\frac{A_1\, K}{RC} \int_{t_o}^{t} P(t)\, dt$$

Noting that $E_o\, A_2\, A_s = D_{t2}(t)$

$$D_{t2}(t) = \frac{A_1 A_2 A_s\, K}{RC} \int_{t_o}^{t} P(t)\ \ dt = \frac{A_1 A_2 A_s K}{RC}\, I(t)$$

The deflection of the trace due to the calibration voltage is

$$D_{c2} = E_{c2}\, A_2 A_s$$

Combining the expressions for $D_{t2}(t)$ and D_{c2}

$$I(t) = \frac{RC\ E_{c2}\ D_{t2}(t)}{A_1\ K\ D_{c2}}$$

The maximum pressure pulse is evaluated at the end of the positive phase duration t_d of the second pressure pulse.

$$I_{max} = \frac{RC\ E_{c2}\ D_{t2}(t_d)}{A_1\ K\ D_{c2}}$$

BLANK

DISTRIBUTION LIST

	No. of Copies
Department of Defense Explosives Safety Board Forrestal Building Washington, D. C. 20314	5
Defense Documentation Center Cameron Station Alexandria, Virginia 22314	12
Director of Defense Research & Engineering Department of Defense Washington, D. C. 20301	1
Chief of Research and Development Department of the Army Washington, D. C. 20310	1
Assistant Chief of Staff for Force Development Department of the Army Director of Doctrine & Systems Washington, D. C. 20310	1
Assistant Chief of Staff for Intelligence Department of the Army Director of Combat Intelligence Washington, D. C. 20310	1
Deputy Chief of Staff for Logistics Department of the Army Attn: COL H. F. Hardin, LOG-DPD Washington, D. C. 20310	1
Deputy Chief of Staff for Personnel Department of the Army Attn: Director of Safety Washington, D. C. 20310	1
Commanding General Army Materiel Command Attn: AMCRD-SP-A Washington, D. C. 20315	1
Commanding General Army Materiel Command Attn: W. G. Queen, AMCSF Washington, D. C. 20315	1

Commanding General 1
Army Materiel Command
Mobility Equipment R&D Center
Fort Belvoir, Virginia 22060

Office, Chief of Engineers 1
Department of the Army
Attn: ENGSA
Washington, D. C. 20314

Office, Chief of Engineers 1
Department of the Army
Attn: Mr. G. F. Wigger, DAEN-MCE-D
Washington, D. C. 20314

Commanding Officer 1
Picatinny Arsenal
Attn; SMUPA-DE
Dover, New Jersey 07801

Commanding General 1
Army Munitions Command
Attn: Mr. E. W. VanPatten
Picatinny Arsenal
Dover, New Jersey 07801

Commanding Officer 1
Ballistic Research Laboratories
Aberdeen Research & Development Center
Attn: Mr. C. N. Kingery
Aberdeen Proving Ground, Md. 21005

Chief of Naval Material 1
Department of the Navy
Attn: MAT 0441B
Washington, D. C. 20360

Chief of Naval Operations 1
Department of the Navy
Attn: Mr. J. W. Connelly, OP-41D
Washington, D. C. 20350

Chief of Naval Operations 1
Department of the Navy
Attn: Capt. J. D. Westervelt, OP-41B
Washington, D. C. 20350

Director 1
Defense Atomic Support Agency
Attn: Mr. E. L. Eagles, J4FE
Thomas Building
Washington, D. C. 20305

Director of Aerospace Safety 1
Headquarters, U. S. Air Force
Attn: Col. J. P. Huffman, IGDSOE
Norton AFB, California 92409

Headquarters, U. S. Air Force 1
Attn: COL W. K. Hillyer, IGDA
Washington, D. C. 20330

Headquarters, U. S. Air Force 1
Attn: AFSSS
Washington, D. C. 20330

Air Force Systems Command 1
ATTN: SCTSW
Andrews Air Force Base
Washington, D. C. 20331

Air Force Systems Command 1
Attn: Mr. Howell, SCIZG
Andrews Air Force Base
Washington, D. C. 20331

Director of Aerospace Safety 1
Headquarters, U. S. Air Force
Attn: Mr. D. E. Endsley, IGDSOE
Norton AFB, California 92409

Headquarters, U. S. Air Force 1
ATTN: Mr. W. Buchholtz, AFPRE
Bolling Air Force Base
Washington, D. C. 20332

Director, Air Force Weapons Laboratory 1
Attn: Mr. F. Peterson, WLDC
Kirtland Air Force Base, N. M. 87117

Central Intelligence Agency 1
Washington, D. C. 20505

Commander 1
Naval Ordnance Systems Command
Attn: ORD-0332
Washington, D. C. 20360

Commander 1
Naval Ordnance Systems Command
Attn: Mr. H. M. Roylance, ORD-048
Washington, D. C. 20360

Commander 1
Naval Ordnance Systems Command
Attn: ORD-04612
Washington, D. C. 20360

Commander 1
Naval Facilities Engineering Command
Attn: Mr. C. J. Stevens, Code 0512E
Washington, D. C. 20390

Commander 1
Naval Facilities Engineering Command
Attn: Mr. A. D. Tolins, Code 04122D
Washington, D. C. 20390

Commander 1
Naval Ordnance Laboratory, White Oak
Attn: EA Division (W. S. Filler)
Silver Spring, Maryland 20910

Commander 1
Naval Weapons Center
Attn: Code 572
China Lake, California 93555

Commanding Officer 1
Naval Ammunition Depot
Attn: WEPEC
Crane, Indiana 47522

Commanding Officer 1
Naval Civil Engineering Laboratory
Port Hueneme, California 93041

Director 1
Defense Atomic Support Agency
Attn: J. R. Kelso, SPLN
Thomas Building
Washington, D. C. 20305

Albuquerque Operations Office 1
Atomic Energy Commission
Attn: ODI
P. O. Box 5400
Albuquerque, New Mexico 87115

Mason & Hanger-Silas Mason Co., Inc. 1
Pantex Plant - AEC
Attn: I. B. Akst, Director of Development
P. O. Box 647
Amarillo, Texas 79105

Atlas Chemical Industries, Inc. 1
Explosives Division
Attn: Dr. W. J. Taylor
Wilmington, Delaware 19899

Commanding Officer 1
Savanna Army Depot
Attn: A. G. Ehringer
Savanna, Illinois 61074

Office of Civil Defense 1
Department of the Army
Rm 3D336, Pentagon
Washington, D. C. 20310

Dr. Robert W. Van Dolah 1
Research Director
Explosives Research Center
Bureau of Mines
Department of Interior
4800 Forbes Avenue
Pittsburgh, Pa. 15213

URS Research Company 1
Attn: Mr. K. Kaplan
155 Bovet Road
San Mateo, California 94402

E. I. du Pont de Nemours & Co. 1
Attn: Mr. Frank A. Loving
Potomac River Development Labs
Martinsburg, West Virginia 25401

Institute of Makers of Explosives 1
Attn: Mr. Harry Hampton
Graybar Building, Rm 2449
420 Lexington Avenue
New York, N. Y. 10017

Assistant Secretary of Defense (I&L) 1
Attn: Mr. Howard Metcalf, IT
Washington, D. C. 20301

Mr. Alex B. Wenzel 1
Department of Mechanical Sciences
Southwest Research Institute
8500 Culebra Road
San Antonio, Texas 78228

Directorate of Safety (Army Dept.) 1
Ministry of Defence
Attn: Mr. R. R. Watson
Lansdowne House, Berkeley Square
London W1, England

Capt. A. Jenssen 1
Norwegian Defence Construction Service
Oslo-MIL
Oslo 1, Norway

Mr. D. S. Allan 1
Arthur D. Little, Inc.
Acorn Park
Cambridge, Mass. 02140

Dr. T. H. Schiffman 1
General American Research Division
General American Transportation Corp.
7449 N. Natchez Ave.
Niles, Ill. 60648